Institute of Hydrology

Albert-Ludwigs-Universität Freiburg i. Br.

Modeling of Flowpaths and Hydrochemistry in Acidified Watershed in the Catskill Mountains, New York, with PHREEQC

by

Angelika Winner

A Thesis in Candidacy for the Degree Diplom-Hydrology under the direction of Prof. Markus Weiler

March, 2009

Pictures

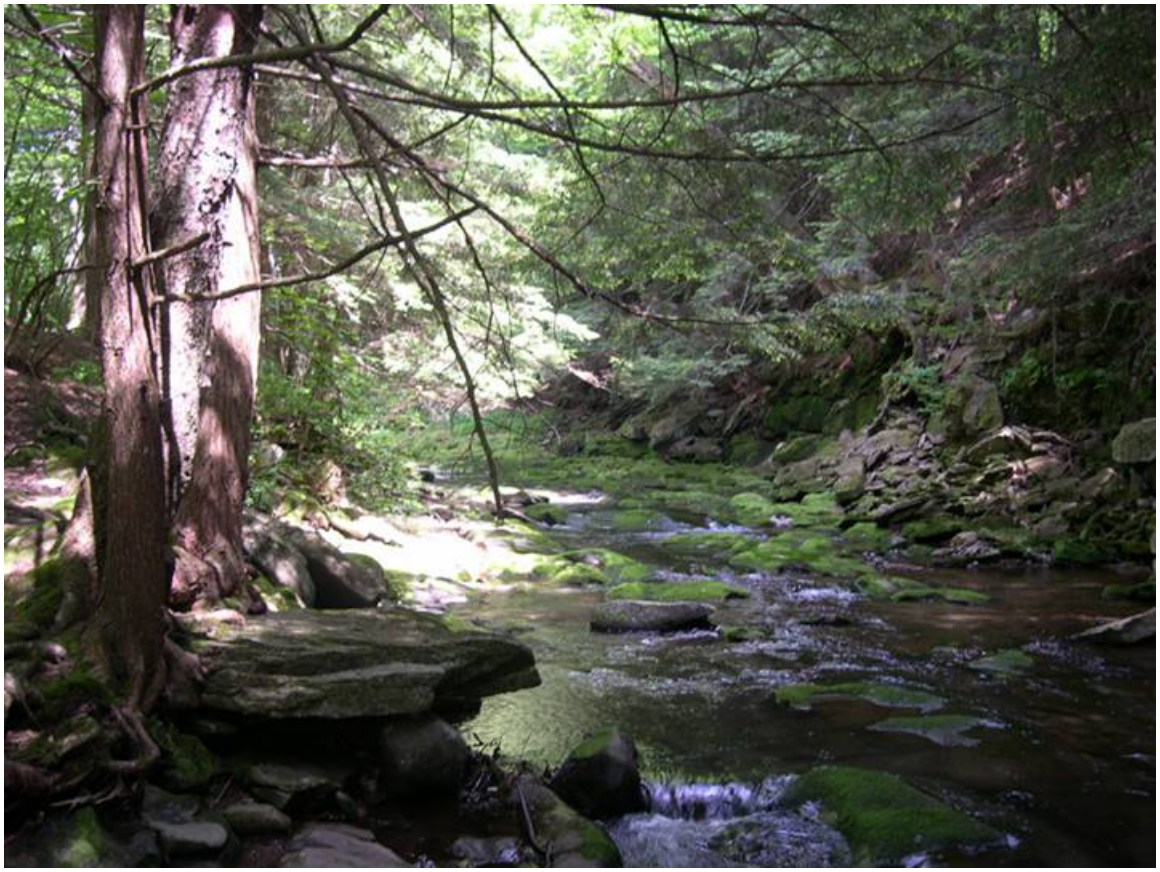

Biscuit Brook above outlet near Frost Valley

Wissen

Wenn einer es weiß, weiß es keiner.

Ludwig Wittgenstein (1889-1951)

Content

List of figures

List of tables

List of Abbreviations

AB	Acid Biscuit
BB	Basic Biscuit
WB	West Biscuit
DOC	Dissolved organic carbon
ANC	Acid neutralizing capacity
1D	One dimensional
CEC	Cation exchange capacity
ARD	Advection-reaction-dispersion equation
EPA	Environmental Protection Agency
LTM	Long-Term-Monitoring
NCDC	National Climatic Data Center
NADP	National Atmospheric Deposition Program
CV	Coefficient of variance
IHF	Institute of Hydrology Freiburg
USGS	US Geological Survey
V-SMOW	Vienna Standard Mean Ocean Water
pCO_2	Partial pressure of CO_2
Al_{im}	Inorganic monomeric Aluminum
SSURGO	Soil Survey Geographic Database
NRCS	Natural Resources Conservation Service
SI	Saturation index
SE	Square error
MSE	Mean square error
AE	Absolute error
MAE	Mean absolute error
pct_err	percent error in charge

atm	Atmosphere
IAEA	International Atomic Energy Agency
SE	Seepwater samples
ST	Streamwater samples
MEC	Mean exchanger composition
gwf	Gram formula weight

List of Symbols

m_{input}	Masses of given substances for input (precipitation)
m_{output}	Masses of given substances for output (stream flow)
Δm	Sinks or sources either by abiotic or by biotic processes
Q_T	Total runoff
$Q_1, Q_2,\ldots Q_n$	Runoff components
$c_1, c_2,\ldots, c_n$	Respective concentrations of one observed tracer t_i
Q_E	Event water
Q_P	Preevent water
c_T	$\delta^{18}O$ concentration in Q_T
c_P	$\delta^{18}O$ concentration in Q_P
c_E	$\delta^{18}O$ concentration in Q_E
a, b, c, d	Number of moles of reactants A, B, and the end products C, D in mass action law
K	Thermodynamic equilibrium or dissociation constant
K_s	Solubility product constant
K_d	Distribution coefficient
K_x	Selectivity coefficient
a_i	Activities with respect to species i
f_i	Activity coefficient
f_i	Relative frequency
I	Ionic strength
m_i	Moles of the species involved
z_i	Charge numbers of species involved (Debye-Hückel-Equation)
a_i, b_i	Ion- specific parameters (Debye-Hückel-Equation)
A, B	Temperature dependent parameters (Debye-Hückel-Equation)

IAP	Ion-activity-product
A^+, B^+	Monovalent ions
R	Exchanger
X	Exchanger
C	Concentration in water [mol/kgw]
t	Time [s]
v	Pore water velocity [m/s]
x	Distance [m]
D_L	Hydrodynamical dispersion coefficient [m²/s] = $D_e + \alpha_L v$
D_e	Effective diffusion coefficient
α_L	Dispersivity [m]
q	Concentration of the solid phase [mol/kgw]
D	Dispersivity
L	Cell length
P_e	Peclet number
$\|v\|$	Velocity [m/s] as a vector, with x, y, z components
‰	Permil (parts per thousand)
$\delta^{18}O$ ‰	Delta-permil notation for stable isotope measurements (example of ^{18}O in water)

Abstract

Acid Deposition is still of great concern, especially in the northeastern US, where recovery of watersheds lacks behind observed recovery of precipitation chemistry. The geochemical model PHREEQC has been applied in the Biscuit Brook basin in the Catskill Mountains, NY, to simulate alterations of water entering the system from rainwater to soilwater, groundwater, and finally to streamwater. Biscuit Brook is an ideal location to study recovery from acid deposition in watersheds, since at least two of the three dilute headwater tributaries have distinctly different chemical characteristics, whereas two are generally alkaline and one acidic.

The concept model, on which the PHREEQC models were based, was established by a combination of geochemical, hydrological, isotope, and soil data, taken in Biscuit Brook in June 2008.

Modeling results indicate that different acidification degrees of the three headwater tributaries are explained by the presence or absence of Calcite, which is derived from till layers that were deposited during the last glaciation. Results showed that streamwater pH is controlled by Calcite dissolution. Thus, streams with headwaters in an area of till deposition should be better buffered, than streams with headwaters in areas of till leaching or lack of till deposits. Observed variations in streamwater and seepwater chemistry in Biscuit Brook could be connected to differences in till deposition and till thickness.

Significant reactions in the Biscuit Brook basin could be detected by a stepwise modeling approach where complexity was gradually increased. The most dominant reactions are weathering processes, with dissolution of Calcite and silica minerals and the formation of clay minerals. Cation exchange is not the dominant process, since cation exchange capacities are generally low in the mineral soil horizons of all tributaries. Sensitivity analyses could prove that the model is not sensitive for cation exchange, since different CEC scenarios hardly changed simulated streamwater concentrations. However, the model seems to be sensitive to pCO_2, which is consequently strongly correlated with the presence of Calcite.

Keywords: *Acidification*, *PHREEQC*, *geochemical modeling*, *multi-component transport modeling*

Zusammenfassung

Anthropogen verursachte Versauerung von Einzugsgebieten durch so genannten „Sauren Regen" ist vielerorts immer noch ein ernstzunehmendes Problem, insbesondere jedoch im Nordosten der USA. Grund ist die verzögerte Erholung der Flussgebiete von dieser sauren Deposition, trotz ansteigenden pH Werten im Niederschlag. Das geochemische Modell PHREEQC wurde im Biscuit Brook Einzugsgebiet in den Catskill Mountains in New York angewandt, um die Veränderungen des Wassers vom Regenwasser, über Boden- und Grundwasser zu Flusswasser zu simulieren. Das Biscuit Brook EZG wurde als sehr geeignet für eine Studie über Versauerung von Flussgebieten angesehen, da mindestens zwei der drei Quelleinzugsgebiete deutlich verschiedene chemische Eigenschaften besitzen: zwei Zuflüsse sind im alkalischen Bereich und ein Zufluss ist im sauren Bereich zu finden.

Das Konzeptmodel auf dem die verschiedenen PHREEQC Modelle aufbauen, wurde mittels geochemischer, hydrologischer und Bodenphysikalischer Daten, sowie Isotopendaten erstellt, die in einer Messkampagne im Juni 2008 in den Quelleinzugsgebieten von Biscuit Brook gewonnen wurden.

Modellierungsergenisse weisen daraufhin, dass die beschriebenen unterschiedlichen Versauerungsgrade in den Zuflüssen durch die Anwesenheit oder Abwesenheit von Calcit erklärt werden können. Dieser stammt von eiszeitlichen Ablagerungen, und bestimmt den pH Wert im Abfluss. Daher sollten Flüsse mit Quelleinzugsgebieten in Gebieten mit Geschiebelehmschichten besser gepuffert sein, als Flüsse, deren Quelleinzusgebiete keine eiszeitlichen Lehmschichten aufweisen. Unterschiede in der Chemie von Fluss- und Quellwasserproben konnten mit der räumlichen Variation der Lehmablagerungen, sowie mit unterschiedlichen Schichtmächtigkeiten in Verbindung gebracht werden.

Signifikante Reaktionen konnten mittels eines schrittweisen Modellierungsansatzes aufgezeigt werden, wobei die Komplexität des Modells graduell erhöht wurde. Verwitterungsreaktionen erwiesen sich als wichtigste Prozesse in Biscuit Brook, mit Calcit und Silikat Lösung, sowie Bildung von Tonmineralien. Überraschenderweise, waren Kationen Austauschreaktionen nicht sonderlich relevant für die Wasserchemie in

Biscuit Brook, was durch eine Sensitivitätsanalyse nachgewiesen werden konnte. Doch das Modell erwies sich als sensitiv für Veränderungen des $pCO_{2,}$ der natürlich eng mit Calcit Lösung und pH zusammenhängt.

Schlagwörter: *Versauerung*, *PHREEQC*, *geochemisches Modellieren*, *Multi-Komponenten Transport Modellierung*

1 Introduction and Objective of this Study

1.1 Acidification of Watersheds

Parts of Eastern North America, Europe and Asia have been affected by atmospheric acid deposition, commonly referred to as "acid rain", for at least 40 years (JENKINS et al., 1999). The strong acidity in precipitations in these areas derives mainly from sulphuric and nitric acids, which are largely produced by burning fossil fuels, primarily coal and oil (BURNS et al., 2008).

The effects on the concerned watersheds can be severe depending on pedology, geology and climate of a given area. Acid deposition is, to a large extent, responsible for increased Aluminum (Al) mobilization and transport in the northeastern United States and Europe ((MCHALE et al., 2007); DISE et al., 2001; REUSS et al., 1985). Al mobilization is of some concern because it is toxic to aquatic biota e.g. trout species (BALDIGO et al., 2005; KAESER et al., 2001). Inorganic monomeric Al can also inhibit Calcium uptake by tree roots and therefore lower stress tolerance of trees (CRONAN, 1995). Another effect of acidification of soils is the depletion of base cations, Ca^{2+}, Mg^{2+}, K^{+}, Na^{+}, through ion exchange with Aluminum species and Hydrogen ions (REUSS et al., 1986).

In the United States the Clean Air Act of 1970, and its amendments of 1990, marked a reversal of environmental impact due to air pollution (MURDOCH et al., 2006). These enactments led to less acidic precipitation in the northeastern US since minimum pH values were reached in the 1970s (LYNCH et al., 2000).

1.1.1 Incorporation of Study Site

The Catskill Mountains are an upland region of the eastern US. This area receives among the highest acid deposition loads in North America (BURNS et al., 2008). The Catskill Mountains are characterized by steep slopes and thin soils with rapid subsurface drainage. The underlying bedrock weathers very slowly. All these factors lead, obviously, to acid-sensitive surface waters and enhancement of the anthropogenic acidification (STODDARD, 1991). Within this region the acidity in

precipitation has decreased since at least 1983 when data collection began (BURNS et al., 2008). Precipitation pH increased significantly by 0.01 units/year during the period of 1987 to 2003 (BURNS et al., 2008). Recent studies showed also that streamwater sulphate concentrations have declined sharply, nitrate decrease was only limited and pH increase significant at many sites (BURNS et al., 2008; MURDOCH et al., 2006).

Within the Catskill Mountains the Neversink River watershed was affected most severely by acid deposition (STODDARD, 1991). Since this river is part of the water supply of New York City, it is imperative to monitor and maintain its water quality. Several trend analyses on precipitation and steam water chemistry in the Neversink River watershed were conducted in recent years (BURNS et al., 2008; MURDOCH et al., 2006; WINNER, 2006 (not published); BURNS et al., 2004). These studies produced similar results but the outcome also depended strongly on the chosen time span. Despite the decrease in atmospheric acid deposition in the last two to three decades the recovery of streamwater chemistry has been only minimal (BURNS et al., 2008; MURDOCH et al., 2006; LAWRENCE et al., 1999).

Therefore the objective of this study was to shed light on this discrepancy between precipitation and streamwater chemistry, to detect significant chemical reactions, and to help better understand the process of recovery from acidification in hydrological systems.

Our approach was to combine chemical, hydrological and isotope data to establish a comprehensive hydrological and geochemical concept model of the study site. Hence, a threepart measurement campaign was carried out in June 2008: Samples were taken along all Biscuit Brook tributaries from headwaters to outlet and soil profiles were dug to obtain information about the exchanger composition in the watershed. Because the data was used to establish the conceptual model, the results of the longitudinal profiles are shown in chapter 6 before the presentation of the PHREEQC model in chapter 7.

The obtained conceptual model was then used to create a hydro-geochemical model with PHREEQC that includes the relevant hydrological processes of the study area, but also the most important chemical reactions related to acidification.

2 Study Site Descriptions

2.1 Physical Setting

The Neversink River watershed lies in the Catskill Mountains of southeastern New York State and has a drainage area of 172.5 km² (BURNS et al., 2008). Figure 2.1 shows a general map of New York State with Biscuit Brook. The mean elevation is 634 m. The catchment has its source at the summit of Slide Mountain, the highest point in the Catskills, with an elevation of 1274 m. The river flows along two principal branches: the West and East Branches of the Neversink River. They join upstream of the man-made Neversink Reservoir, which is part of the New York City water supply, at an elevation of 450 m (BURNS et al., 2008).

Figure 2.1: General Map of New York State, showing the study site in the Catskill Mt. (Big Indian is the highest point in Biscuit Brook) and the Neversink Reservoir (after Google Earth, modified)

The data for this present study were collected in Biscuit Brook, a headwater basin with a drainage area of ~ 10 km² that drains into the Neversink River and ultimately into the Delaware River (MURDOCH et al., 2006).

Biscuit Brook is divided in three headwater tributaries: Basic Biscuit, the main branch, West Biscuit and Acid Biscuit. As the names already indicate, Basic and West Biscuit have basic pH values above 6.5, whereas pH in Acid Biscuit is < 5 (COSTELLO-WALKER, 1995). Biscuit Brook has been monitored for discharge and water quality at the basin outlet near Frost Valley by the U.S. Geological Survey (USGS) since 1983 (MURDOCH et al., 2006). Several studies have also been conducted in the basin itself (e.g. BURNS et al., 2008; MURDOCH et al., 2006; LAWRENCE et al., 1999; BURNS et al., 1998; MURDOCH et al., 1993) so that a preliminary conceptual hydrological model could be established as shown in figure 2.2 which will be discussed in more detail in the next section below.

2.2 Geology, Hydrogeology and Pedology

2.2.1 Geology and Hydrogeology

The Catskill Mountains are an erosionally dissected plateau rather than a mountain range and approximately 1000 m higher than the surrounding terrain (SHAMAN et al., 2004). All streams in the region are underlain by flat-lying Devonian age sedimentary bedrock, which was deposited as a massive westwards flowing delta (MURDOCH et al., 1991). Bedrock consists primarily of sandstone with a few conglomerates, which makes up to 60 %, and the remaining 40 % consists of shale and siltstone (ETHRIDGE, 1977). Bedrock is overlain by glacial till deposits and alluvium, which is generally only a few meters wide in the headwater streams like Biscuit Brook but widens to several hundred meters downstream (SHAMAN et al., 2004; BURNS et al., 1998). These till deposits vary spatially according to the flow path of former glaciers, and are generally thicker in the valley bottoms than on slopes. Stream-channel material consists mainly of sand, gravel and boulders that have been altered by alluvial processes (BURNS et al., 1998). The stream flows directly on exposed or submerged bedrock in most parts of Biscuit Brook (BURNS et al., 1998). Figure 2.3 and Figure 2.4 show a map of bedrock geology and surficial geology of Biscuit Brook respectively.

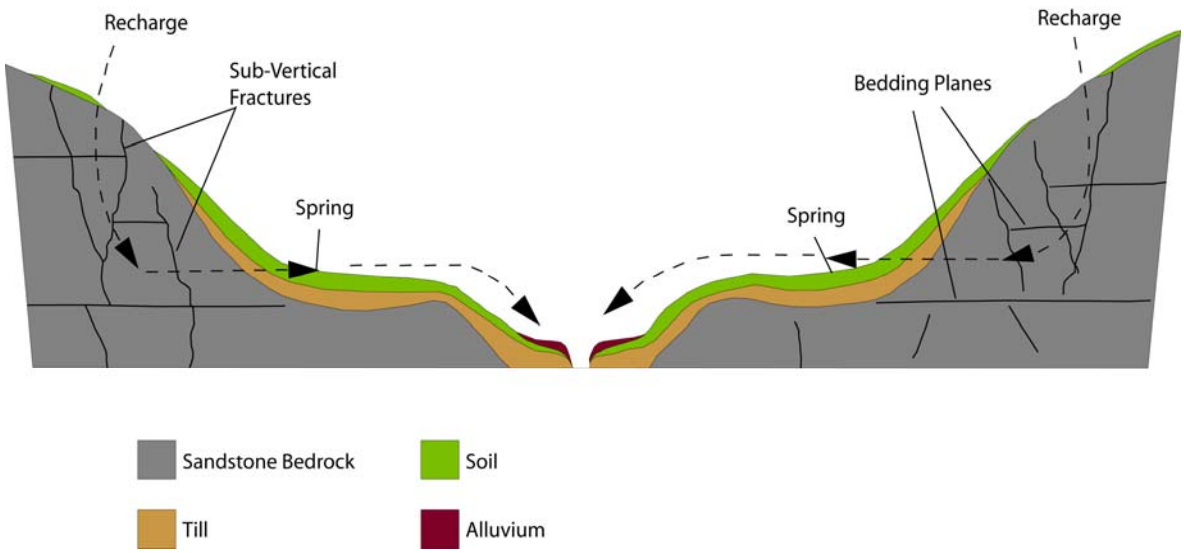

Figure 2.2: Conceptual hydrological model of study site (after SHAMAN et al., 2004)

Figure 2.2 shows the conceptual groundwater flow system for Biscuit Brook. The bedding plane of the sandstone bedrock lays almost horizontal and most of the beds are cut by three nearly perpendicular sets of fissures, one of which is nearly parallel to the bedding plane (PARKER, 1964). These patterns of fractures lead to groundwater springs at the base of steep slopes in the Catskills and throughout the Appalachian Plateau (SHAMAN et al., 2004). So typically spring water passes through till and soil layers during recharge and discharge. The till mainly originates from the local bedrock and was deposited during the last glaciation around 14 000 years ago (SHAMAN et al., 2004). This glacial till layer varies in thickness between 0.25 to 1.5 m, and can range from clay-size particles to boulders (BROWN et al., 1999). Some of the till has been redeposited as alluvium near stream channels in lowland areas (SHAMAN et al., 2004). The sandstones show only little variation when taken as a whole. Two main groups could be detected (WAY, 1972): the gray to green colored and the red to brown colored sandstones. The first group of sandstones is influenced by the metamorphic source terrain, which contributed low rank metamorphic minerals, especially chlorite. The latter group is influenced by iron oxide minerals. The dominant minerals are quartz, chlorite and iron oxides (WAY, 1972). K-feldspar, mica and plagioclase feldspar vary as secondary components present (ETHRIDGE, 1977). Since the cement of the sandstones does not feature Calcite as a binding agent, the glacial till

layers can be seen as the only Calcite source in the Catskill Mountains (COSTELLO-WALKER, 1995).

Thus, the bedrock states a moderate to poor aquifer and is chemically unreactive (MURDOCH et al. (1991)).

2.2.2 Pedology

Soils in this region have been classified as Inceptisols of the Arnot-Oquaga-Lackawanna series and range from 0.1 to 1.5 m in depth, with a mean soil depth of 1 m (SHAMAN et al., 2004; BURNS et al., 2008). Inceptisols have a low SO_4^{2-} adsorption capacity and a moderate to high acidity, with an averaged pH of 4.4 and a low mean CEC of 6 meq/100 g soil (MURDOCH et al., 1993). They are excessively to moderately well drained, very steep, and medium textured on uplands (BURNS et al., 2008).

Inceptisols are soils of humid and subhumid regions with altered horizons. They are characterized by a loss of bases, iron and aluminium, but retain still some weatherable minerals. Typically Inceptisols do not have an illuvial horizon enriched with silicate, clay or with amorphous mixture of aluminum and organic carbon but some profiles in Biscuit Brook show redoximorphic features.

Figure 2.5 shows a pedological map of the study site Biscuit Brook.

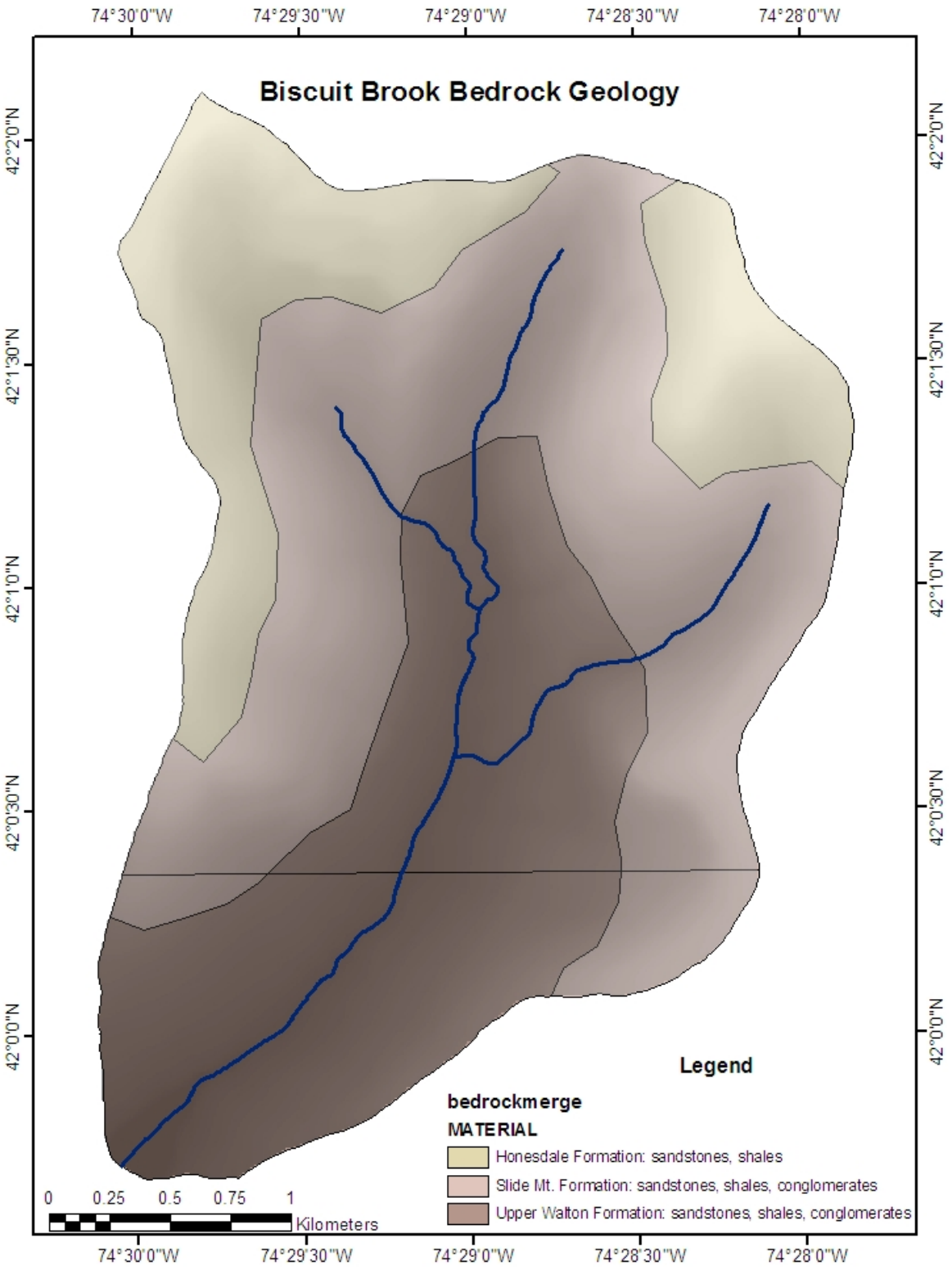

Figure 2.3: Bedrock geology map of Biscuit Brook

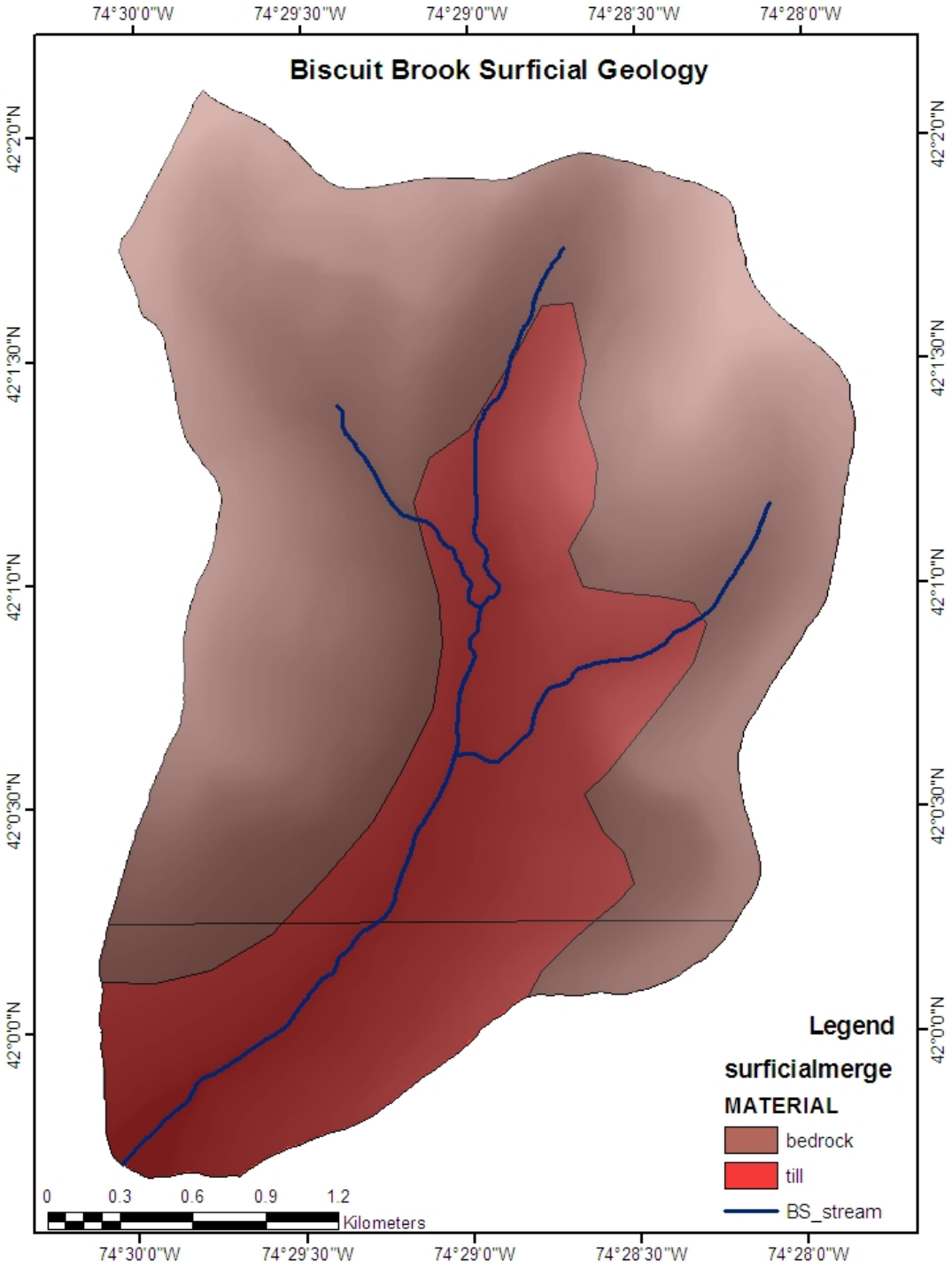

Figure 2.4: Surficial geology of Biscuit Brook

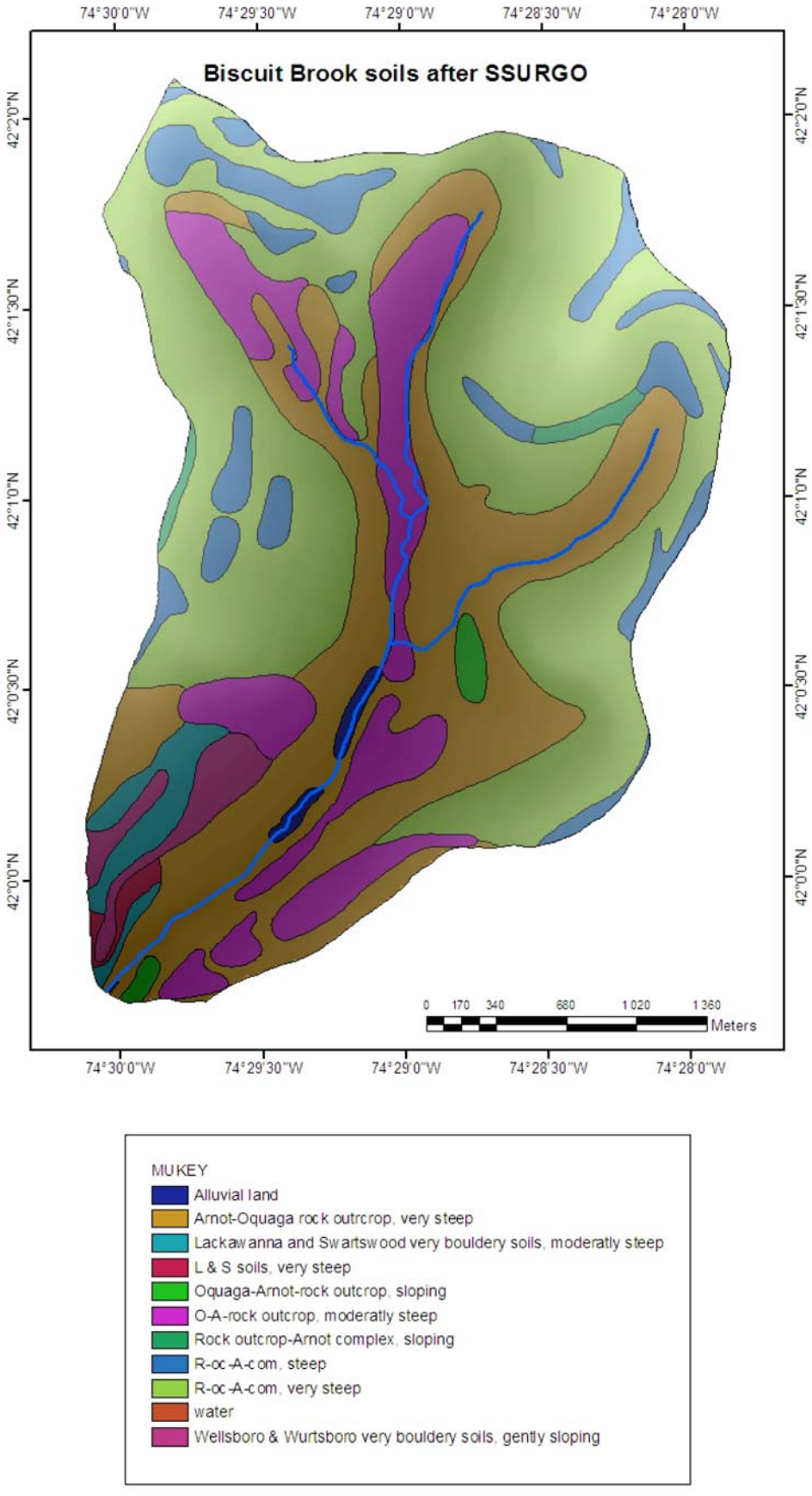

Figure 2.5: Soil map for Biscuit Brook after US SSURGO

2.3 Meteorology and Hydrology

2.3.1 Meteorology

The climate in the Catskill region is categorized as humid continental with cold winters and moderately warm summers (BURNS et al., 1998). Mean annual air temperatures range from 5.2 °C at the Slide Mountain weather station at an elevation of 807 m, which lays about 2 km downstream of the headwaters of the West Branch of the Neversink River, to 7.2 °C at Liberty (elevation 472 m), which is 30 km southwest of the basin (1971-2000 means) (BURNS et al., 2008). Figure 2.6 shows the 1991 to 2007 temperature timeline at Slide Mt. Mean annual precipitation varies between 1611 mm at Slide Mountain weather station and 1268 mm at Liberty (BURNS et al., 2008). Figure 2.7 presents the 1991 to 2007 precipitation timeline as well as the daily hydrograph for that period. Snowfall at the Slide Mountain weather station averages 18 % of total precipitation (1974-1985 means), 173 mm/yr fall as snow, and snow cover typically lasts from mid-December to mid-March (MURDOCH et al., 1992; MURDOCH et al., 2006). Precipitation in the region derives from coastal storms, frontal systems from the west, and local thunderstorms (MURDOCH et al., 1992).

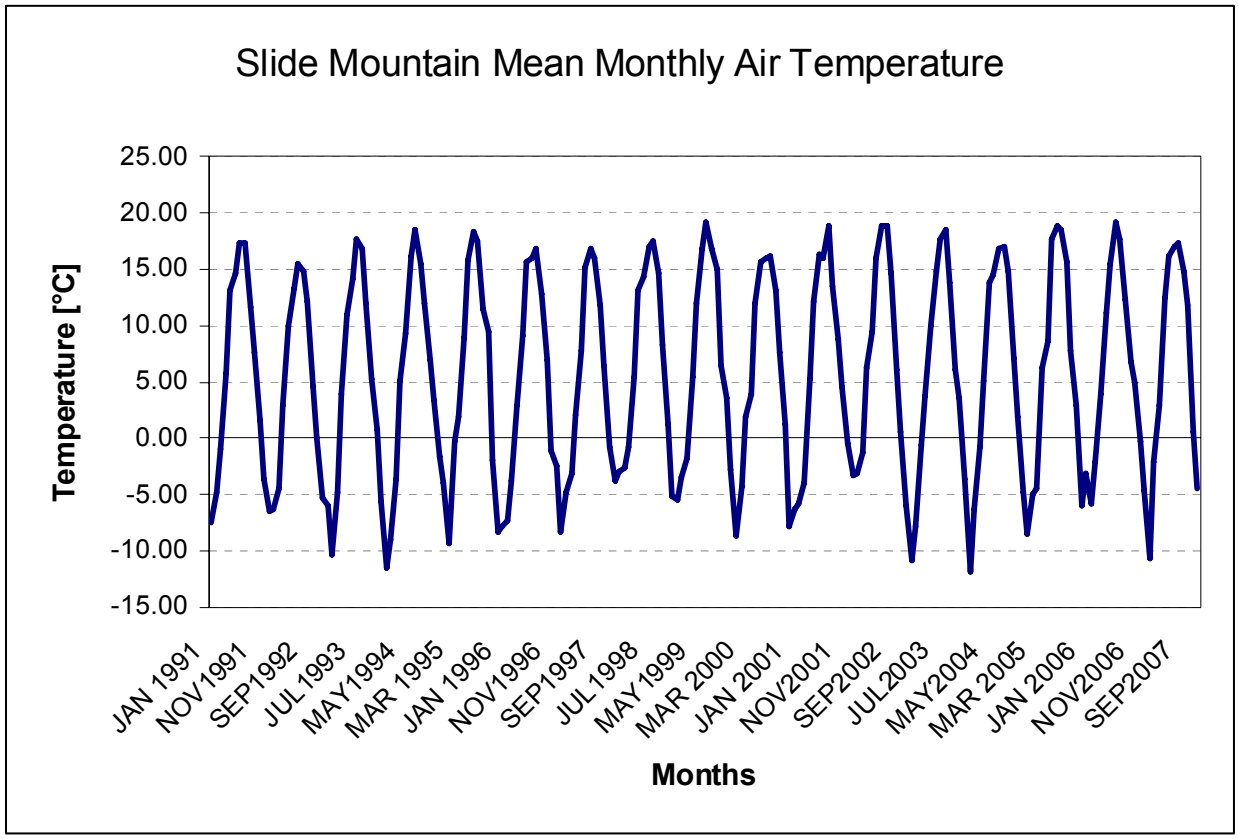

Figure 2.6: Mean monthly air temperature measured at Slide Mt. weather station for water years 1991 to 2007; data collected by National Climatic Data Center

2.3.2 Hydrology

Annual discharge regime in the Biscuit Brook basin is influenced by two main peaks as shown in figure 2.8, which presents the Pardé coefficient calculated over the period 1991 to 2007. The Pardé coefficient is obtained by dividing the mean monthly discharge through the mean annual discharge. Biscuit Brook Discharge behavior is controlled by two factors: The first factor is snowmelt leading to the main peak between March and May (MURDOCH et al., 2006). Rainstorms lead to the secondary peak in fall- winter (November to January), but rain is involved in both maxima. The discharge regime can be called "nival-pluvial".

Mean annual discharge for the water years 1992 to 2007 was 0.9 m^3/s or 300 mm respectively, measured at the gaging site above Frost Valley just above the outlet of the basin. As already mentioned, figure 2.7 shows the Biscuit Brook hydrograph for water years 1992 to 2007, as well as the daily precipitation at Slide Mt. weather station.

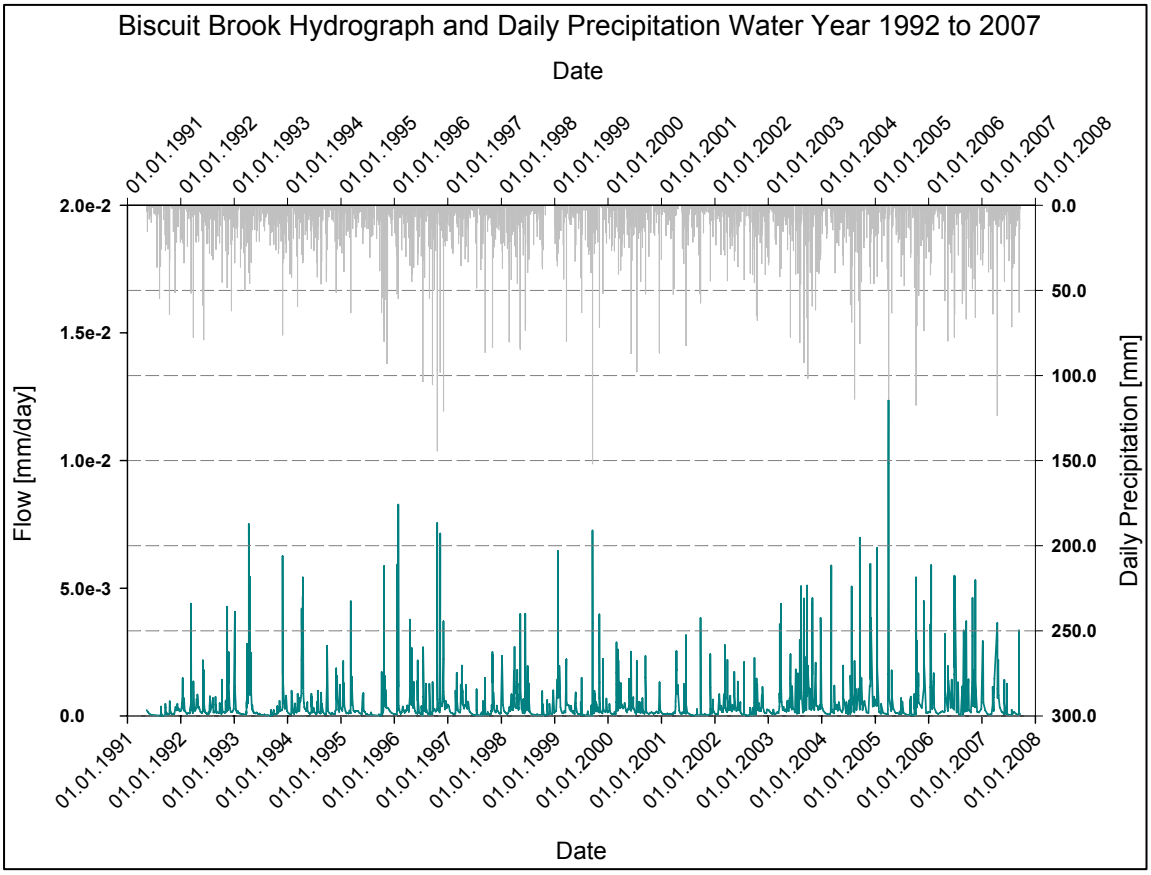

Figure 2.7: Daily hydrograph and precipitation for water years 1992 to 2007, measured at Frost Valley, just above the outlet of Biscuit Brook; units are [mm/d]; data collected by National Climatic Data Center

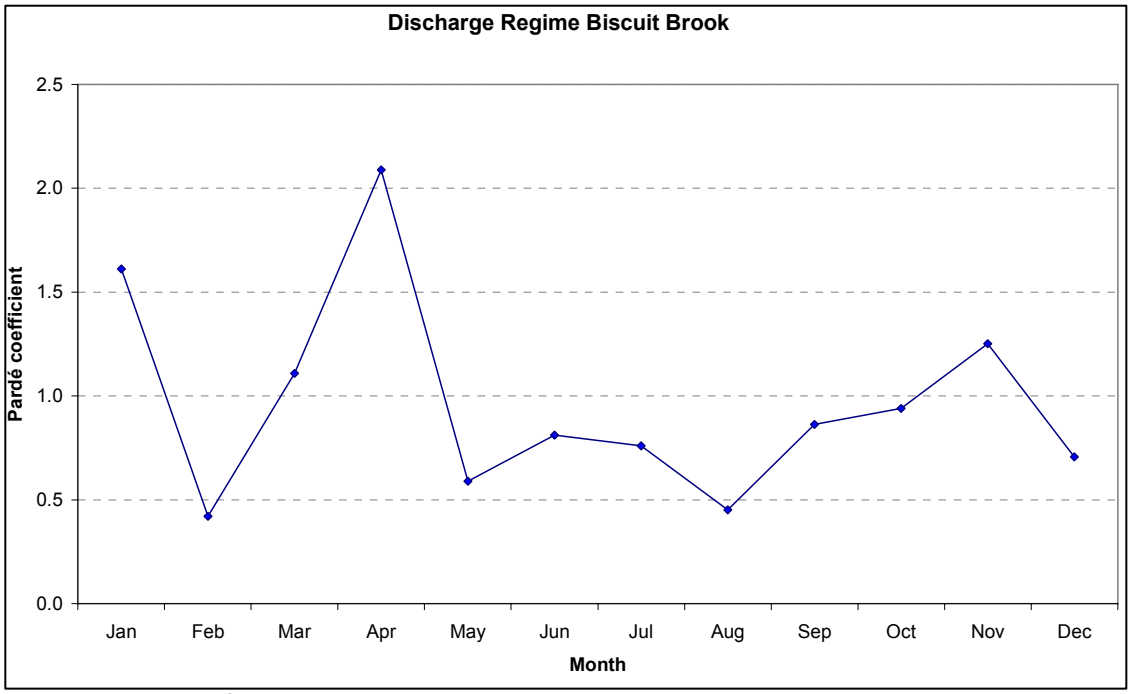

Figure 2.8: Pardé coefficient calculated over period 1991 to 2007 to establish a flow regime

The greatest amount of runoff usually occurs in spring (March-April), when snowmelt and spring storms produce 32 % of total annual runoff, whereas runoff during growing season (May-September) only accounts for 28 % of the annual total (FIRDA et al., 1996).

March and late fall are principal groundwater recharge periods, and residence time of groundwater, based on ^{18}O and ^{35}S analyses, is 6 to 22 months (BURNS et al., 1998). Mean annual recharge is maximally 170 mm, 1984 to 1994 means (BURNS et al., 1998).

2.4 Vegetation and Landuse

Biscuit Brook is 100 % forested and has not been logged for at least 60 years (MURDOCH et al., 2006). Vegetation is mainly northern hardwood forest; the most dominant tree species are American beech, sugar maple, red maple and yellow birch (BURNS et al., 2008). Above higher elevation (> 1100 m), red spruce and balsam fir dominate (BURNS et al., 2008).

In the 19th century, the forest below an elevation of 850 m was harvested extensively, but above an elevation of 850 m logging was minimal (BURNS et al., 2008). Biscuit Brook has been state owned since the beginning of the 20th century, so the forest remained relatively undisturbed.

Currently, less than 1000 people, with scattered homes and little agriculture, live in the whole upper Neversink River watershed (BURNS et al., 2008).

3 State of the Art

3.1 Hydrological Outlook

For the purpose of this study it is of great need to identify and understand major hydrological processes, as well as significant chemical reactions in the hydrological system, the Biscuit Brook watershed. Therefore, the following chapter gives an overview of past studies already conducted in the study area in respect to dominant hydrological and chemical processes.

3.1.1 Flow Paths and Residence Times in Biscuit Brook

Several studies explored flow paths and residence times in Biscuit Brook. BURNS et al. (1998) examined the effect of groundwater springs on NO_3^- concentrations during summer in the upper Neversink River watershed. The fact that data were collected in summer is especially of interest because flow conditions were comparable to those in the present study. The objective of the study of Burns et al. was to explore the effects of groundwater recharge, storage and discharge on the seasonal dynamics of stream nitrate concentrations. They could detect evidence for two different groundwater flow systems by collected groundwater and streamwater data (1991-1996): a shallow flow system within the soil and till and a deep flow system within bedrock fractures and bedding planes. This deep groundwater discharges as perennial springs. In a comparable watershed nearby (Shelter Creek), it could be proofed by data from eight wells, finished close to the till/bedrock interface, that saturated conditions are not maintained in the shallow flow system during most summers.

In Biscuit Brook the different tributaries react differently during low flow conditions. In Acid Biscuit the contribution of deep groundwater seems to be much smaller than in West and Basic Biscuit respectively. This could be shown by two sets of flow measurements made in each stream. Discharge in Acid Biscuit was approximately half the runoff in West and Basic Biscuit on two days in September 1992 and June 1994 respectively. The 11 year (1984-1994) hydrologic budget for the Biscuit Brook watershed showed

that March and late autumn are principal groundwater recharge periods. Mean net recharge for the period 1984 to 1994 was almost 170 mm.

For the Shelter Creek watershed estimates of residence time of base flow were obtained from $\delta^{18}O$ and ^{35}S data. Shelter Creek is an adjacent watershed with comparable geology and pedology. Residence times generally ranged from six months to almost two years.

3.1.2 Flow Generation and Streamflow Components

Evans et al. (1999) related stream hydrochemical variations to processes of flow generation and episodic acidification through plots of solute concentrations against discharge using data from 1989 to 1990 of four streams in the Catskill Mountains, Biscuit Brook and three adjacent watersheds. Results indicate a two component-system of shallow and deep saturated subsurface flow, in which the two components respond simultaneously during hydrologic events. This seems to support the results of BURNS et al. (1998) for high flow conditions. Additional qualitative information could be obtained by a "sea-salt" event that occurred during the study period and where high Na^+ inputs served as a natural tracer for event water. Pre-event water is thought to be displaced by infiltrating event water, which becomes dominant in the falling limb. NO_3^- for example shows a clear and consistent compositional difference between water from the two sources, evident as hysteresis loop in concentration-discharge plots. Nitrate concentrations appear to be elevated in event water after percolation through organic horizon. Therefore, the most acidic, high nitrate conditions during an episode generally occur after peak discharge.

Brown et al. (1999) explored summer storm runoff components and the effect of catchment size on water sources by monitoring seven nested headwater watersheds (Shelter Creek and six nested subcatchments) in the Catskill Mountains during five summer rain events. Event-water contribution, obtained by two-component isotopic hydrograph separation, near the time of peak flow ranged from 49% in Shelter Creek to 62% in the smallest subcatchments during the highest intensity event. The proportion of event water was greater than justified by direct precipitation on saturated areas alone. Also, DOC concentrations in stormflow were strongly correlated with stream ^{18}O composition. Therefore, bivariate mixing plots showed that the large event water contributions were likely

derived from O-horizon soil flow and three end-members could be detected: throughfall, O-horizon soil flow and groundwater. This indication could be reinforced by two-tracer, three-component hydrograph separations which revealed that throughfall and O-horizon soilwater components together could account for the estimated contribution of event water to stormflow. The groundwater component generally dominated the hydrograph in each of the subcatchments, but throughfall and O-horizon soil flow were also significant contributors to stormflow. Maximum throughfall and groundwater contribution occurred at peak runoff and dominated the rising limb of the hydrograph. Maximum O-horizon soil flow contribution on the other hand was detected after peak flow and played a more important part in the falling limb of the hydrograph with declining groundwater and throughfall contributions. These results suggest that perched, shallow subsurface flow provides a significant contribution to summer stormflow in the study catchments.

In those relatively small watersheds, the hydrographs of the monitored summer events showed a rapid response to rainfall and a steep recession. Steep recessions usually indicate rapid drainage either as overland flow or flow through macropores, but overland flow was observed to be minimal during the monitored events, and is generally negligible in the headwaters of the Neversink River watershed due to its dense plant cover. Runoff coefficient, the percentage of quickflow relative to net throughfall (Q_F /P_{Thfall}) represents the fraction of the watershed contributing to stormflow. Runoff coefficients ranged from 0.1% to 5.9%, which is low in comparison to other values reported by DUNNE et al. (1978) for the northeastern US. A quick development of a groundwater table above the soil-bedrock interface could be observed on the hillslopes in response to precipitation, which declined slowly over the next few days. Steeper slopes of the water content recession curves for the shallower soils (10 to 30 cm) indicated a more rapid drainage from shallower soils than from deeper soils (30 to 70 cm). In the deeper soils, water tended to remain in storage because of the low gradient of the underlying bedrock surface.

With regard of catchment size some information could be obtained through the collected hydrometric data and the two-component isotopic separation. The hydrometric evidence showed that catchment size affected the runoff response. Peak runoff and runoff coefficients increased significantly with increasing catchment size. The maximum event water

contribution decreased with increasing catchment size after the results from the isotopic hydrograph separation.

3.2 Geochemical Outlook

3.2.1 Characterization of Streamwater Chemistry in Biscuit Brook

Headwaters of the Neversink River are dilute waters with low ionic strength; most of them are chronically acidified. Mean streamwater pH of the Neversink River for water years 1991 to 2006 ranged from 6.25 at the basin outlet to 4.5 at the headwater (WINNER, 2006, unpublished). Even though Biscuit Brook is one of the headwaters, mean streamwater pH was close to neutral (6.0) for water years 1991 to 2007 for mean flow conditions, but it acidifies episodically during high flow conditions. Table 3.1 shows mean temperature, conductance, pH and streamwater concentrations [mg/L] for Biscuit Brook for water year 1991 to 2007 and figure 3.1 shows the chemical composition averaged over the period of study in Biscuit Brook. The dominant cation is clearly Calcium, followed by Magnesia, Sodium, Ammonia, and Aluminum. Sulphate is the dominant anion, which is succeeded by Nitrate, Chloride, and Hydrogen-Carbonate, as well as Nitrite.

Table 3.1: Mean temperature, conductance, pH and streamwater concentrations [mg/L] for Biscuit Brook for water year 1991 to 2007

Parameter	Units	Value
Temp	°C	7.7
Cond	µS/cm²	20.6
pH	pH units	6.0
ANC	µeq/L	23.6
DOC	µeq/L	184.1
Ca	mg/L	2.2
Mg	mg/L	0.5
NH_4	mg/L	2.7E-02
Na	mg/L	0.3
K	mg/L	0.2
Al_{im}	mg/L	1.7E-02
SiO_2	mg/L	1.0
SO_4	mg/L	4.8
NO_3	mg/L	1.3
Cl	mg/L	0.5
HCO_3	mg/L	0.5
NO_2	mg/L	1.3E-02

It is well worth mentioning that the calculated charge balance for Biscuit Brook streamwater was unequal zero, but a positive "excess" charge could be detected.

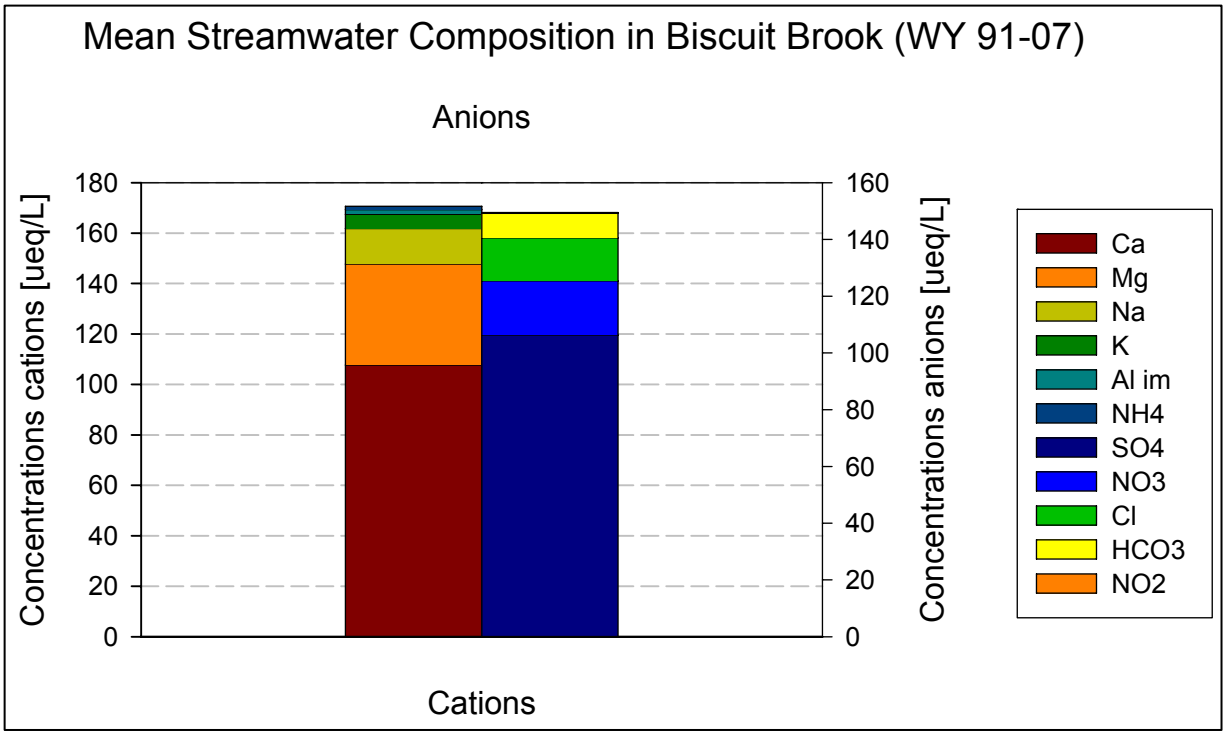

Figure 3.1: Mean streamwater composition in Biscuit in µeq/L; shown as stocked vertical bars for cations and anions for water years 1991 to 2007

In past studies DOC was called to account for this imbalance (Burns & Lawrence, 2008, personal communication). But typically CO_2 species were not taken into consideration at all. The most significant difference among the data sets of streamwater from the different tributaries of the Neversink River basin is Ca^{2+} and, to a lesser extend, Mg^{2+}, concentration; ANC and pH generally follow this pattern (MURDOCH et al., 1993). Concentrations of all other constituents are relatively uniform among streams. Differences in stream acidity in the Neversink River basin are correlated with the differences in concentration of base cations and not with the differences in mineral acid concentrations, which could be proofed by applying an analysis of variance of mean Sulphate and Nitrate concentrations, as well as Calcium, Magnesia and ANC concentrations (MURDOCH et al., 1993). Results of monitoring stream chemistry in the

streams of the Neversink basin indicate that H_2SO_4, HNO_3, and organic acids all contribute to stream acidity (MURDOCH et al., 1993).

3.2.2 Alkalinity in Biscuit Brook Stream Water

A Master Thesis by COSTELLO-WALKER (1995), who explored surface water alkalinity in two tributaries of Biscuit Brook, was an important basis for this present study. Alkalinity is a measure of the acid neutralizing capacity of natural waters. Results of field measurements indicated that these two tributaries, Acid Biscuit and Basic Biscuit, have distinctly different chemical characteristics, which are already described by the name of the respective tributary. Figure 3.2 shows a map, taken from Costello Walkers work, showing all three headwater tributaries in Biscuit Brook. Results also showed that alkalinity measurements and ultimately also pH values are generally underestimated with standard analysis methods, because of degasing of CO_2. Costello-Walker also simulated alkalinity in Biscuit Brook with the geochemical model PHREEQE. Modeling Results indicated that alkalinity in Biscuit Brook is predominantly Carbonate alkalinity, with a small but consistent addition of organic alkalinity. Calcite dissolution could be identified as the source of Carbonate alkalinity in Basic Biscuit, whereas alkalinity in Acid Biscuit was seen as a reflection of precipitation inputs.

Costello-Walker also detected flowpath as the most influential factor controlling surface water alkalinity because of its affect on subsurface residence time and exposure to varying lithologies. Variations in flowpath could be connected to differences in till deposition and compaction. Streams with headwaters in areas of till deposition should have better buffered systems than streams whose headwaters are in areas of till scouring or lack of deposition.

3.2.3 Streamwater and Precipitation Chemistry Trends

A multitude of past studies detected temporal trends in precipitation and stream chemistry in the Catskill region, but results varied depending on chosen time spans. All studies used the Seasonal Kendall trend analysis to account for changes in precipitation and stream chemistry. This statistic test detects trends independently from stream flow correlated or seasonal variations in concentrations. MURDOCH et al. (1993) could not detect any significant trends for precipitation chemistry at the Biscuit Brook

catchment for the period 1983-1989. But they observed decreasing trends for SO_4^{2-} streamwater concentrations, whereas NO_3^- concentrations generally increased in the period of study. In a later study by MURDOCH et al. (2006) decreasing Sulphate concentrations in Biscuit Brook streamwater could be affirmed for the time span 1983 to 2002. Ca^{2+} and Mg^{2+} concentrations decreased at a steady but slower rate than SO_4^{2-}; ANC showed no trends. No significant trends could be observed for Nitrate streamwater concentrations with the Seasonal Kendall trend test.

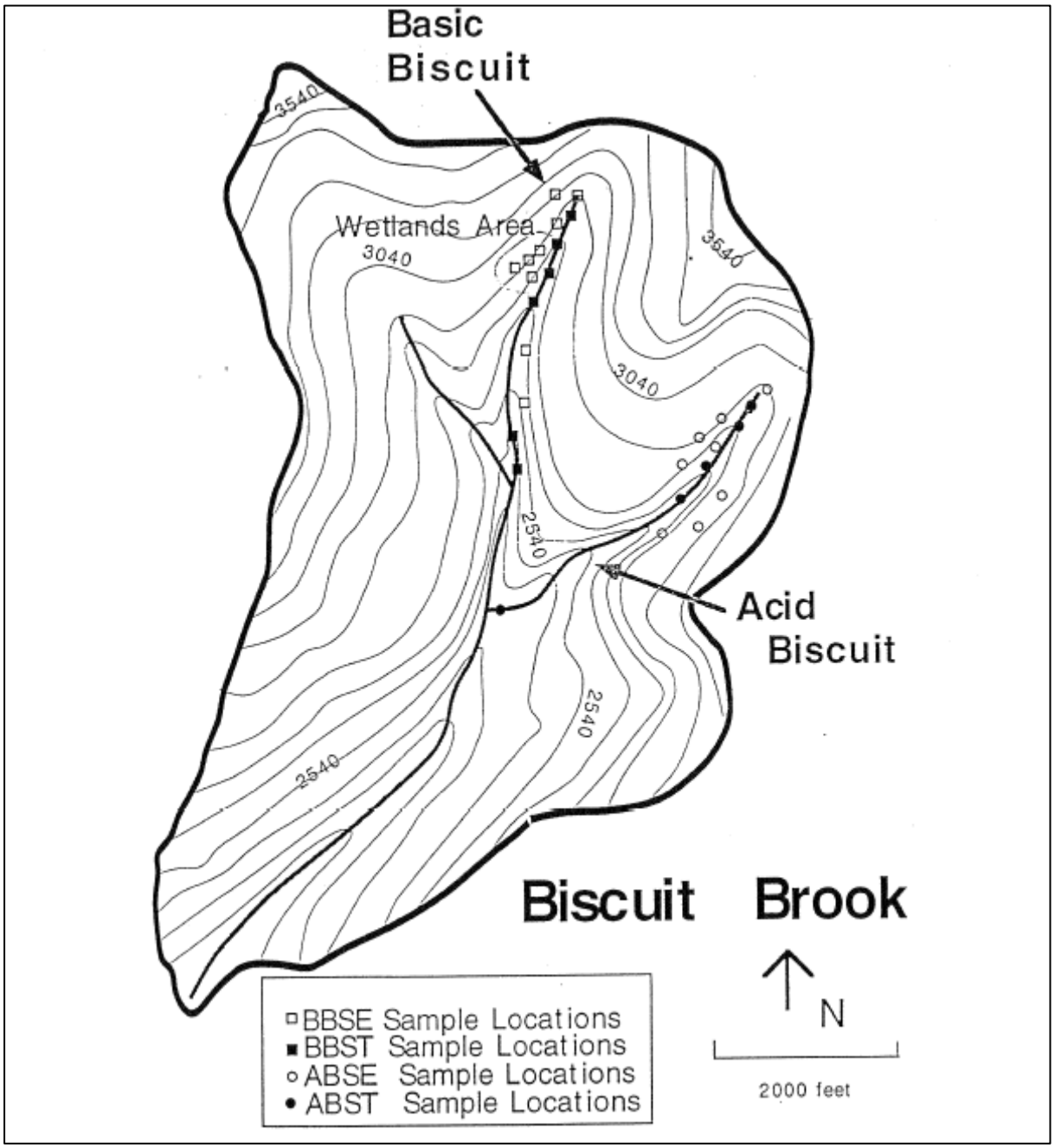

Figure 3.2 Conceptual map of Biscuit Brook, taken from COSTELLO-WALKER (1995)

A more recent study of BURNS et al. (2008), which included a trend analysis of stream and precipitation chemistry for water years 1987-2003, and an unpublished work by WINNER (2006), water years 1991 to 2006, covered the longest time span. Winner also conducted trend analysis for low, medium and high flow conditions to evaluate the influence of runoff generation and residence time on stream chemistry. For precipitation

trends both studies detected a recovery of pH of +0.01 pH units/year, as well as a decreasing trend for Sulphate. Burns et al. also found an increasing trend in Biscuit Brook streamwater pH, but a parallel significant increasing trend in acid neutralizing capacity (ANC) and a decreasing trend in Al^{3+} concentrations could not be detected. This increase in stream pH could not be affirmed by the trend analysis conducted by Winner, where pH trends for Biscuit Brook streamwater were not significant for all flow conditions. But Winner found also a significant decreasing trend for Sulphate and, in contrast to Burns' study, a decrease in Al^{3+}, SiO_2, and an increase in dissolved organic carbon (DOC) streamwater concentrations for all flow conditions.

There might possibly be several reasons for this wide range of results: First of all, a long period of record is generally required for a performance of a Seasonal Kendall Trend Test. Calculated trends, based on timelines shorter than 20 years, might be significant for the given period, but may not represent long-term trends in terms of centuries. Secondly, different acidification states of the catchment over time can lead to negation of trends, when long time periods are observed.

3.2.4 Bio-Geochemical Modeling in Biscuit Brook

Some geochemical and eco-hydrological modeling has been done in Biscuit Brook. COSTELLO-WALKER (1995) used PHREEQE for speciation and for alkalinity calculations. Her results indicated that Calcite is the main source of alkalinity in Biscuit Brook.

Chen et al. (2004) applied the integrated biogeochemical model PnET-BGC in Biscuit Brook and four watersheds in the Adirondack Mountains. PnET-BGC was formulated to simulate the response of soil and surface waters in northern forest ecosystems to changes in atmospheric deposition and land disturbance. Results indicated that model-simulated surface water chemistry generally agreed well with the measured data. Sulphur budgets showed little retention of inputs of Sulphur. Biscuit Brook also showed little retention of NO_3^-. It also exhibited the highest rates of base cation output. Atmospheric deposition was found to be the greatest source of acidity; cation exchange and mineral weathering served as most important sources for ANC.

4 Geochemical Modeling

4.1 Geochemical Models

The first generation of geochemical modeling programs was developed in the beginning of the 1970s and since the early 1980s it became possible to install these programs on personal computers (MERKEL & PLANER-FRIEDRICH, 2005).

The most frequently used models are MINTEQA2 (Allison et al. 1991), WATEQ4F (Ball & Nordstrom 1991), PHREEQC (PHREEQE) (Parkhurst & Appelo 1999, Parkhurst 1995 & Parkhurst et al. 1980) and EQ 3/6 (Wolery 1992a and 1992b) (in MERKEL & PLANER-FRIEDRICH, 2005).

In comparison with the other mentioned models, it seems that PHREEQC is the optimal program for the solution of simple and more complex problems and for one-dimensional transport modeling with regard to user-friendliness, numerical stability, compactness and clarity of the data format as well as flexibility (MERKEL & PLANER-FRIEDRICH, 2005).

This was also substantiated by several Diplom students of the Institute of Hydrology at the University of Freiburg, who worked with geochemical models, in particular PHREEQC. The work of CARSTENS (2007), who modeled adsorption and transport of heavy metals in the saturated zone using PHREEQC, was an important basis for the present study, since modifications of Carstens' PHREEQC-inputfiles were used in the geochemical model.

4.2 Introduction of PHREEQC

PHREEQC version 2 is a computer program that is designed to perform a wide variety of low-temperature aqueous geochemical calculations (PARKHURST et al., 1999). It uses the ion dissociation theory to describe the water-gas-rock-interaction in aquatic systems, and PHREEQC is capable of (1) speciation and saturation-index calculations; (2) batch-reaction and one-dimensional (1D) transport calculations involving (2a) reversible reactions, which include among other things aqueous, mineral, gas, solid-solution, and ion exchange-equilibria, and (2b) irreversible

reactions, which include inter alia kinetically controlled reactions, mixing of solutions, and temperature changes; and (3) inverse modeling with a variety of features (PARKHURST et al., 1999). The species distribution is calculated from thermodynamic data sets by solving the non-linear set of equations resulting from equilibrium constants and mass balance in the system, which, naturally, implies the establishment of chemical equilibrium and mass balance (MERKEL & PLANER-FRIEDRICH, 2005).

PHREEQC is based on the FORTRAN program PHREEQE (PARKHURST et al., 1980), which was capable of simulating a variety of geochemical reactions for a system. PHREEQC version 1 was a completely new program written in C programming language that included all of the capabilities of PHREEQE, and added many more that were not available previously (PARKHURST et al., 1999).

PHREEQC version 2, which was used in the present study, is a modification of PHREEQC version 1. Several new capabilities have been added, including among others: (1) kinetically controlled reactions; (2) diffusion or dispersion in 1D transport. An improvement of user-friendliness was achieved by adding several keywords, which allow writing user-defined quantities to the primary output file and/or to a file suitable for importation into a spreadsheet (PARKHURST et al., 1999).

Despite the general flexibility of PHREEQC, several limitations have to be considered (PARKHURST et al., 1999):

In the aqueous model PHREEQC uses ion-dissociation theory and DEBYE-HÜCKEL expressions to account for non-ideality of aqueous solutions. This model is adequate at low ionic strength, but may brake down at higher ranges, e.g. seawater. Since Biscuit Brook streams are dilute waters with low ionic strength, this limitation did not affect the present study.

The other limitation in the aqueous model is the lack of internal consistency in the data of the databases. PHREEQC offers three databases, *phreeqc.dat*, *wateq4f.dat* and *minteq.dat.* The log K-values and enthalpies of reactions have been taken from various literature sources, and no systematic attempt has been made to determine the aqueous model used to develop individual log K's. This requires careful selection of aqueous species and thermodynamic data by the users of the program.

In the following only processes that were relevant for the present study will be addressed more thoroughly.

4.2.1 Speciation and equilibrium calculations with PHREEQC

Chemical reactions determine occurrence, distribution, and behavior of aqueous species in water. The aqueous species is defined as organic or inorganic substances dissolved in water in contrast to colloids and particles (MERKEL & PLANER-FRIEDRICH, 2005). This definition includes free anions and cations as well as complexes.

Chemical reactions can be described by thermodynamics; these reactions are expressed by the mass-action law, thermodynamically reversible, and independent of time. In contrast, kinetic processes are time dependent reactions, e.g. decay processes. In this section, the equations used within PHREEQC to define thermodynamic activities of aqueous species are presented. The unknowns for each aqueous species i are the activity, a_i, activity coefficient, f_i, molality, m_i, and moles in solution, n_i (PARKHURST et al., 1999). The unit molality gives the number of moles per kg of H_2O; and in fresh water, molality equals molarity [mol/L] (APPELO & POSTMA, 2005).

Mass action law

In principle, any chemical equilibrium reaction can be described by the mass-action law.

$$aA + bB \leftrightarrow cC + dD \qquad \text{Eq.(4.1)}$$

$$K = \frac{\{C\}^c * \{D\}^d}{\{A\}^a * \{B\}^b} \qquad \text{Eq.(4.2)}$$

With a, b, c, d = number of moles of reactants A, B, and the end products C, D, respectively for the given reaction

K = thermodynamic equilibrium or dissociation constant

In particular, K is defined in relation to the following types of reaction using the mass-action law (MERKEL & PLANER-FRIEDRICH, 2005):

- Dissolution/ Precipitation (chapter 4.2.1): K_s = solubility product constant
- Sorption (chapter 4.2.2): K_d = distribution coefficient
  K_x = selectivity coefficient
- Complex formation// destruction of complexes: K = complexation constant, stability constant
- Redox Reactions: K = stability constant

It must be clearly mentioned, that given K-values are only valid for the given standard state, e.g. T = 25°C and ionic strength I = 0 (MERKEL & PLANER-FRIEDRICH, 2005).

Equations for aqueous, exchange, and surface species, used within PHREEQC, are derived from the mass-action expression for the moles of each species in the chemical system in terms of the master unknowns. These equations, after being differentiated with respect to the master unknowns, will be substituted into the constituent mole-balance, charge-balance, and phase-equilibria functions (PARKHURST et al., 1999).

The total numbers of moles, n_i, of an aqueous species i can be derived from the mass action expression (PARKHURST et al., 1999).

Activities and Ionic strength

For the mass-action law, quantities of substances are presented in activities, a_i, and not in concentrations, c_i, with respect to species i.

$$a_i = f_i * c_i \qquad \text{Eq.(4.3)}$$

In Eq. 3, the activity coefficient f_i is an ion-specific correction factor describing how interactions among charged ions influence each other (MERKEL & PLANER-FRIEDRICH, 2005). Therefore, activity is always lower than concentration, for the reason that oppositely charged ions interact with each other to reduce the available charge. In the ideal case of an infinitely dilute solution, f_i is 1, interactions among ions are zero, and activity equals concentration.

Ionic strength

Ionic strength I describes the summation of the ionic forces in a given solution.

$$I = 0.5 * \sum m_i * z_i^2 \qquad \text{Eq.(4.4)}$$

With m_i = moles of the species involved

z_i = charge numbers of species involved

Theory of ion dissociation

The activity coefficient can be calculated using several approximation equations, if the ionic strength of the solution from the chemical analysis is given. All of these equations are derived from the DEBYE-HÜCKEL equation and differ in the range of the ionic strength they can be applied for (MERKEL & PLANER-FRIEDRICH, 2005). Some are presented here.

DEBYE-HÜCKEL equation (Debye & Hückel, 1923)

$$\log(f_i) = -A * z_i^2 * \sqrt{I} \text{ , I < 0.005 mol/kg} \qquad \text{Eq.(4.5)}$$

DAVIES equation (Davies 1962, 1938)

$$\log(f_i) = -A * z_i^2 \left(\frac{\sqrt{I}}{1+\sqrt{I}} - 0.3 * I \right) \text{, I < 0.5 mol/kg} \qquad \text{Eq.(4.6)}$$

"*WATEQ" DEBYE-HÜCKEL* equation

$$\log(f_i) = \frac{-A * z_i^2 * \sqrt{I}}{1 + B * a_i * \sqrt{I}} + b_i * I \text{ , I < 1 mol/kg} \qquad \text{Eq.(4.7)}$$

With f = activity coefficient

z = valence

I = ionic strength

a_i, b_i = ion- specific parameters (depend on the ion radius)

A, B = temperature dependent parameters, calculated from empirical equations (for details see MERKEL & PLANER-FRIEDRICH (2005) page 10-11)

Per default, activity coefficients of aqueous species are defined with the DAVIES equation in PHREEQC (PARKHURST et al., 1999). But it is generally possible to use the extended DEBYE-HÜCKEL equation or the WATEQ-DEBYE-HÜCKEL equation.

Dissolution and Precipitation

Dissolution and precipitation can be described by the mass-action law as reversible and heterogeneous reactions. Generally, the solubility of a mineral is defined as the mass of a mineral, which can be dissolved within a standard volume of the solvent (MERKEL & PLANER-FRIEDRICH, 2005). In PHREEQC, one way of addressing dissolution and precipitation, is by equilibrium reactions between the aqueous phase and pure phases, including gases with fixed partial pressures (PARKHURST et al., 1999). Equilibrium equations are included in the model through heterogeneous mass-action equations and mole-balance equations. The additional master unknown for each pure phase is the moles of the pure phase present in the system, n_p, where p refers to the p^{th} phase.

Solubility product

According to the mass-action law the dissolution of a mineral AB into its components A and B occurs as follows:

$$AB \leftrightarrow A + B \qquad \text{Eq.(4.8)}$$

$$K_{sp} = \frac{\{A\} * \{B\}}{\{AB\}} \qquad \text{Eq.(4.9)}$$

Because for a solid phase AB the activity is assumed to be constant at 1, the equilibrium-constant of the mass-action law results in a solubility product constant K_{sp} or ion-activity-product IAP as below:

$$K_{sp} = IAP = \{A\} * \{B\} \qquad \text{Eq.(4.10)}$$

The solubility product depends on the mineral, the solvent, the pressure or partial pressure of certain gases, the temperature, pH, redox potential E_h, and on ions previously dissolved in the water (MERKEL & PLANER-FRIEDRICH, 2005).

Saturation Index

The saturation index SI indicates, if a solution is in equilibrium with a solid phase or under-saturated and super-saturated in relation to a solid-phase respectively.

$$SI = \log \frac{IAP}{K_{sp}} \qquad \text{Eq.(4.11)}$$

The IAP is calculated from activities that are derived from analytically determined concentrations by considering ionic strength, temperature, and complex formation. The solubility product K_{sp} is calculated in a similar manner, but using equilibrium solubility data corrected to the appropriate water temperature (MERKEL & PLANER-FRIEDRICH, 2005).

Positive SI values signify supersaturation, negative values undersaturation, and SI = 0 means equilibrium with the solid-phase. In practice, equilibrium can be assumed for a SI range of -0.2 to 0.2. A value of 1 signifies a ten-fold supersaturation, a value of -2 a hundred-fold undersaturation in relation to a certain mineral phase (MERKEL & PLANER-FRIEDRICH, 2005).

When equilibrium reactions are calculated with PHREEQC, the user has to specify the target saturation index for the given phase. It is possible to choose a positive, zero, or negative value, specifying supersaturation, equilibrium, or undersaturation for the mineral with respect to the solution (PARKHURST et al., 1999).

4.2.2 Modeling Ion Exchange with PHREEQC

Ion exchange describes the replacement of one adsorbed, readily exchangeable ion by another (STUMM & MORGAN, 1996). The ability of solid substances to exchange cations or anions with ions in aqueous solution is called ion-exchange capacity (MERKEL & PLANER-FRIEDRICH, 2005).

In natural systems cations are exchanged more readily than anions, and form a succession of decreasing exchange intensity: $Ba^{2+}>Sr^{2+}>Ca^{2+}>Mg^{2+}>Be^{2+}$ and $Cs^{+}>K^{+}>Na^{+}>Li^{+}$. Generally, multivalent ions, like Ca^{2+}, are more strongly bound than monovalent ions (Na^{+}), but selectivity decreases with increasing ionic strength (STUMM & MORGAN, 1996).

Ion exchange capacity is pH dependent, because cations are inter alia adsorbed electrostatically due to proton charge. Therefore ion exchange capacity increases with pH (MERKEL & PLANER-FRIEDRICH, 2005).

If one assumes a complete reversibility of sorption, the ion exchange can be described through the mass-action law.

$$A^+ + B^+R^- \leftrightarrow A^+R^- + B^+$$

$$K_B^A = \frac{\{A^+R^-\} * \{B^+\}}{\{A^+\} * \{B^+R^-\}} = \frac{\{A^+R^-\} / \{A^+\}}{\{B^+R^-\} / \{B^+\}} \qquad \text{Eq.(4.12)}$$

With A^+, B^+ = monovalent ions

R = exchanger

K_x = selectivity coefficient

The selectivity coefficient is considered here as an equilibrium constant, even though it depends not only on external conditions (temperature, pressure, pH), but on specific properties of the respective solid phase (MERKEL & PLANER-FRIEDRICH, 2005). Thus, the composition of an exchanger will be in equilibrium with the resident water under steady-state conditions. If the water composition changes as a result of e.g. acidification, the exchanger acts as a temporary buffer by adjusting its

composition to the new water concentrations (APPELO & POSTMA, 2005). This may completely alter the concentrations in water through a process known as ion chromatography.

Equation 12, after rewriting and inserting Ca^{2+} and Na^{+} for A and B respectively, becomes the GAINES-THOMAS convention (Gaines & Thomas, 1953):

$$Na^{+} + 0.5 * CaX_2 \leftrightarrow NaX * 0.5Ca^{2+}$$

$$K_{Ca}^{Na} = \frac{\{NaX\} * \{Ca^{2+}\}^{0.5}}{\{CaX_2\} * \{Na^{+}\}} \qquad \text{Eq.(4.13)}$$

With X= exchanger

K_x= selectivity coefficient

The most important cation exchangers of soils are clay minerals and organic matter, whereas metal oxides and hydroxides are only of minor importance (SCHEFFER & SCHACHTSCHABEL, 2002). MERKEL & PLANER-FRIEDRICH (2005) also mention aluminous silicates as important ion exchanger.

Mathematically, ion exchange can be described by a range of equations, extending from simple empirical equations (sorption-isotherm) to complicated mechanistic models, like e.g. diffuse-double layer and triple layer model which are based on surface complexation theory. For more detailed descriptions of determination of cation exchange with the models, mentioned above, please see STUMM & MORGAN (1996).

Ion-exchange equilibria are included in the model through heterogeneous mass-action and mole-balance equations for exchange sites. The approach is based on half-reactions between aqueous species and a fictive unoccupied exchange site for each exchanger (PARKHURST et al., 1999).

For using the ion-exchange model in PHREEQC appropriate, it is often necessary to base the application on field data of the given study area.

4.2.3 Modeling Transport with PHREEQC

In the previous part of this chapter chemical processes and models were described without consideration of transport in aqueous systems. But PHREEQC allows simulating reactive mass transport, which means the combination of thermodynamic equilibrium reactions and kinetic processes with convective and dispersive transport. Thus, it becomes possible to model the spatial distribution coupled to the chemical behavior (MERKEL & PLANER-FRIEDRICH, 2005). Within PHREEQC, it is possible to include advection, diffusion, advection with dispersion, as well as advection with dispersion, considering diffusion in stagnant zones, in 1D-transport modeling (PARKHURST et al., 1999). For any transported substance applies, in consideration of mass balance, the Advection-Reaction-Dispersion equation (ARD):

$$\frac{\partial C}{\partial t} = -v * \frac{\partial C}{\partial x} + D_L * \frac{\partial^2 C}{\partial x^2} - \frac{\partial q}{\partial t} \qquad \text{Eq.(4.14)}$$

With C = concentration in water [mol/kgw]

t = time [s]

v = pore water velocity [m/s]

x = distance [m]

D_L = hydrodynamical dispersion coefficient [m²/s] = $D_e + \alpha_L v$

De = effective diffusion coefficient

α_L = dispersivity [m]

q = concentration of the solid phase [mol/kgw]

The first term on the right hand side of the equation considers advective transport; the second term represents dispersive transport, and the third term exhibits changes in concentrations in the solid phase through reactions. Figure 4.1 presents a schematic diagram of the components of the ARD. The transport term of the equation is solved by using the finite-difference method. For every time step, chemical interactions and reactions are calculated separate from transport computations. For a more detailed discussion please see APPELO & POSTMA (2005) chapter three.

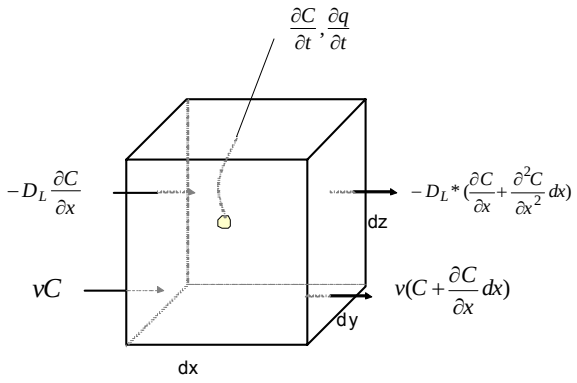

Figure 4.1: Presentation of the components of the ARD (after PARKHURST et al., 1999)

Transport calculation starts with computation of advection, then all chemical reactions are computed, and afterwards dispersive transport is determined; ultimately a computation of chemical equilibria and kinetic reactions is executed. This approach is exhibited in figure 4.2 , on the basis of a flowpath, that is discretized in several cells.

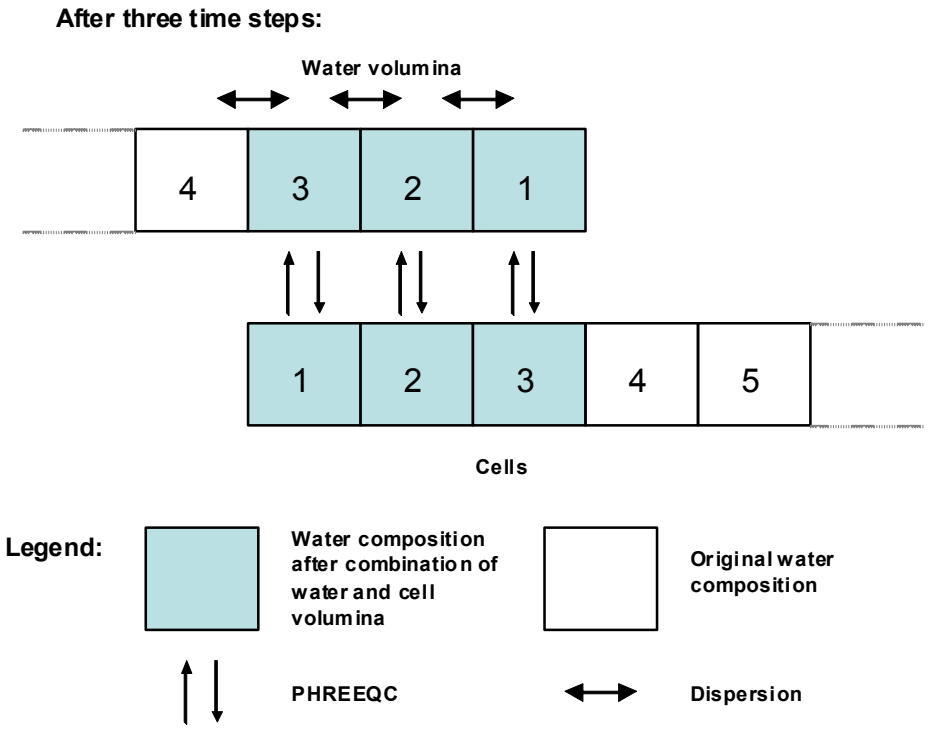

Figure 4.2 PHREEQC approach of simulating transport coupled with reaction, shown for a 1D flowpath (after APPELO & POSTMA, 2005; CARSTENS, 2007, modified)

Two general problems occur when using the finite-difference method: Numeric dispersion and oscillation, as shown in figure 4.3. Both, the spatial discretization and the choice of the type of the differences, meaning where the nodes of cells are set (e.g. central), have a strong influence on the result (MERKEL & PLANER-FRIEDRICH, 2005). This fuzziness which is caused by the application of different methods is called "numeric dispersion"; and it can be eliminated largely by a high resolution discretization. The Grid-Peclet number, P_e, helps for the definition of cell size, MERKEL & PLANER-FRIEDRICH (2005) recommends it to be ≤ 2.

$$P_e = \frac{|v| * L}{D} \qquad \text{Eq.(15.)}$$

With D = dispersivity

L = cell length

and $|v| = \sqrt{v_x^2 + v_y^2 + v_z^2}$ = velocity [m/s] Eq.(4.16)

The high-resolution discretization leads to extremely long computing times. Additionally, the stability of the numeric finite-differences method is influenced also by the discretization of time (MERKEL & PLANER-FRIEDRICH, 2005).

The Courant number is a criterion, so that the transport of a particle is calculated within at least one time step per cell.

$$C_o = \left| v * \frac{dt}{L} \right| < 1 \qquad \text{Eq.(4.17)}$$

Besides the strong attenuation (numeric dispersion) there is another problem with the finite-differences method and that is oscillation, which is characterized by a strong vibration.

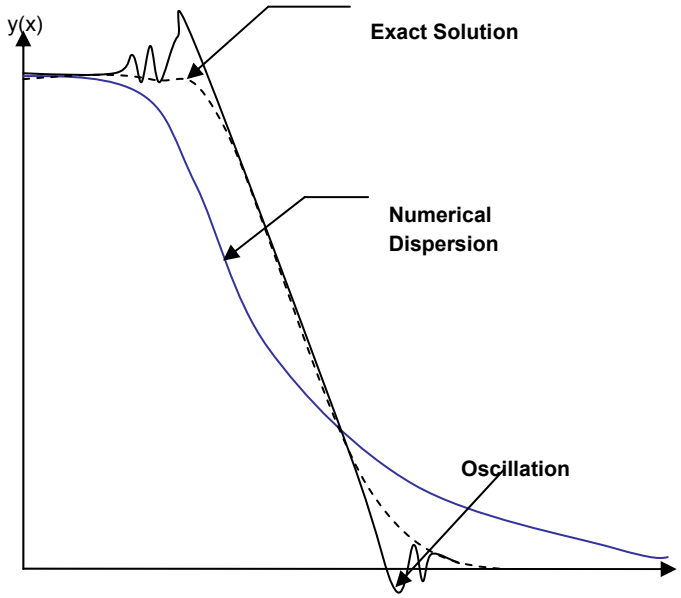

Figure 4.3: Numeric dispersion and oscillation effects for the numeric solution of transport equation (after MERKEL & PLANER-FRIEDRICH, 2005, modified)

4.2.4 Applications of PHREEQC

Several successful applications of reactive transport modeling with PHREEQC have been published. In the following, only several exemplary studies that were operated at larger scales are presented.

CHARLET et al. (2007) used PHREEQC to model different scenarios of arsenic transport in an aquifer in India, where the complexity of the transport model could be extended by including several geochemical processes. The module for inverse modeling was applied by MACHADO et al. (2007) to explore an aquifer in northeastern Brazil. Study objective was to proof evidence of flow-systems connecting the upper with the lower part of the catchment. MAHLKNECHT et al. (2006) used PHREEQC to establish a mass balance model for the Independence Basin in Mexico, as well as to reconstruct water ages through Carbonate isotopes.

In regard to acidification of watersheds, no examples of applications of PHREEQC transport modeling could be found.

5 Field Measurements: Material and Methods

As already mentioned in the introduction, our field work approach was a threepart measurement campaign: (1) streamwater samples for stream chemistry data; (2) streamwater and precipitation samples for isotope data; (3) soil samples for exchanger data.

Generally, samples were taken before, at, and after the inflow of small seeps or tributaries to explore possible differences in water-type, water-origin, contact times and flow paths.

5.1 Long Term Monitoring Program

The USGS, in cooperation with the US Environmental Protection Agency (EPA), has established the Long-Term Monitoring (LTM) Project at seven stream monitoring stations in 1983, and one in Biscuit Brook for the continuous monitoring of streamwater quality and discharge (MURDOCH et al., 1993). The monitoring station in Biscuit Brook is located just above the outlet of the catchment, in Frost Valley. Therefore, it will be revered to as Frost Valley from now on. All streams in the LTM Program have been sampled regularly for major ions, dissolved Al, and DOC concentrations since 1987 up to the present time. Timelines of flow and major-ions concentrations are routinely tested for outliers and consistency (McHale, personal communication, 2009).

Daily precipitation volume data was obtained from the Slide Mountain weather station (808 m elevation) of the National Climatic Data Center for the period 1991 to 2008. Monthly wetfall chemistry data were received from the National Atmospheric Deposition Program site (NY-68; 634 m elevation) in Biscuit Brook.

5.2 Analyses of Long-Term-Data

Charge Balance

To assure data quality for stream flow and precipitation timelines, charge balances were performed for water years 1991 to 2006. Therefore, it is necessary to convert concentrations into activities. This was done by using the DAVIES equation, see chapter 4.2.1, since it is suitable for

predominant ranges of ionic strength. Then percent errors of charge balance were calculated:

$$percent\_error = \frac{\sum cations - \left|\sum anions\right|}{\sum cations + \left|\sum anions\right|} \qquad \text{Eq.(5.1)}$$

Mass Balance

To develop a better understanding of water chemistry in Biscuit Brook, mass balances were performed, following the simple approach:

$$m_{output} - m_{input} + / - \Delta m = 0 \qquad \text{Eq.(5.2)}$$

Where m_{input}, m_{output} are masses of given substances for input (precipitation) and output (stream flow); Δm expresses any sinks or sources in the catchment, inducted either by abiotic or by biotic processes.

5.3 Longitudinal Streamwater Chemistry Profile of Biscuit Brook

The measurement campaign was carried out on three days in June 2008, the 3rd, 4th and 12th, during low flow conditions. Water samples were taken along all three tributaries to obtain a longitudinal streamwater chemistry profile. Our approach was to come as close as possible to sampling points of a former study by COSTELLO-WALKER (1995) who sampled two of the three tributaries of Biscuit Brook, to examine the evolution of streamwater chemistry closer. Figure 5.1 presents a topographic map of the study site with all sampling points.

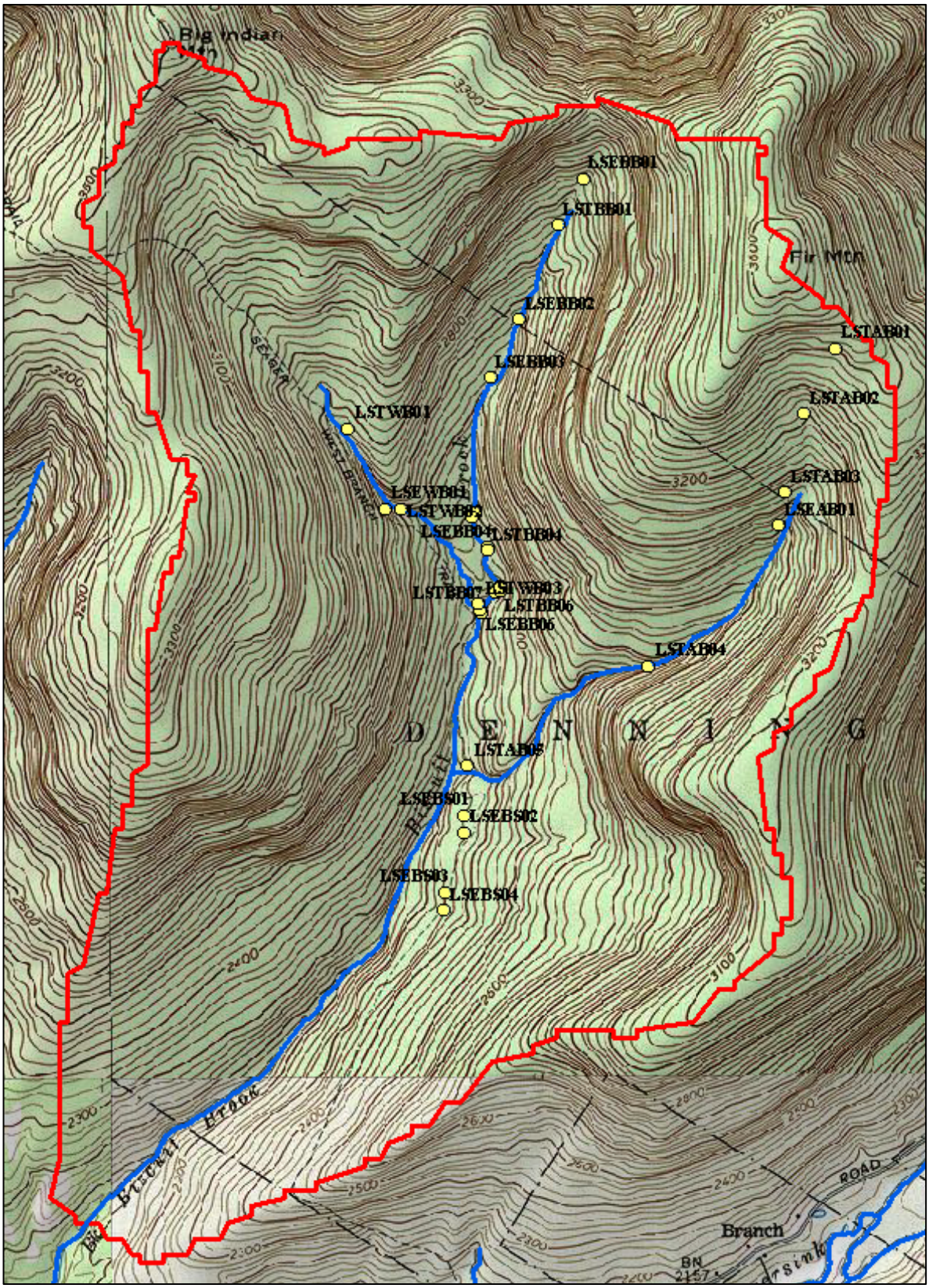

Figure 5.1: Topographic map of Biscuit Brook, presenting all streamwater sampling points for the measurement campaign in June 2008

5.3.1 Sampling and Laboratory Methods

Water samples were taken manually in 0.5 Liter Teflon™ bottles and refrigerated until they were analyzed for major ions, Al, Fe and DOC in the USGS laboratory in Troy. Field water temperatures and latitude and longitude of the sampling points were also recorded, except for water temperatures at several sampling points on the first day of measuring, the 3rd of June. Samples were analyzed for SO_4^{2-}, NO_3^-, and Cl^- concentrations and for base cations (Ca^{2+}, Mg^{2+}, Na^+, and K^+) by ion chromatography.

Ion chromatography

This is a form of liquid chromatography where retention is predominantly controlled by ionic interactions between the ions of the solute and *counter ions* that are situated in, or on, the stationary phase (URL 1). Its greatest utility is for analysis of anions for which there are no other rapid analytical methods, but it is also commonly used for cations and biochemical species such as amino acids and proteins (URL 2). To separate cations, for example, the stationary phase must contain immobilized anions as counter ions, with which the cations can interact. Most ion-exchange separations are done with pumps and metal columns (URL 2).

All samples were recorded within 11% error and coefficient of variance (CV) of 10%, CV equals the ratio of arithmetic mean to standard derivation. DOC was analyzed by infrared detection according to the analytical method described by LAWRENCE et al. (1995a & b) and LINCOLN et al. (2005) and reported within 15% error and CV of 15%. Aluminum and Iron concentrations were determined by direct coupled plasma and AA techniques. ANC was measured by Gran plot titration, and pH was measured by a low ionic strength electrode for all samples taken on the 3rd and the 4th of June. Unfortunately, samples taken on the 12th of June were not analyzed for pH and ANC due to a misunderstanding with the USGS laboratory. Thus, a regression analysis was performed to define the substance with the greatest pH control, which was NO_3^- with an R^2 of 0.7. Missing pH values were then calculated by inserting the respective Calcium concentrations in the regression equation.

All reported laboratory analyses met US EPA's quality assurance program guidelines, which include analysis of blind audit, duplicate, split, and blank samples. Table 5.1 shows reporting limits and data-quality objectives for the respective substances.

Details of analytical methods, quality assurance and quality control procedures used at the USGS laboratory in Troy, New York are provided in LAWRENCE et al. (1995a), LAWRENCE et al. (1995b) and LINCOLN et al. (2005).

Prior to the analyses, aliquots of all the samples were taken and later sent to the Institute of Hydrology in Freiburg (IHF), Germany, where they were analyzed for $\delta^{18}O$ by mass spectrometry.

Table 5.1: Reporting limits and data-quality objectives (percent error and CV respectively) for solution analyses performed by the USGS laboratory in Troy, NY, May 1991 through June 1993 (after Lawrence, 1995; modified)

	Reporting Limit	**Percent Error**	**CV[3]**
	µmol/L	*%*	*%*
ANC[1]	-	10	10
pH	-	10	20
DOC[2]	41	15	10
Al $_{\text{total monomeric}}$	1.5	10	10
NH_4	2.0	15	10
Ca	2.0	10	10
Cl	2.0	10	10
Mg	1.0	10	10
NO_3	2.0	10	10
K	1.0	10	10
SiO_2	6.0	15	10
Na	1.0	10	10
SO_4	2.0	10	10
Mean	2	11	10

[1] DOC is presented as µmol carbon/L water; [2] ANC in µeq/L; [3] CV = coefficient of variance

Annotation:

The USGS laboratory does not routinely analyze HCO_3. Thus, it was necessary to calculate hydrogen Carbonate concentration by applying equilibrium calculations, which depend on water temperature, pH, and pCO_2. Water was assumed to be in equilibrium with atmospheric pCO_2. First H_2CO_3 concentration were calculated, then HCO_3, and finally CO_3. But Bicarbonate concentrations were, as expected at given pH ranges, extremely low, so only hydrogen Carbonate was considered in the PHREEQC models.

5.4 Isotope Analyses

Our approach for the $\delta^{18}O$-analyses consists of two parts: (1) $\delta^{18}O$-event analyses to explore event-preevent water contributions for all seasons and several flow conditions and to gain additional information about seasonality and elevation effects, which bias ^{18}O distribution in precipitation and streamwater; (2) Generation of longitudinal isotope profiles to examine the spatial distribution of $\delta^{18}O$-concentrations, as well as to identify possible water types.

All samples for both parts of the $\delta^{18}O$-analyses were analyzed by mass spectrometry at the IHF. All Values were reported relative to V-SMOW and with a mean precision of 0.2 ‰.

5.4.1 Isotope Hydrology and Gas Source Mass Spectrometry

Stable isotopes are measured as the ratio of the two most abundant isotopes of a given element, e. g. for ^{18}O: $^{18}O/^{16}O$. But measuring an absolute isotope ratio is not easily done and would not lead to comparable results. Since hydrologists are mainly interested in comparing variations in stable isotope concentrations rather than actual abundance, not the absolute but an apparent ratio is measured. By measuring a sample at the same time as a known reference, one can compare sample and reference and eliminate, mathematically, the error m between the apparent and the true ratio. This is expressed using the delta (δ) notation:

$$\partial^{18}O_{sample} = \left(\frac{(^{18}O/^{16}O)_{sample}}{(^{18}O/^{16}O)_{reference}} - 1 \right) * 1000‰\ VSMOW \qquad \text{Eq.(5.3)}$$

VSMOW is the name of the reference used: Vienna Standard Mean Ocean Water.

For measuring $\delta^{18}O$ by gas source mass spectrometry it is necessary to equilibrate the water first with CO_2 and then analyzing the CO_2. The basis of gas source mass spectrometry is to bend a beam of charged molecules in a magnetic field into a spectrum of masses (CLARK & FRITZ, 1997).

Global and Local Effects on $\delta^{18}O$-distributions

It is temperature that controls partitioning of isotopes in precipitation, and provides the variable input function, e.g. used to trace groundwater

recharge (CLARK & FRITZ, 1997). The stable isotope distributions in meteoric waters are controlled by a series of temperature-based mechanisms that drive the rainout process. These include on a global scale continental and latitude effects, and at a local scale altitude and seasonal effects (CLARK & FRITZ, 1997). Usually, only partitioning processes on a local scale can be considered. The International Atomic Energy Agency (IAEA) in Vienna provides isotope data from stations around the world, which makes it possible to explore seasonal and altitude effects on ^{18}O distribution. Unfortunately, only three IAEA stations are located on the east coast, Chicago (Illinois), Hatteras (North Carolina), and Coshocton (Ohio).

Since this is not an isotope study, descriptions of mass spectrometry measurements and theoretical background of isotope hydrology are kept minimal. Please see Clark & Fritz (1997), chapter 1 and 2, for more details.

5.4.2 δ ^{18}O-Event Analyses

Aliquots of streamwater and precipitation samples were stored routinely at the USGS depot in Troy, NY, since water year 2006. Table 5.2 shows sampled and analyzed events for water years 2006 to 2007, measured at the continuous monitoring station above the outlet of Biscuit Brook. The Criterions for including a given event were the availability of sufficient samples for base flow, rising limp, peak flow, and falling limp, as well as the existence of corresponding precipitation samples. Precipitation samples were obtained as bulk weekly samples and originate from the Slide Mt. weather station.

Hydrograph Separations

Hydrograph separations are based on the steady-state mass balance equations of water and tracer fluxes in a catchment (HOEG et al., 2000). In the case of n runoff components and $n-1$ observed tracers $t_1, t_2,\ldots, t_{n-1}$ the following n linear mixing equations can be written:

$$Q_T = Q_1 + Q_2 + Q_n \qquad \text{Eq.(5.4)}$$

$$c_T^{t_i} * Q_T = c_1^{t_i} * Q_1 + c_2^{t_i} * Q_2 + ... + c_n^{t_i} * Q_n \qquad \text{Eq.(5.5)}$$

With: Q_T = total runoff; $Q_1, Q_2,...Q_n$ = runoff components; c_1, c_2,..., c_n = respective concentrations of one observed tracer t_i.

The application of these equations is based on certain assumptions (HOEG et al., 2000):

- significant difference between tracer concentrations of different components
- constant tracer concentrations in space and time, or variations are accounted for
- no significant contributions of an additional component
- conservative mixing of tracers
- no collinearity between the tracers of the components

Table 5.2: Compilation of events, which were partly used for $\delta^{18}O$- event-analyses; streamflow samples were obtained from the USGS in Troy, NY

Event Number	Date and Time	Flow [m³/s]	Flow [mm/week]	Comments	Precipitation Date
Event 1 baseflow	11.01.2006 11:30	0.16	9.5E-03	Winter storm	04.01.06-10.01.06
Event 1 baseflow	11.01.2006 21:35	1.28	7.8E-02	Winter storm	04.01.06-10.01.06
Event 1	14.01.2006 08:10	4.11	2.5E-01	Winter storm	11.01.06-17.01.06
Event 1	18.01.2006 06:20	1.70	1.0E-01	Winter storm	11.01.06-17.01.06
Event 2 baseflow	08.03.2006 11:00	0.09	5.7E-03	spring base flow	08.03.06-14.03.06
Event 2	22.03.2006 11:50	0.15	9.2E-03	spring base flow	22.03.06-28.03.06
Event 3 baseflow	09.08.2006 10:30	0.03	1.9E-03	Summer storm	03.08.06-08.08.06
Event 3	19.08.2006 23:15	1.32	8.1E-02	Summer storm	09.08.06-15.08.06
Event 3	23.08.2006 10:45	0.03	1.8E-03	Summer storm	09.08.06-15.08.06
Event 4 baseflow	07.02.2007 13:00	0.09	5.7E-03	Snow melt	31.01.07-06.02.07
Event 4 baseflow	22.02.2007 12:00	0.06	3.4E-03	Snow melt	21.02.07-27.02.07
Event 4	07.03.2007 13:45	0.09	5.5E-03	Snow melt	07.03.07-13.03.07
Event 4	14.03.2007 22:45	0.51	3.1E-02	Snow melt	07.03.07-13.03.07
Event 4	15.03.2007 12:30	1.30	8.0E-02	Snow melt	07.03.07-13.03.07/14.03.07-20.03.07
Event 4	21.03.2007 13:00	0.22	1.3E-02	Snow melt	14.03.07-20.03.07/ 21.03.07-27.03.07
Event 4	23.03.2007 02:05	0.83	5.1E-02	Snow melt	21.03.07-27.03.07
Event 5	24.03.2007 21:45	1.02	6.3E-02	Snow melt/ Spring storm	21.03.07-27.03.07
Event 5	27.03.2007 10:15	1.68	1.0E-01	Snow melt/ Spring storm	21.03.07-27.03.07/28.03.07-03.04.07
Event 5	15.04.2007 21:35	4.17	2.5E-01	Snow melt/ Spring storm	11.04.07-17.04.07
Event 5	16.04.2007 22:45	3.40	2.1E-01	Snow melt/ Spring storm	11.04.07-17.04.07
Event 5	17.04.2007 10:15	1.22	7.4E-02	Snow melt/ Spring storm	11.04.07-17.04.07/18.04.07-24.04.07
Event 5	18.04.2007 07:50	0.79	4.8E-02	Snow melt/ Spring storm	18.04.07-24.04.07
Event 6 baseflow	11.09.2007 09:25	0.10	6.4E-03	Late Summer/ early fall storm	05.09.07-11.09.07
Event 6	11.09.2007 10:55	3.84	2.3E-01	Late Summer/ early fall storm	05.09.07-11.09.07
Event 6	11.09.2007 15:25	0.68	4.2E-02	Late Summer/ early fall storm	05.09.07-11.09.07
Event 6	12.09.2007 11:15	0.14	8.5E-03	Late Summer/ early fall storm	12.09.07-18.09.07

Two-component hydrograph separations

After equations 5.4 and 5.5, the contribution of event water Q_E and preevent water Q_P to total runoff Q_T can be estimated using:

$$\frac{Q_E}{Q_T} = \frac{c_{T_{18_O}} - c_{P_{18_O}}}{c_{E_{18_O}} - c_{P_{18_O}}} \qquad \text{Eq.(5.6)}$$

$$\frac{Q_P}{Q_T} = \frac{c_{T_{18_O}} - c_{E_{18_O}}}{c_{P_{18_O}} - c_{E_{18_O}}} \qquad \text{Eq.(5.7)}$$

With c_T = $\delta^{18}O$ concentration in Q_T; c_P = $\delta^{18}O$ concentration in Q_P; c_E = $\delta^{18}O$ concentration in Q_E.

Per definition, the event component is the part of total runoff that entered the hydrological system during the rainfall event, whereas the preevent component is defined as that part of Q_T, which was already stored in the catchment (HOEG et al., 2000). Therefore, it is legitimate to use base flow prior to the analyzed event as an approximation for preevent $\delta^{18}O$ concentration.

Corrections for Altitude and Seasonal Effects

Additional isotope information was obtained by including three north-American IAEA-stations: Hatteras (North Carolina) at 3 m above sea level, Chicago (Illinois) at 189 m.a.s.l., and Coshoton (Ohio) at 344 m above sea level. Unfortunately, these stations are located pretty far away from the study site and also situated at different latitudes and climate zones than Biscuit Brook. Figure 5.2 presents the ^{18}O distribution in precipitation for the three mentioned IAEA stations for the period 1966 to 1971, which was the only overlapping time period available for these stations. Timelines show a high spatial variability because of the already mentioned overlapping of global and local effects. This overlapping makes an interpretation of the isotope data from the IAEA stations very hard. Another drawback is the available time period for the used stations, which is from 1966 to 1971.

5.4.3 Longitudinal $\delta^{18}O$-profiles

Aliquots were taken from all the streamwater samples, received from the measurement campaign in June 2008, and sent, together with the

precipitation aliquots, to the IHF laboratory. Unfortunately, it was not possible to conduct a preevent-event water hydrograph separation with the samples from June 2008, because there were no base flow/ preevent samples available from within the Biscuit Brook catchment and its tributaries.

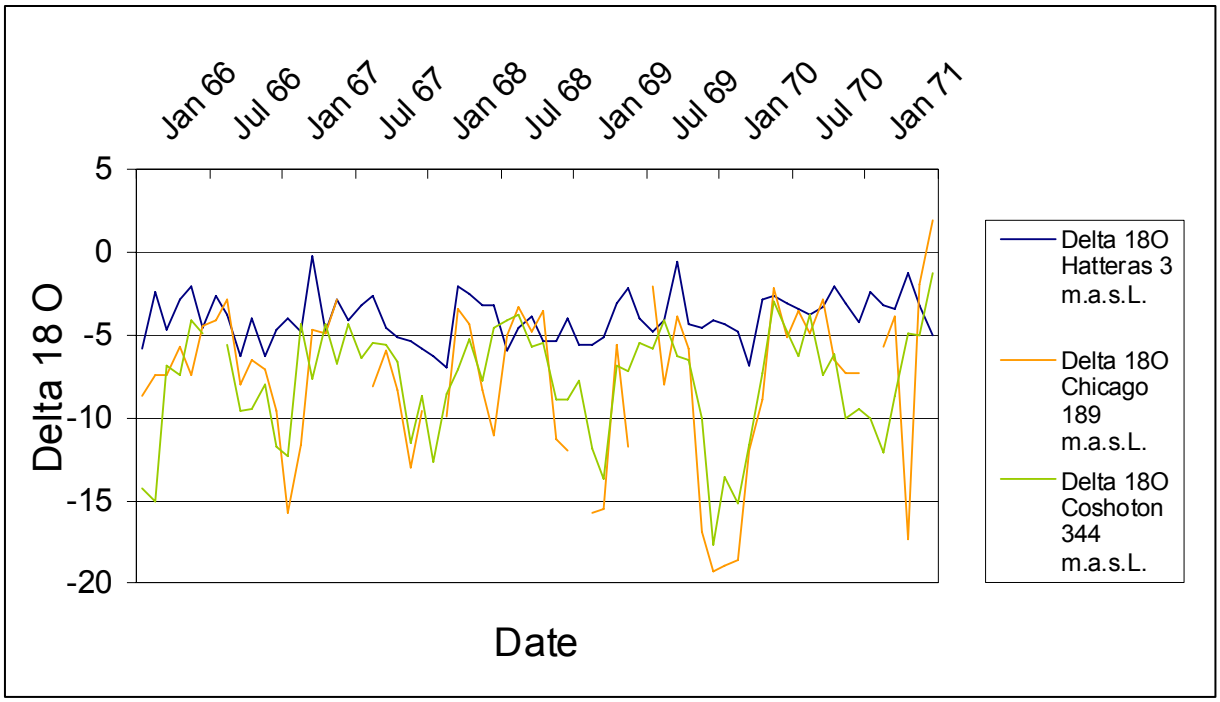

Figure 5.2: Timeline δ18O for 3 US-IAEA stations form 1966 to 1971

5.5 Soil Sampling

On June 12th 2008, soil profiles were dug in every tributary: Basic Biscuit, West Biscuit, and Acid Biscuit. In each subcatchment 1 deep profile, reaching down to the lower B/ upper C horizon (1m), and 4 shallow profiles were taken respectively at 4 compass directions, around 15-20 m from the deep pits away. This should give at least some spatial information about soil exchanger composition. Locations for soil profiles were chosen because of possible till deposition at these sites. Mineral soil samples were comprised of equal volumes of soil collected from each 10 cm increment from the soil profile. The samples were air dried, passed through a 2 mm sieve, and then subsampled for measuring soil moisture content by weighting before and after drying at 105°C (LAWRENCE, personal communication, 2008). oil samples were analyzed for

exchangeable base cations Ca^{2+}, Mg^{2+}, K^{+} and Na^{+} by extraction with 1 mol/L NH_4Cl, followed by flame aspiration atomic adsorption spectrophotometry. Exchangeable acidity, H^{+} and Al^{3+}, was determined by extraction with 1 mol/L KCl, followed by titration. Soil pH was detected in 0.01 $CaCl_2$ solutions. Details for soil sample treatment and analyses are described in BLUME et al. (1990).

6 Results Field Measurements

In this section, results of field measurements and various streamwater and precipitation chemistry analyses are presented to provide a basis for the conceptual model used in PHREEQC.

6.1 Results Long-Term Data

Charge Balance

Both, precipitation and streamwater data, feature relatively high mean percent errors, resulting from an apparent disproportionate charge balance. Mean percent error in the charge balance of Biscuit Brook streamwater for period 1991 to 2006 was 5%, the respective error for precipitation was 10%. Figure 6.1 shows a timeline of calculated percent error in charge for Biscuit Brook stream flow.

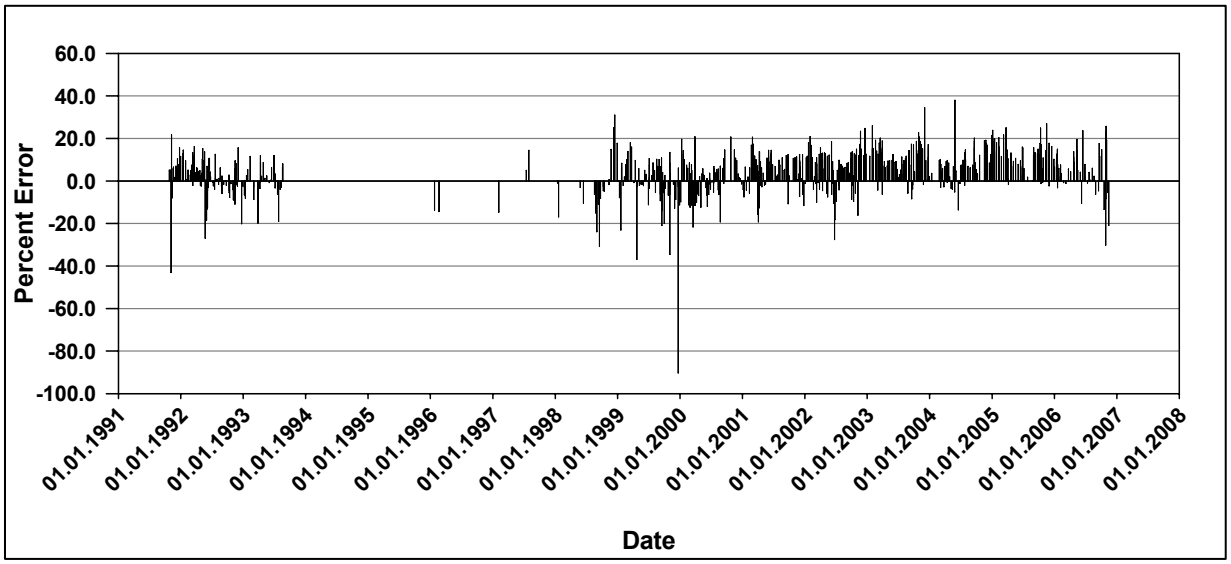

Figure 6.1: Percent error in charge of Biscuit Brook Streamwater in µeq/L for water years 1991 to 2006

High percent errors in charge are due to several reasons. First of all, the lower the ionic strength of a solution the higher is the charge error in the solution and headwaters in the Catskills are dilute waters with a very low degree of ionization. Secondly, not all species that contribute to the charge balance are routinely measured in the USGS laboratory in Troy, NY. Hydrogen Carbonate, for instance, is not measured, and was

calculated. Also, DOC was not included in the charge balance, since no data about charge or speciation of DOC was available.

Mass Balance

Results showed only for H^+ and NH_4^+ negative annual mass balances, which means that input loads were larger than output loads, and indicates storage of the respective substances in the watershed. For all base cations, as well as for SO_4^{2-} and NO_3^-, positive mass balances were detected, which shows that annual output loads were greater than annual input loads, and indicates leaching.

6.2 Results Longitudinal Streamwater Chemistry Profiles

Table 6.1 shows minimal and maximal concentrations for major ions, acid neutralizing capacity (ANC), DOC, as well as minimal and maximal pH, temperature, pCO_2 and specific conductance as measured during the field campaign in June 2008. The complete data set is shown in the Appendix in table 0.1. Figures 6.2 to 6.8 show longitudinal profiles of selected streamwater chemistry for all tributaries.

Table 6.1: Minimal and maximal concentrations of major ions, ANC, DOC, SC = specific conductance, and minimal and maximal values for other chemical and physical variables from longitudinal samples, measured in June 2008; numbers in brackets indicate gfw

		BASIC BISCUIT		ACID BISCUIT		WEST BISCUIT		BISCUIT	
Source		**Min**	**Max**	**Min**	**Max**	**Min**	**Max**	**Min**	**Max**
Temp	*°C*	8.1	13.2	10.5	11.3	11.1	11.3	10.4	14.5
Charge	*eq/L*	4.18E-12	3.01E-09	6.65E-12	1.95E-09	-5.70E-10	1.74E-10	-4.61E-06	5.19E-06
Percent Error	*%*	0.00	0.00	0.00	0.00	0.00	0.00	-2.82	1.94
pH		5.71	7.05	4.52	4.90	5.78	7.22	5.07	6.50
ANC	*µeq/L*	63.28	184.49	-30.25	-6.49	8.71	288.95	-0.44	44.42
DOC	*µeq/L*	79.36	226.24	161.50	601.31	79.77	153.02	83.78	136.39
SC	*µS/cm²*	21.20	30.20	16.36	25.10	15.42	41.10	15.67	19.01
Cl (35.45)	*mg/L*	0.3	0.5	0.3	0.4	0.1	0.3	0.2	0.4
Ca (40.08)	*mg/L*	2.8	9.2	0.5	1.2	1.6	7.0	0.8	2.0
Fe (55.85)	*mg/L*	1.9E-03	3.4E-02	8.9E-05	0.2	3.5E-04	7.2E-03	3.0E-03	1.8E-02
Mg (24.31)	*mg/L*	0.5	0.9	0.2	0.4	0.3	0.7	0.3	0.6
K (39.1)	*mg/L*	2.7E-02	0.4	4.3E-02	0.1	0.1	0.1	4.2E-02	0.2
Si (28.09)	*mg/L*	0.9	1.3	0.4	1.0	0.7	1.2	0.7	1.0
Na (22.99)	*mg/L*	0.3	1.0	0.2	0.3	0.2	0.3	0.2	0.3
NH_4 (18.04)	*mg/L*	1.3E-02	0.6	1.5E-02	3.2E-02	1.8E-02	2.3E-02	8.6E-03	2.1E-02
NO_3 (62.0)	*mg/L*	4.8E-01	1.3	0.1	0.5	0.3	0.8	4.8E-01	1.0
NO_2 (46.01)	*mg/L*	5.1E-04	1.3E-02	4.0E-03	7.5E-03	3.3E-03	5.1E-03	1.2E-03	6.3E-03
SO_4 (96.06)	*mg/L*	8.0	9.0	7.7	8.0	2.2	8.3	7.2	8.3
Al_{im} (26.98)	*mg/L*	7.6E-03	9.6E-03	3.3E-02	0.2	1.3E-02	2.1E-02	9.4E-03	0.1
HCO_3 (61.02)	*mg/L*	6.2	22.4	0.6	2.3	1.6	16.9	4.0E-02	3.3
pCO_2	*bar*	-3.5	-1.9	-2.1	-1.4	-3.0	-2.6	-4.0	-2.5

Figure 6.2 presents pH profiles that show very clearly the discrepancy in streamwater of the different tributaries. In Basic Biscuit (BB), as well as in West Biscuit (WB), pH ranges between 6 and 7, whereas in Acid Biscuit (AB) observed pH-values are < 5. After the confluence of the three tributaries, pH in Biscuit Brook streamwater lies between 5 and 6.5.

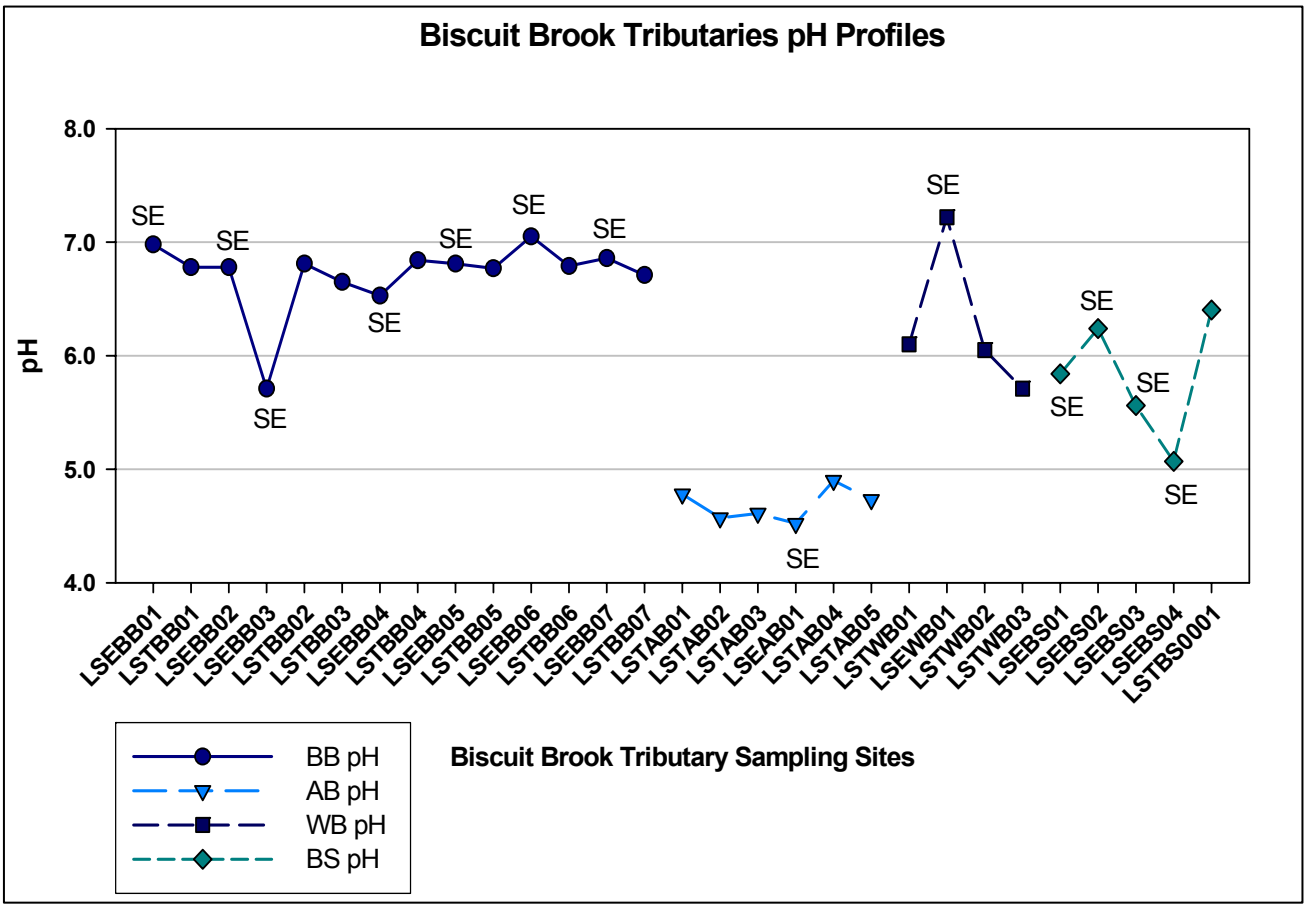

Figure 6.2: Biscuit Brook Tributaries pH profiles, measured in June 2008; SE stands for seepwater sample, the others are streamwater samples; LSTAB01: L for LTM-project, ST ≙ streamwater sample, AB ≙ ACID Biscuit; 01 ≙ headwater sample; LSEAB01: SE ≙ seepwater sample; BB ≙ BASIC Biscuit; WB ≙ WEST Biscuit

In BB some seeps show opposite patterns: some have a slightly higher pH than streamwater (LSEBB01, LSEBB06) and some have a slightly lower pH (LSEBB04). But most peculiar is LSEBB03 with the lowest pH of 5.71 in Basic Biscuit. There is no general increase or decrease in pH with increasing flow path visible in BB.

In Acid Biscuit, almost all seeps ran dry during the measurement, so only a single seep could be sampled. LSEAB01 had the lowest pH of 4.5 observed in Biscuit Brook. It seems like there is a slight increase in pH downstream.

In West Biscuit, LSEWB01 catches ones attention: it has the highest pH of 7.22 of all samples in Biscuit Brook. Because only three samples could be taken in WB, it is harder to recognize patterns in streamwater chemistry, but it seems like there is a slight decrease in downstream pH noticeable.

In Figure 6.3 Calcium profiles are presented that show very similar patterns.

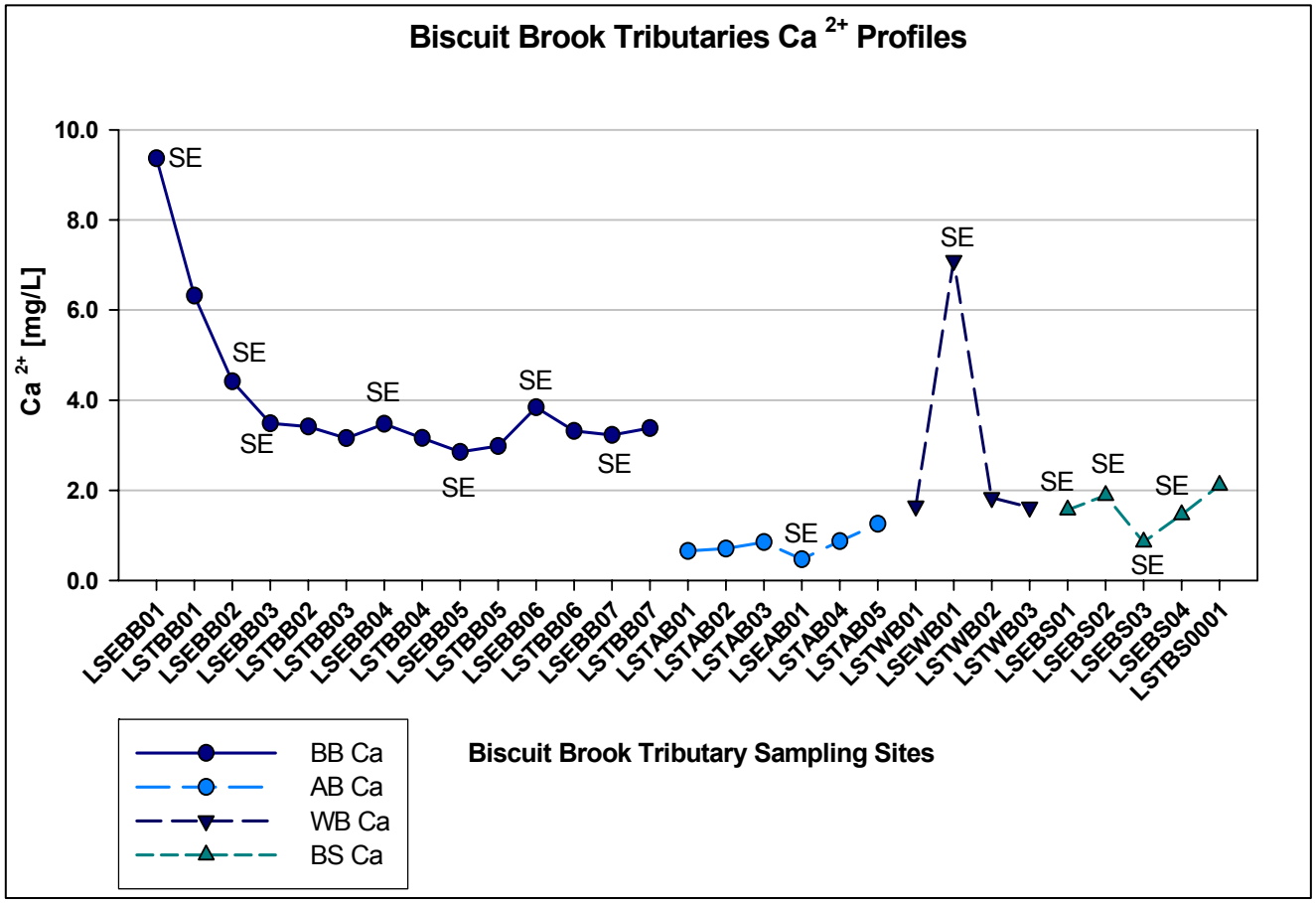

Figure 6.3: Biscuit Brook Tributaries Ca^{2+} profiles in mg/L, measured in June 2008; SE stands for seepwater sample, the others are streamwater samples; for further descriptions see figure 6.2

BB has the highest Calcium concentrations, which clearly decrease with increasing flow path. LSEBB03 Ca^{2+} concentrations do not follow observed pH. Since pH was lowest in LSEBB03, one should expect a lower Ca^{2+}

concentration. But Ca^{2+} concentration at LSEBB03 are in the same range than Ca^{2+} concentrations of sampling sites further downstream, which lies between 3 and 4 mg/L . Only LSEBB01 and LSTBB01 showed considerably higher Calcium concentrations of 9.4 and 6.3 mg/L respectively.

Of all tributaries AB has the lowest range of Ca^{2+} concentrations with concentrations around 0.8 mg/L. As already seen in the pH profile for AB, LSEAB01 has also slightly lower Calcium concentrations (0.5 mg/L) as in all streamwater samples. It also seems that Ca^{2+} concentrations are increasing with increase in flow path, which corresponds to increasing pH.

The WB Calcium profile also matches the observed pH profile. All streamwater samples have lower Ca^{2+} concentrations of around 1.7 mg/L, whereas LSEWB01 has the highest Ca^{2+} concentration and is far above the range of the streamwater samples with Calcium concentration of 7.1 mg/L.

BS seepwater Calcium concentrations were more in the range of WB and AB streamwater Ca^{2+} concentrations with values around 1.5 mg/L, whereas BS streamwater samples had slightly higher concentrations of 2.0 mg/L.

Biscuit Brook Mg^{2+}, Na^{+}, and K^{+} concentrations also show higher concentrations in BB and WB than in AB. These results are not shown here. But differences in concentrations where not as pronounced as for Calcium.

Figure 6.4 presents NO_3^- profiles for all three tributaries, in which BB has generally the highest and AB the lowest Nitrate concentrations. A couple of BB seep samples, LSEBB03 and LSEBB06, are much below the range of concentration of the other samples, which lies between 1.0 and 1.3 mg/L, with a Nitrate concentration of 0.5 and 0.004 mg/L respectively. This could be a sign for denitrification but corresponding NO_2^- concentration did not confirm this pattern. Generally, Nitrate concentrations seem to slightly decrease downstream.

AB NO_3^- concentrations seem to increase from 0.2 at the headwaters to 0.5 mg/L at the outlet of AB. LSEAB01 is below the range of the streamwater samples with a Nitrate concentration of 0.1 mg/L.

West Biscuit Nitrate concentrations lie in between BB and AB NO_3^- concentrations, and are generally in the same range around 0.8 mg/L. However, one streamwater sample, LSTWB02, is clearly below this range

with a Nitrate concentration of only 0.3 mg/L. But again, corresponding NO_2^- concentration did not confirm this pattern.

In BS, after the confluence of all tributaries, seepwater samples show clearly lower Nitrate concentrations than streamwater samples, with a range for the seepwater samples of ~0.5 mg/L in comparison to 1.0 mg/L in BS streamwater. One seep sample, LSEBS03, is far below the general range of seepwater samples with a Nitrate concentration of 0.004 mg/L.

These different ranges in observed Nitrate concentrations might be connected with redox conditions in the respective tributary.

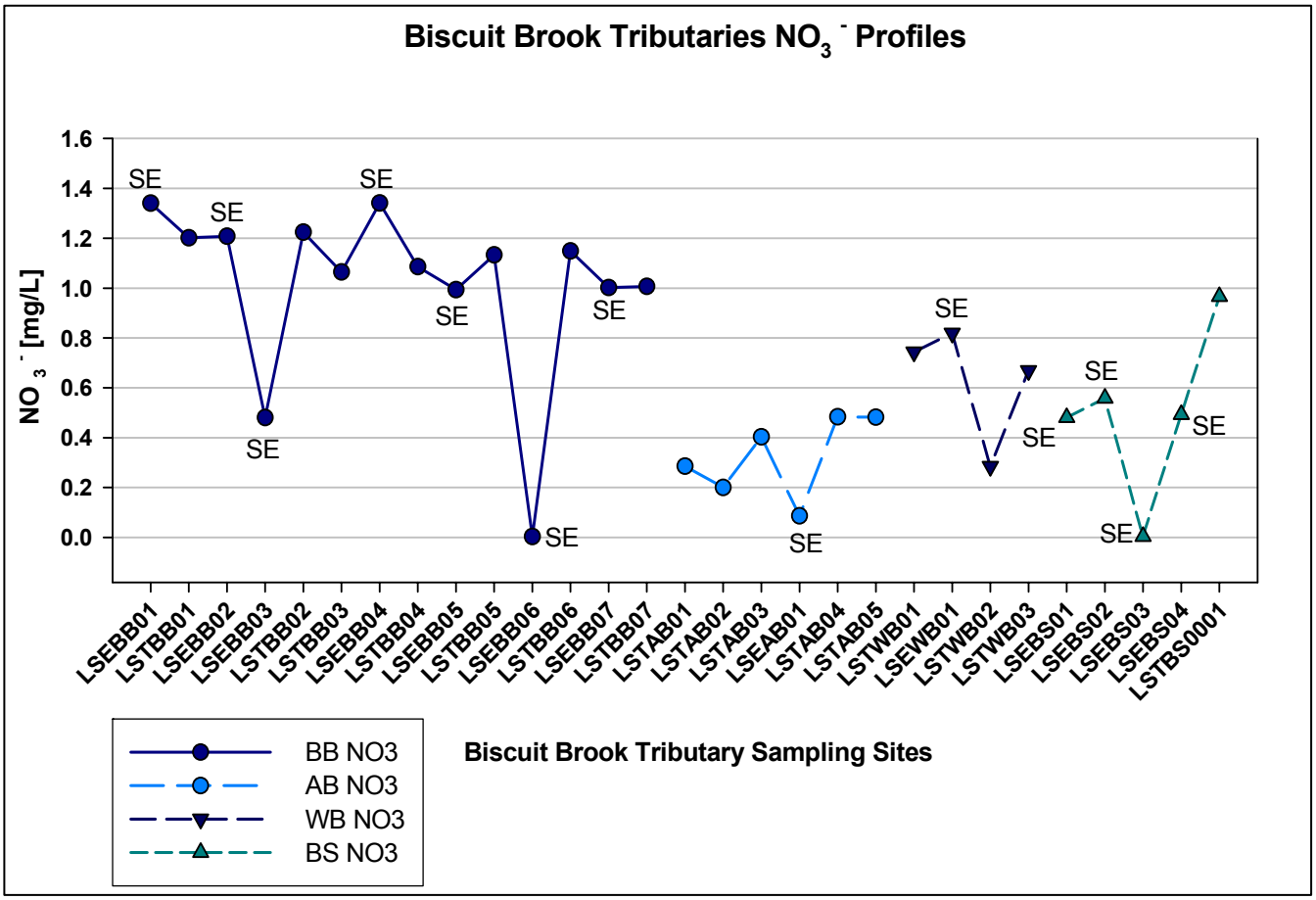

Figure 6.4: Biscuit Brook Tributaries NO_3^- profiles in mg/L, measured in June 2008; SE stands for seepwater sample, the others are streamwater samples; for further descriptions see figure 6.2

In figure 6.5 Silica profiles are presented. In BB the general range of Silica concentrations lies around 1 mg/L. With 1.3 mg/L, LSEBB06 has a noticeably higher Silica concentration than the other samples.

In Acid Biscuit Silica concentrations are close to those in BB, except for LSEAB01, which is with 0.5 mg/L below the general range of ~0.8 mg/L.

In WB Silica concentrations are also in a general range of 0.8 mg/L, except LSEWB01, which exceeds streamwater Silica concentration with a concentration of 1.2 mg/L.

After the confluence of the three tributaries, streamwater and seepwater Silica concentrations are very close. The streamwater sample LSTBS0001 has a Silica concentration of 1.0 mg/L; the seepwater samples have concentrations between 0.8 and 1.0 mg/L.

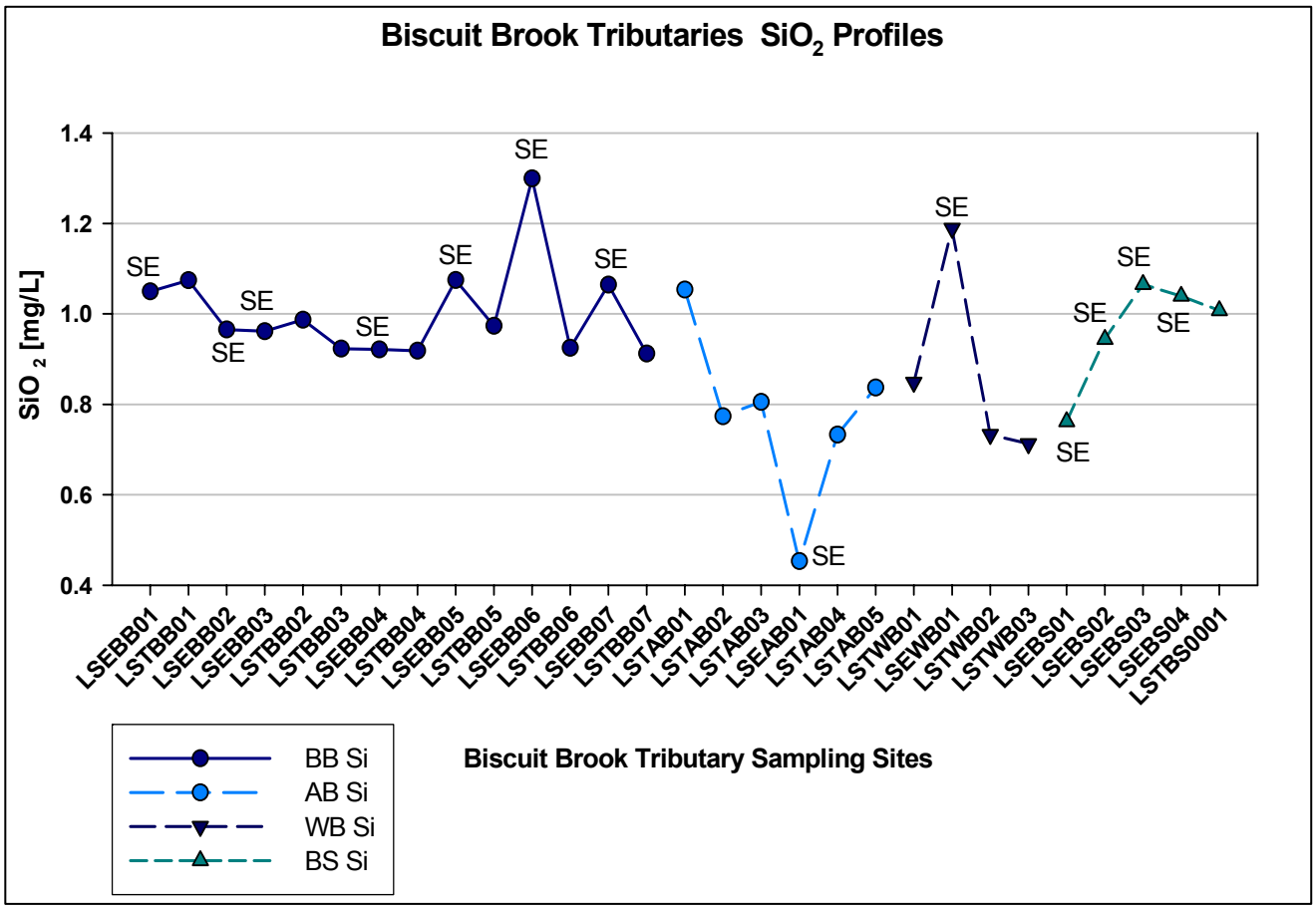

Figure 6.5: Biscuit Brook Tributaries SiO_2 profiles in mg/L, measured in June 2008; SE stands for seepwater sample, the others are streamwater samples; for further descriptions see figure 6.2

In figure 6.6 longitudinal Al_{im} profiles are displayed. Al_{im} means inorganic monomeric Aluminum, Al^{3+}. Since Al^{3+} mobilization is pH dependent, Aluminum concentrations in the different tributaries follow the respective

pH ranges. Thus, Al^{3+} concentrations in BB are low, between 7.6E-03 and 9.6E-03 mg/L.

AB has Aluminum concentrations that are almost two orders of magnitude higher than those in BB, and one order of magnitude higher than in WB. LSEAB01 has the maximum Al^{3+} concentration with a very high value of 0.2 mg/L. After McHale (personal communication, 2008), this is one of the highest Aluminum value ever reported in the LTM streams. Of course, this value corresponds to the lowest pH measured in June 2008 in Biscuit Brook.

In comparison to BB, WB has slightly higher concentrations in the range of 1.3E-02 to 2.1E-02 mg/L.

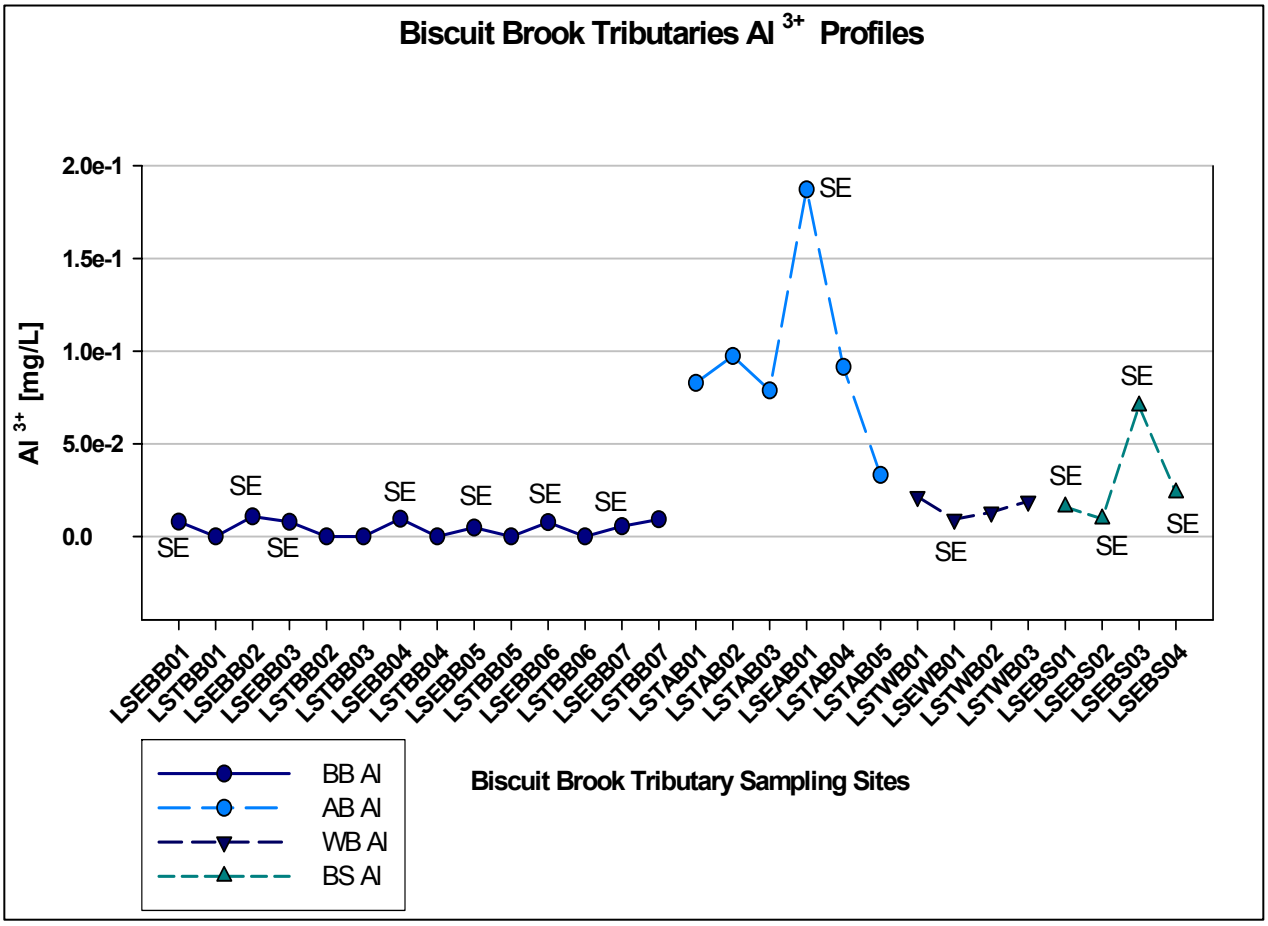

Figure 6.6: Biscuit Brook Tributaries Al^{3+} profiles in mg/L, measured in June 2008; SE stands for seepwater samples, the others are streamwater samples; for further descriptions see figure 6.2

Figure 6.7 presents longitudinal pCO_2 profiles for all tributaries in Biscuit Brook as measured in June 2008. As mentioned in the previous chapter, HCO_3 and ultimately pCO_2 had to be computed based on equilibrium calculations. First, water was assumed to be in equilibrium with atmospheric pCO_2 of $10^{-3.5}$ atm. But this resulted in an underestimation and in some cases to an overestimation of HCO_3 concentrations and to large percent errors in charge. Therefore, pCO_2 was adjusted to minimize the charge error. This was seen as the most straight forward approach, since in natural aquatic systems charge balance is commonly achieved by assimilating HCO_3 concentrations.

PH has a major influence on the amount of dissolved CO_2 (H_2CO_3*), at pH < 5 CO_2 (aq.) becomes the dominant Carbonate species (STUMM & MORGAN, 1997; see chapter 4). Therefore, partial pressures of CO_2 are higher and Hydrogen-Carbonate (HCO_3) concentrations are lower in the acidic tributary, AB, than in the more basic tributaries, BB and WB.

In BB, partial pressures of CO_2 are generally higher further upstream, with pCO_2 values around $10^{-2.7}$ bar, and decrease gradually with increasing flow path to values around $10^{-3.1}$ atm. Seep samples LSEBB04 and LSEBB06 show different patterns than adjacent streamwater samples. LSEBB04 has the highest calculated pCO_2 with $10^{-1.9}$ atm, which also corresponds to the lower pH measured at this site. LSEBB06 has with $10^{-3.5}$ atm a lower partial CO_2 pressure than the surrounding streamwater samples.

Partial CO_2 pressures in Acid Biscuit range from $10^{-2.6}$ to $10^{-1.6}$ atm. Two streamwater samples, LSTAB01 and LSTAB04, have noticeably lower pCO_2 values. It is even more remarkable that LSTAB05, which is directly downstream of LSTAB04, seems not to be influenced by the minimal pCO_2 measured at LSTAB04. If LSTAB04 and LSTAB05 are not taken into consideration, a slight increase in pCO_2 can be observed downstream.

WB has generally low pCO_2 values between $10^{-2.8}$ and $10^{-3.2}$ atm. There is a slight increase observable downstream.

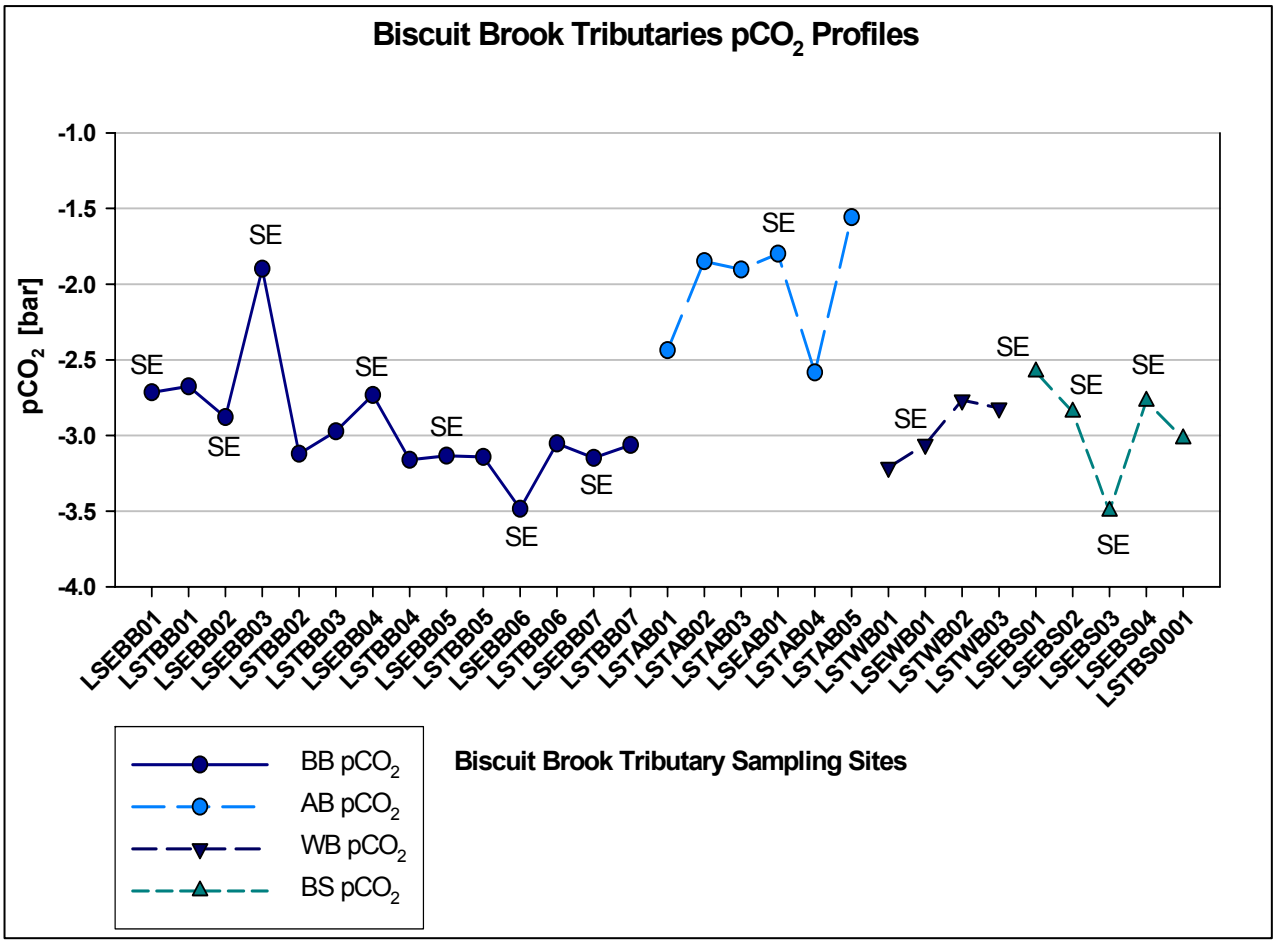

Figure 6.7: Biscuit Brook Tributaries pCO_2 profiles shown as Log(pCO_2) in atm, measured in June 2008; SE stands for seepwater samples, the others are streamwater samples; for further descriptions see figure 6.2

Partial CO_2 pressures in BS generally have a similar range than WB and BB, from $10^{-2.6}$ to $10^{-3.5}$ atm.

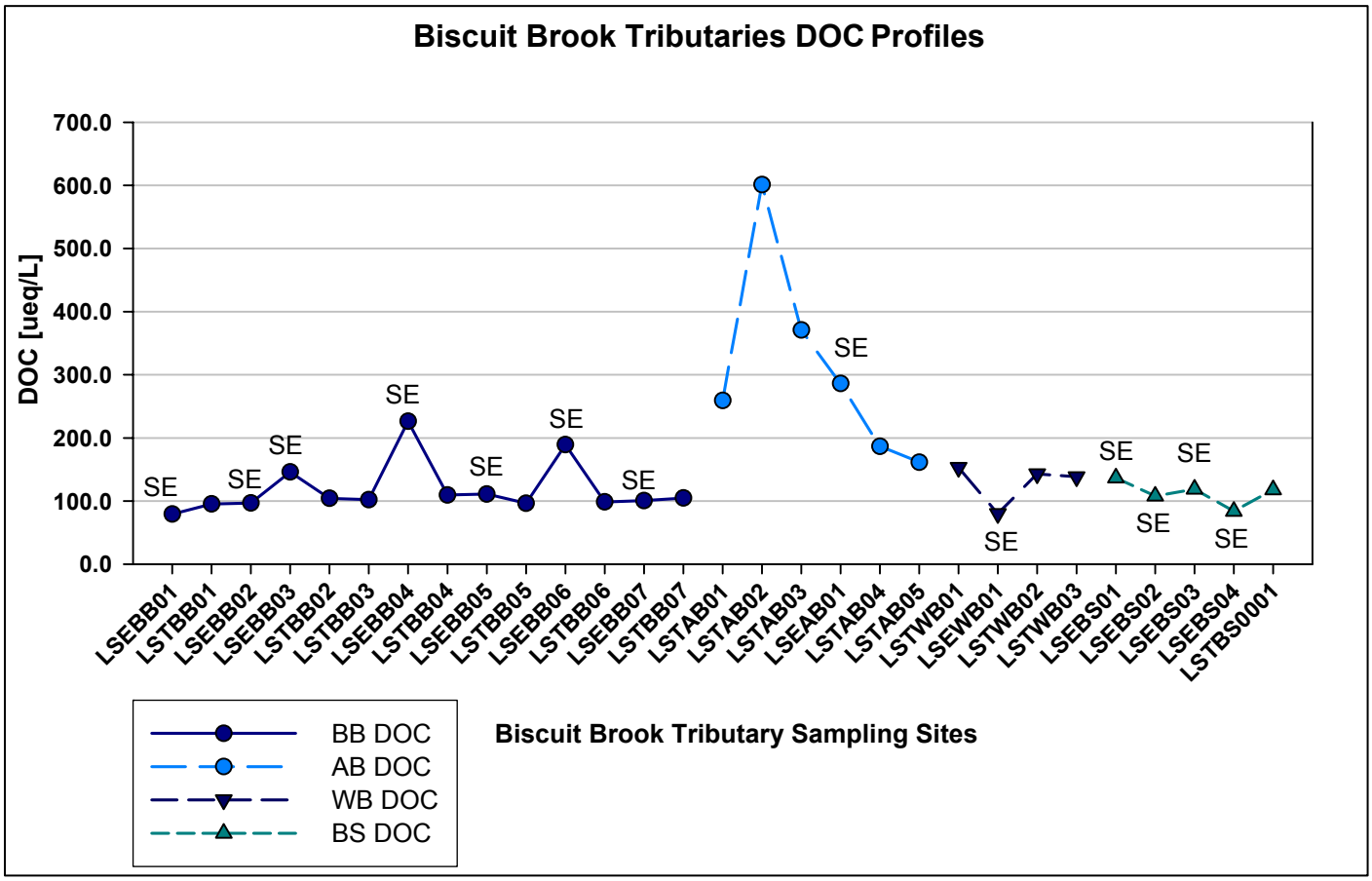

Figure 6.8: Biscuit Brook Tributaries DOC profiles in µeq/L, measured in June 2008; SE stands for seepwater samples, the others are streamwater samples; for further descriptions see figure 6.2

Interesting are also longitudinal DOC profiles, which also show the difference in water chemistry between BB/WB and AB. BB, WB and also BS samples have much lower DOC concentrations ranging from around 100 to 200 µeq/L.

DOC concentrations in AB, on the other hand, lie between 200 and 600 µeq/L, the latter was measured at LSTAB02. But DOC concentrations gradually converge towards WB/BS DOC range downstream.

6.3 Results Isotope Analyses

6.3.1 Results $\delta^{18}O$-Event Analyses

Tables 6.2 and 6.3 present measured and elevation corrected $\delta^{18}O$-values for selected events between 2006 and 2007 in precipitation and streamwater, respectively. Figures 6.9 and 6.12 visually represent these results. The $\delta^{18}O$-Inputfunction is characterized by high variability. Winter precipitations can have $\delta^{18}O$ concentrations as light as -17.2 ‰, and summer precipitations can be as heavy as -3.3 ‰. This can be explained by consideration of the major climate systems, which deliver precipitation to the region. Generally, the Catskill Mountains are located in the west wind zone. Thus, the general climate can be described as continental. But, since the Catskill Mountains are only approximately 150 km away from the Atlantic Ocean (linear distance), they are sometimes affected by local systems that originate in the northeastern coastal Atlantic region. Additionally, during winter the Catskill region can be influenced by very cold air masses from Central Canada, and in summer the region can be affected by warm air masses from the Gulf of Mexico. Because of the strong δ-T relationship, precipitation formed at higher latitudes tends to have more negative $\delta^{18}O$ values than precipitation formed at lower latitudes (CLARK & FRITZ, 1997).

Table 6.2: $\delta^{18}O$-Precipitation in [‰] for analyzed events, precipitation and snowfall amount for corresponding time periods

Number	Time Period	Precipitation N_i *[mm/week]*	Snowfall S_i *[mm/week]*	$\delta^{18}O$ *[‰]*	Comments
1	04.01.06-10.01.06	14.5	139.7	-13.1	Winter storm
2	11.01.06-17.01.06	50.3	50.8	-9.3	Winter storm
3	08.03.06-14.03.06	18.0	0.0	-5.0	Spring base flow
4	22.03.06-28.03.06	7.4	101.6	-12.8	Spring base flow
5	03.08.06-08.08.06	6.1	0.0	-5.3	Summer storm
6	09.08.06-15.08.06	10.9	0.0	-3.3	Summer storm
7	31.01.07-06.02.07	5.8	114.3	-17.2	Winter storm
8	21.02.07-27.02.07	18.3	292.1	-8.4	Winter storm/ Snow melt
9	07.03.07-13.03.07	15.7	0.0	-16.9	Winter storm/ Snow melt
10	14.03.07-20.03.07	75.2	609.6	-7.2	Snow melt
11	21.03.07-27.03.07	17.3	0.0	-7.4	Snow melt
12	28.03.07-03.04.07	4.1	0.0	-9.6	Snow melt
13	04.04.07-10.04.07	13.7	76.2	-7.9	Snow melt
14	11.04.07-17.04.07	180.8	355.6	-10.7	Snow melt
15	18.04.07-24.04.07	2.3	12.7	-5.4	Snow melt
16	05.09.07-11.09.07	8.6	0.0	-10.7	Late summer/early fall storm
17	12.09.07-18.09.07	79.0	0.0	-5.4	Late summer/early fall storm

The frequency distribution of $\delta^{18}O$ values in Biscuit Brook precipitation shown in figure 6.10 confirms the described variability, since it follows clearly not a Gaussian distribution.

Table 6.3: $\delta^{18}O$-Streamflow in [‰] for analyzed events, as well as discharge for corresponding time periods

Number	Date and Time	Flow [m³/s]	$\delta^{18}O$ [‰]	Comments	Precipitation Date
1	11.01.2006 11:30	0.16	-9.4	Winter storm	04.01.06-10.01.06
2	11.01.2006 21:35	1.28	-5.1	Winter storm	04.01.06-10.01.06
3	14.01.2006 08:10	4.11	-11.6	Winter storm	11.01.06-17.01.06
4	18.01.2006 06:20	1.70	-10.3	Winter storm	11.01.06-17.01.06
5	08.03.2006 11:00	0.09	-10.1	spring base flow	08.03.06-14.03.06
6	22.03.2006 11:50	0.15	-10.5	spring base flow	22.03.06-28.03.06
7	09.08.2006 10:30	0.03	-9.6	Summer storm	03.08.06-08.08.06
8	19.08.2006 23:15	1.32	-7.7	Summer storm	09.08.06-15.08.06
9	23.08.2006 10:45	0.03	-8.3	Summer storm	09.08.06-15.08.06
10	07.02.2007 13:00	0.09	-9.0	Snow melt	31.01.07-06.02.07
11	22.02.2007 12:00	0.06	-8.2	Snow melt	21.02.07-27.02.07
12	07.03.2007 13:45	0.09	-9.4	Snow melt	07.03.07-13.03.07
13	14.03.2007 22:45	0.51	-10.9	Snow melt	07.03.07-13.03.07
14	15.03.2007 12:30	1.30	-11.4	Snow melt	07.03.07-13.03.07/14.03.07-20.03.07
15	21.03.2007 13:00	0.22	-9.7	Snow melt	14.03.07-20.03.07/ 21.03.07-27.03.07
16	23.03.2007 02:05	0.83	-9.5	Snow melt	21.03.07-27.03.07
17	24.03.2007 21:45	1.02	-10.8	Snow melt	21.03.07-27.03.07
18	27.03.2007 10:15	1.68	-10.4	Snow melt	21.03.07-27.03.07/28.03.07-03.04.07
19	15.04.2007 21:35	4.17	-10.8	Snow melt	11.04.07-17.04.07
20	16.04.2007 22:45	3.40	-10.4	Snow melt	11.04.07-17.04.07
21	17.04.2007 10:15	1.22	-11.0	Snow melt	11.04.07-17.04.07/18.04.07-24.04.07
22	18.04.2007 07:50	0.79	-10.8	Snow melt	18.04.07-24.04.07
23	11.09.2007 09:25	0.10	-10.1	Late Summer/ early fall storm	05.09.07-11.09.07
24	11.09.2007 10:55	3.84	-10.2	Late Summer/ early fall storm	05.09.07-11.09.07
25	11.09.2007 15:25	0.68	-10.1	Late Summer/ early fall storm	05.09.07-11.09.07
26	12.09.2007 11:15	0.14	-9.1	Late Summer/ early fall storm	12.09.07-18.09.07

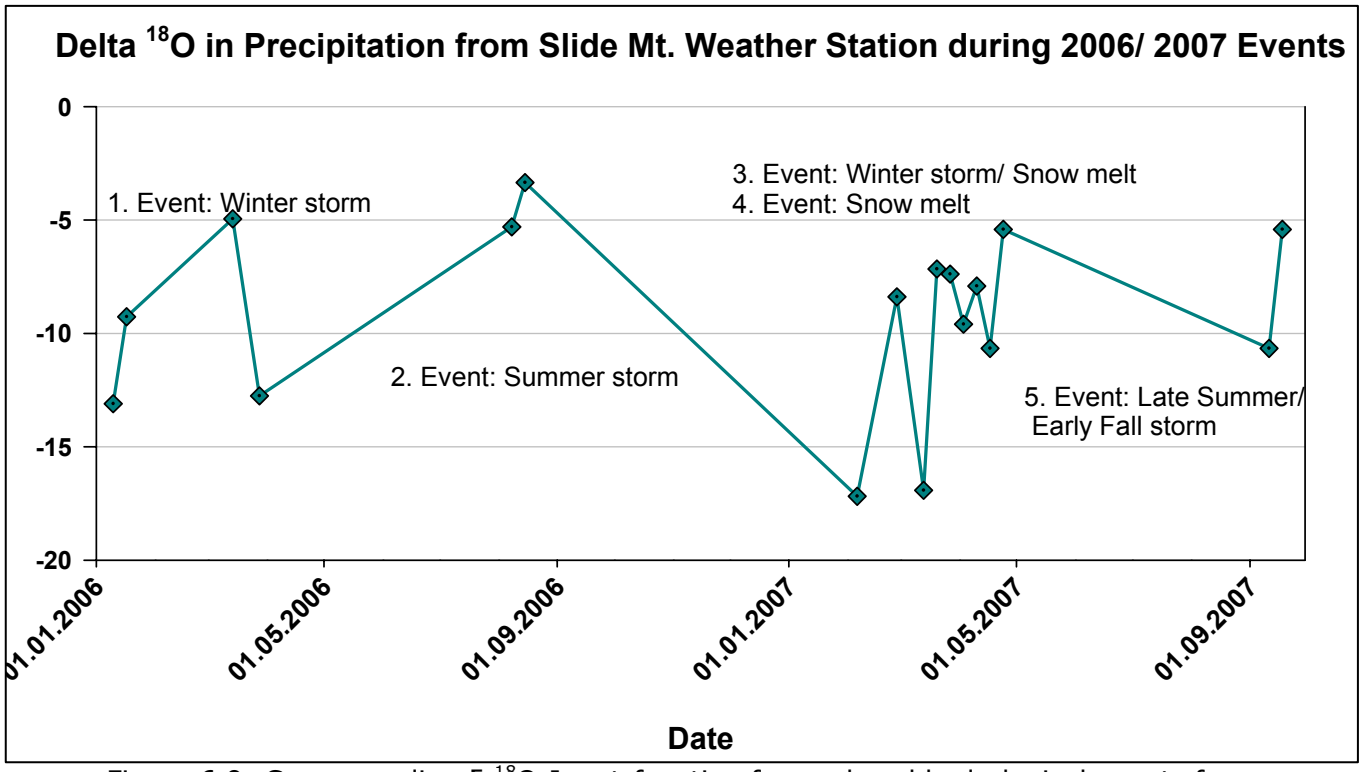

Figure 6.9: Corresponding δ ^{18}O-Input-function for analyzed hydrological events from 2006 through 2007; precipitation samples from Slide Mt. weather station

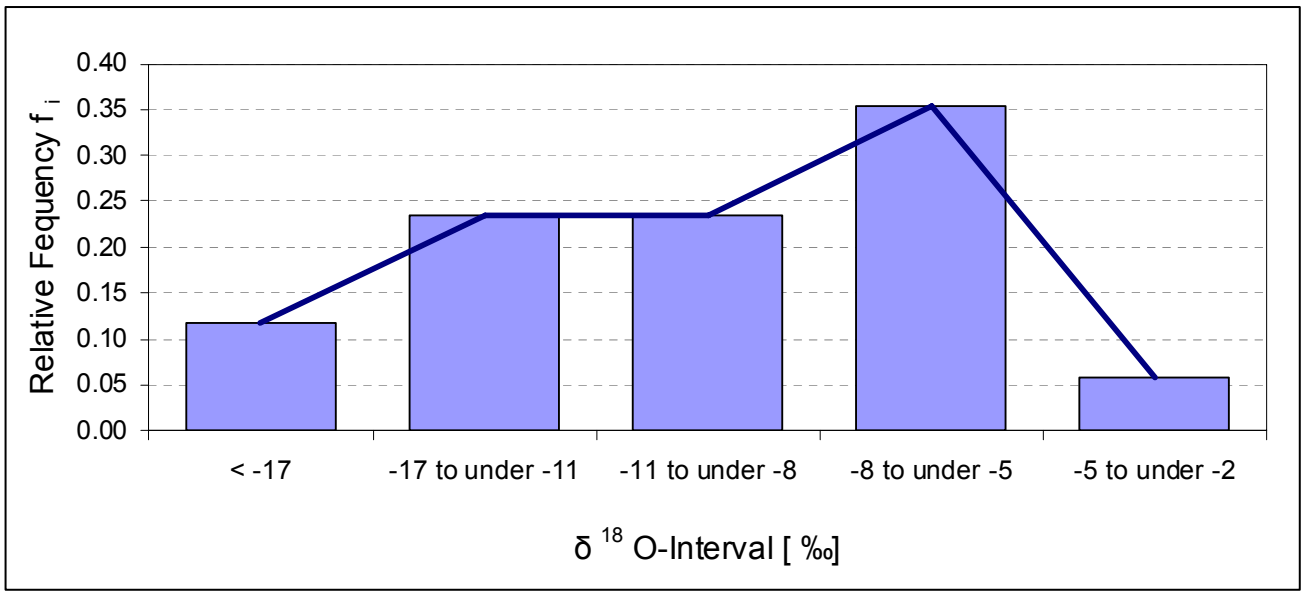

Figure 6.10: Frequency distribution of δ^{18}O for analyzed events from 2006 through 2007 in Slide Mt. precipitation

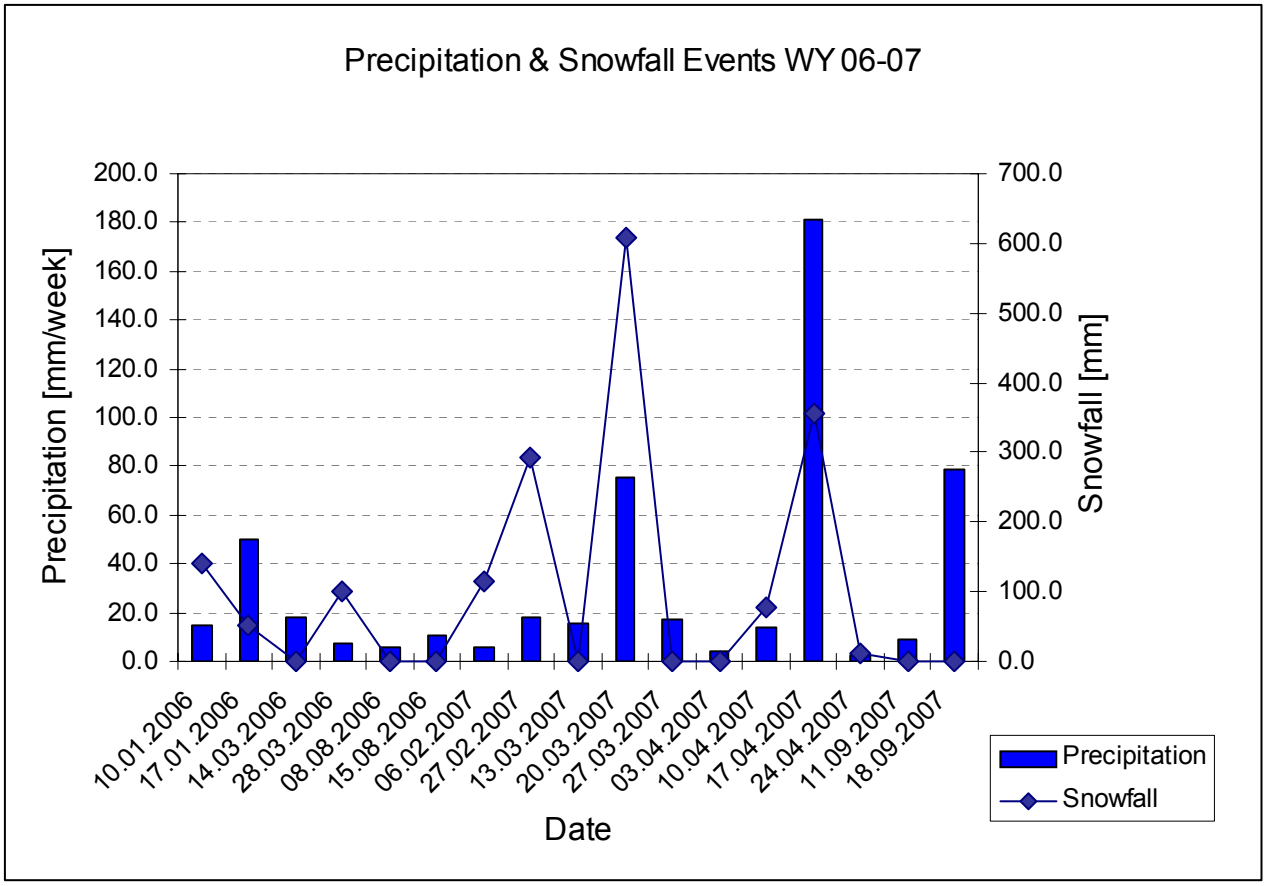

Figure 6.11: Corresponding Slide Mt. precipitation and snowfall amounts for analyzed events from 2006 through 2007

Figure 6.11 shows corresponding weekly precipitation and snowfall amounts [mm] for analyzed events in the given time period. In both years winter precipitation is composed of snow and rain, which reflexes the influence of warmer air masses. Figure 6.11 also shows that the minimal $\delta^{18}O$ values from February and March 2007 probably fell as snow.

In comparison to the $\delta^{18}O$-input function the system-response function is more balanced or damped, as shown in figure 6.12. This is also confirmed by the frequency distribution of $\delta^{18}O$ in Biscuit Brook streamwater, which is presented in figure 6.14, and moves closer to a Gaussian distribution. The range of $\delta^{18}O$-concentrations is much smaller, with values between -11.6 and -5.1 ‰. The minimal value is found in winter, but, surprisingly, the maximal value is also found in winter (peak flow sample of 1st analyzed event). This could be due to influence of Atlantic weather systems that are enriched in heavier isotopes. This is also supported by comparing corresponding discharge amount, as shown in figure 6.13, and isotope concentration: the first winter event in January 2006 has one of the highest discharge amounts of all analyzed events.

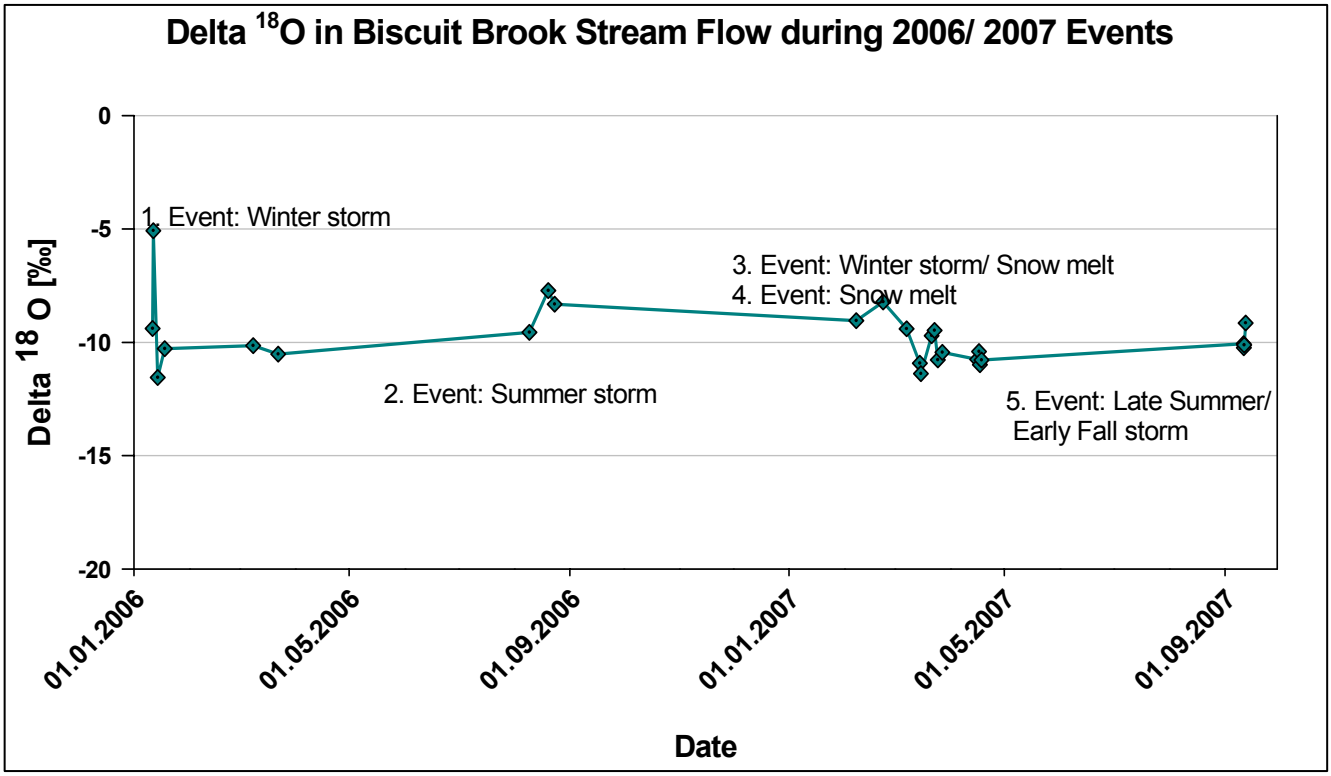

Figure 6.12: system-respond-function for analyzed events from 2006 through 2007 in Biscuit Brook streamwater

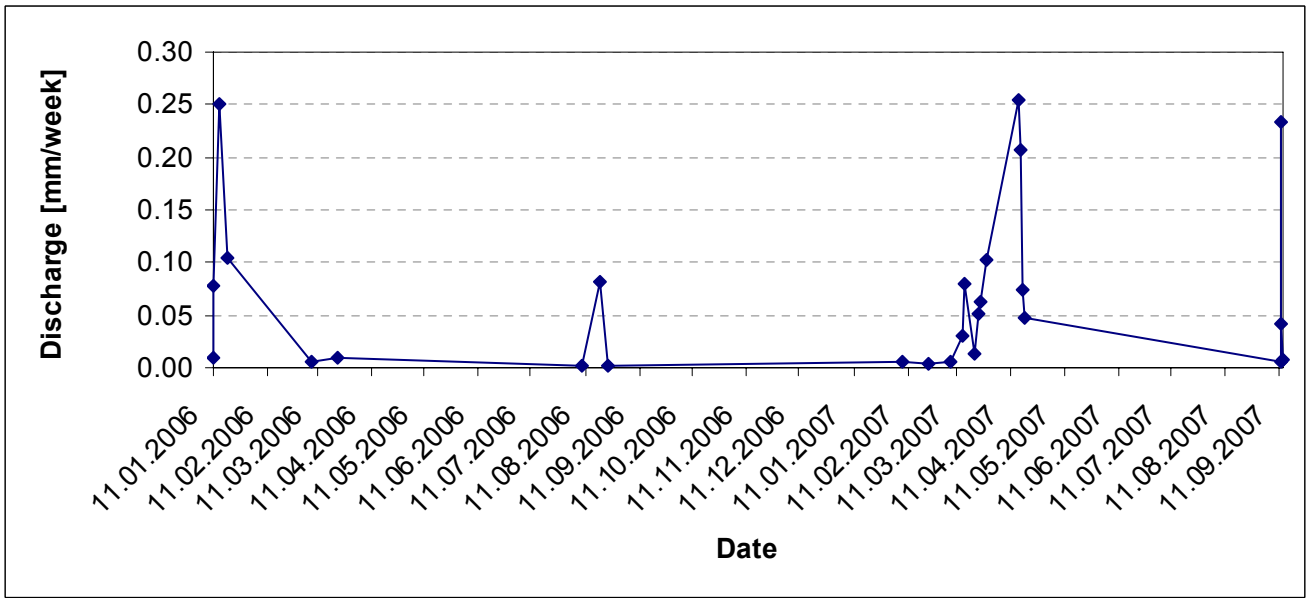

Figure 6.13: Biscuit Brook discharge in [mm/week] for selected analyzed events between 2006 and 2007

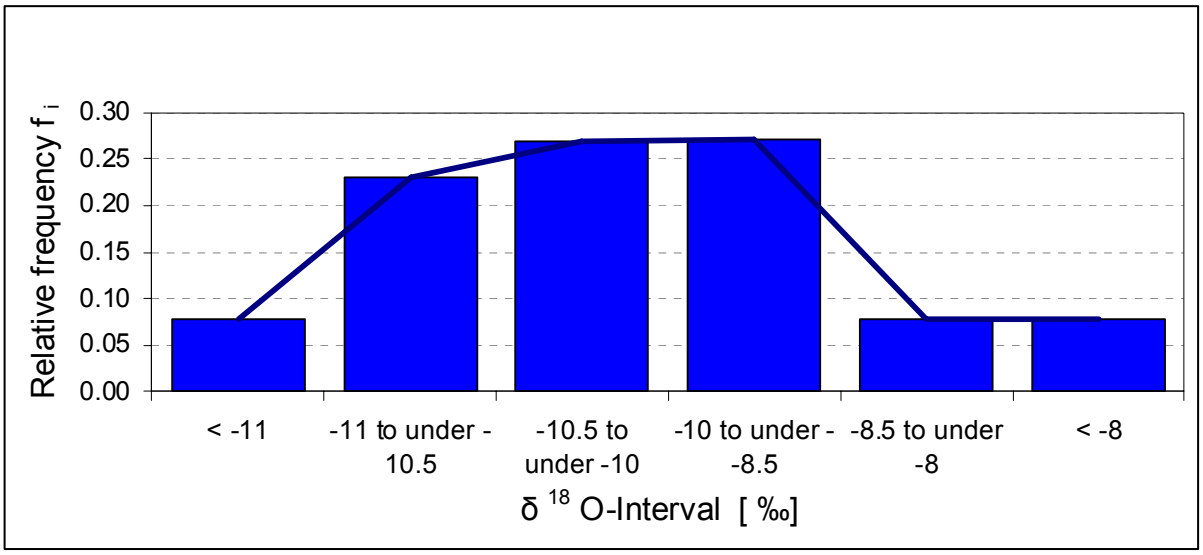

Figure 6.14: Frequency distribution of $\delta^{18}O$ for analyzed events from 2006 through 2007 in Biscuit Brook streamwater; measured at Frost Valley

Elevation Correction

$\delta^{18}O$ concentrations [‰] of three IAEA stations at different altitudes in the Northern US were obtained from the IAEA-website to analyze the influence of elevation on $\delta^{18}O$-signature in precipitation. Figure 6.15 shows mean annual $\delta^{18}O$-values for the three stations. Hatteras, North Carolina, is the station with the lowest elevation of 3 m.a.s.l. The Chicago, Illinois, station is located at 189 m.a.s.l. and the station in Coshoton, Ohio, at 344 m.a.s.l. But, as figure 6.15 shows, the $\delta^{18}O$-concentrations do not always follow the expected pattern, meaning lower altitude stations should have less negative $\delta^{18}O$-values than higher altitude stations. Correspondingly, Hatteras has the least negative values, but the other two stations do not show this pattern so clearly.

In fact, when calculating the $\delta^{18}O$ altitude gradient (Δ ($\delta^{18}O$)/100m), it showed that other effects, such as continental and latitude effect for example, must interfere, since computed gradients are unrealistically high with values > -1‰. But maximally possible is only a gradient of –0.36‰/100m.

Therefore a different approach was used to compute elevation gradients: elevations of the longitudinal seep sample sites, sampled in June 2008, were used to calculate a mean gradient of -0.33‰/100m, which is shown in table 6.4.

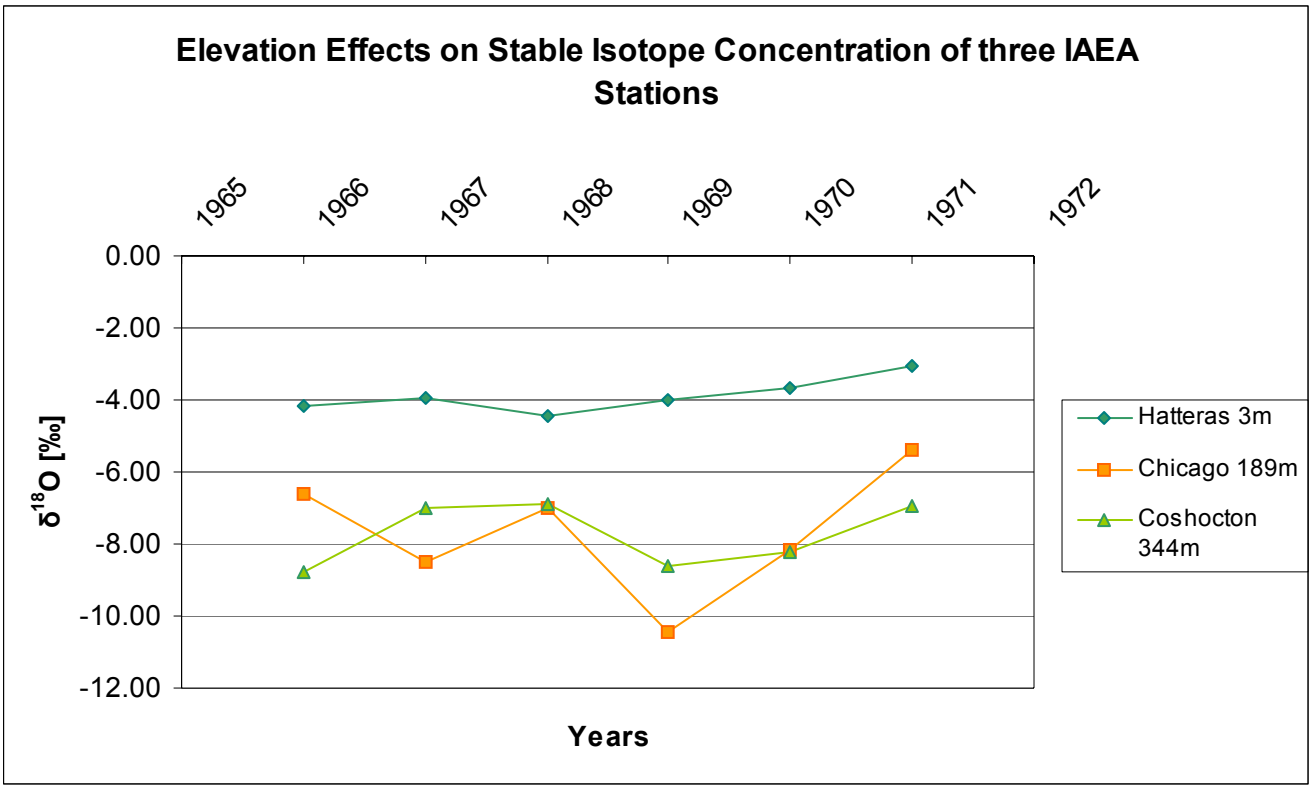

Figure 6.15: Mean annual $\delta^{18}O$ concentrations [‰] for 3 IAEA stations in the northern US for period 1966 to 1971

Table 6.4: Elevation gradients for Biscuit Brook seep samples (June 2008); please note: seep sample number 3 and 11 with gradients > -0.36‰/100m and were not included in gradient computation

Number	Sample ID Seeps	Date	Elevation *m*	$\delta^{18}O$ ‰	$\delta^{18}O$ difference *‰ / 100m*
1	LSEBB01	12.06.2008	892	-9.54	
2	LSEBB02	12.06.2008	809	-9.51	0.04
3	LSEBB03	12.06.2008	797	-9.87	3.02
4	LSEBB04	03.06.2008	749	-9.91	0.09
5	LSEBB05	03.06.2008	736	-10.00	0.68
6	LSEBB06	04.06.2008	748	-9.83	
7	LSEBB07	04.06.2008	736	-9.89	0.56
8	LSEAB01	04.06.2008	903	-9.14	
9	LSEWB01	03.06.2008	809	-9.34	0.21
10	LSEBS01	04.06.2008	730	-9.41	
11	LSEBS02	04.06.2008	721	-9.49	0.93
12	LSEBS03	04.06.2008	712	-9.52	0.30
13	LSEBS04	04.06.2008	730	-9.45	0.40
MEAN			774.77	-9.61	0.33

6.3.2 Two-component Hydrograph Separation

During the preevent-event water contribution analysis several problems occurred. First of all, the precipitation samples were weekly bulk samples. Since the event component is the part of total runoff entering the hydrological system during the rainfall event, whereas the preevent component was already stored in the catchment, the $\delta^{18}O_{event}$ concentration has to be zero before the rainfall event. Expressed differently, before the event, streamwater is only biased by $\delta^{18}O_{preevent}$ concentration. But for some analyzed events, preevent $\delta^{18}O$ in streamwater was biased by event $\delta^{18}O$, because of overlapping time periods for precipitation and base flow samples. This resulted in preevent contributions > 100%, which is of course not possible. Results for event and preevent contributions are presented in table 6.5, please note events 1 and 4 with preevent contributions > 100%. Mean event water contribution was 25% and mean preevent water contribution was 75%, which is in accordance with results of Brown et al. (1999). They found mean event and preevent water contributions in Shelter Creek, an adjacent but smaller catchment, of 30 and 70%, respectively.

Table 6.5: Calculated event and preevent water contributions in [%] for 5 selected events; Q_e/Q_t = event water contribution, Q_p/Q_t = preevent water contribution; please note events 1 and 4 with Q_p/Q_t > 100%

Events	Q_e/Q_t [%]	Q_p/Q_t [%]
1. Event	34.3	134.3
2. Event	*28.3*	71.7
3. Event	*26.4*	73.6
4. Event	*41.9*	141.9
5. Event	*18.9*	81.1
MEAN	*25*	75

Another reason for this unrealistically high preevent water contribution is shown in figure 6.11, which presents precipitation and snowfall amounts for selected events. All analyzed winter events, like event 1 and event 4, are also influenced by snowfall. But no snowfall samples were available to take the $\delta^{18}O$ concentrations of the snow-component into account. As mentioned in 5.4.2, several assumptions for the application of these

equations have to be done. One is that no significant contributions of an additional component should be present in stream flow. But this is the case in the present study. Therefore, preevent water contributions calculated here can only be seen as maximal possible preevent water proportions.

6.3.3 Results Longitudinal $\delta^{18}O$-Profiles

These results also support the present of different water types as clearly visible in figure 6.16. BB had to be divided in two series because the headwaters were sampled approximately 1 week later (June 12th) than the rest of the samples (June 3rd and 4th) and it rained in between. The general ranges of $\delta^{18}O$-concentrations are more negative in BB, WB, and in BS than in AB.

For BB (June 3rd and 4th), seepwater samples and streamwater samples seem to build two separate clusters, where seepwater samples are noticeable lighter than the streamwater samples with $\delta^{18}O$-values around -10‰. Interestingly, streamwater samples are hardly affected by the lighter seepwater samples, since the range of $\delta^{18}O$ still is around -9‰ even after the respective confluence.

In WB, $\delta^{18}O$ concentrations are slightly less negative than in BB, with values in the range of -9.5‰. The only taken seepwater sample, LSEWB01, does not show a much different $\delta^{18}O$-signature than LSTWB01. It is remarkable, that the following streamwater sample, LSTWB02, has with -9.8‰ a significantly lighter $\delta^{18}O$-signature than the rest of the WB samples. Maybe a small tributary with a lighter signature was not sampled.

In AB $\delta^{18}O$ concentrations range between -9.1 and -9.4‰, this is significantly higher than in BB and WB. There seems to be a slight decrease in $\delta^{18}O$-values downstream. Interesting is the sudden drop of $\delta^{18}O$ at LSTAB04. Again, it could be possible that a smaller tributary with a lighter isotope signature was not sampled.

After the confluence of the three tributaries, BS has $\delta^{18}O$ concentrations of ~-9.5‰.

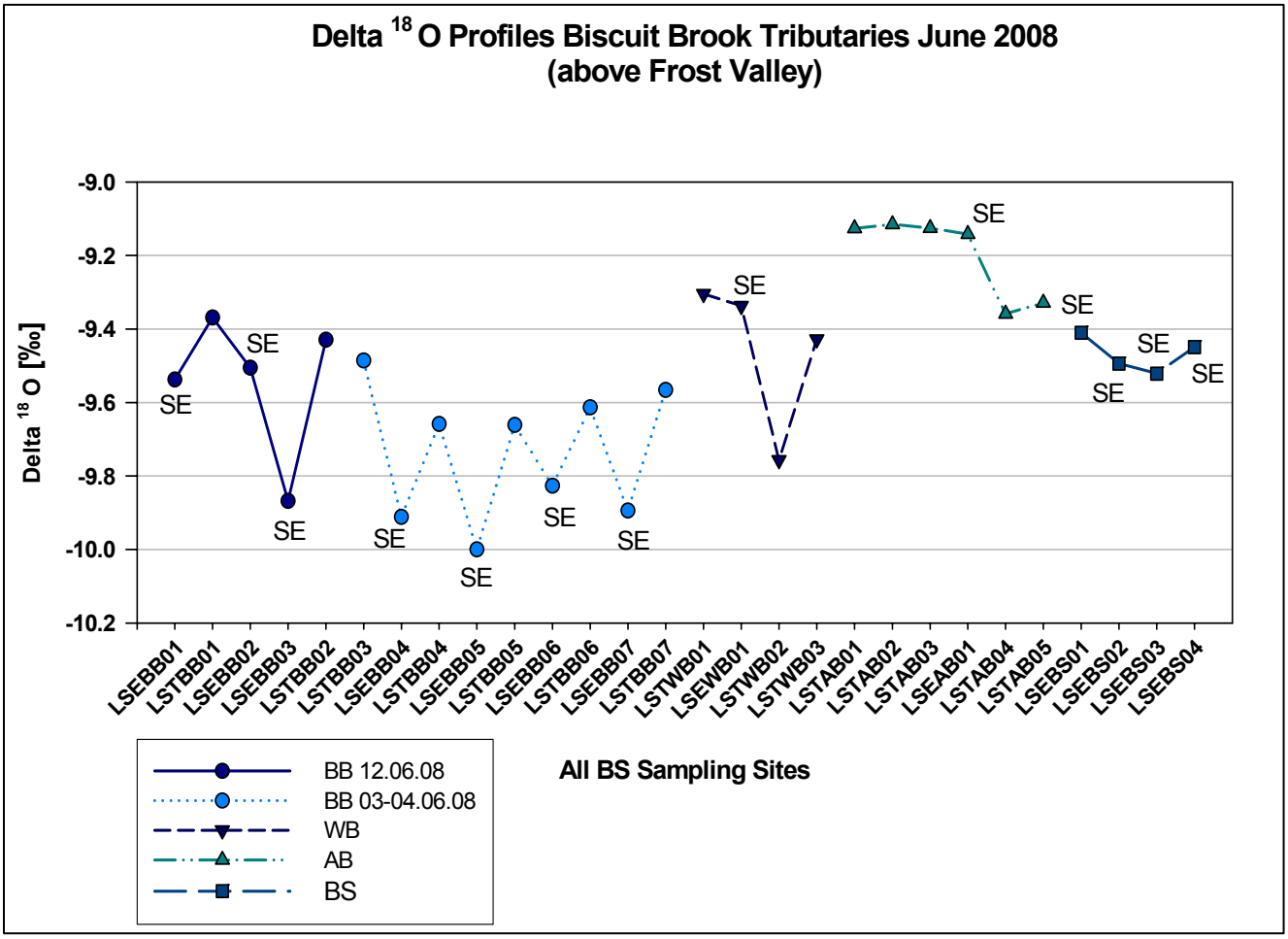

Figure 6.16: Longitudinal $\delta^{18}O$-profiles of Biscuit Brook tributaries, measured in June 2008; SE stands for seepwater samples, all others are streamwater samples; LSTAB01: L stands for LTM-project, ST ≙ streamwater sample, AB ≙ ACID Biscuit; 01 ≙ headwater sample; LSEAB01: SE ≙ seepwater sample; BB ≙ BASIC Biscuit; WB ≙ WEST Biscuit

6.4 Results Soil Profiles

Table 6.6 summarizes the results for the mean exchanger composition (MEC) in Biscuit Brook tributaries and table 6.7 presents calculated mean cation exchange capacities (CEC) for O-, (E-), B1-, B2-, and (C-) horizons for each tributary. CEC was calculated by adding the respective exchanger composition (Ca, Mg, Na, K, Al, H) for each horizon and for all mineral horizons respectively.

Typically, soils in the Catskills are classified as Inceptisols (see chapter 2) with O-, B-, and C-horizons. But the deep soil pits in Acid Biscuit and West Biscuit are definitely Spodosols with a clearly defined elluvial (E-horizon) and alluvial horizon (B_h-horizon). Signs of redoxiemorphosis could be

detected in both soil pits. In the deep AB soil pit the C-horizon could not be sampled, because of a shallow groundwater table at this site (-0.5 m).

In general, CEC is high in Biscuit Brook O-horizons, but decreases significantly in the mineral soil, where, with values between 3 and 8 $Cmol_C/kg$, CEC has to be classified as low.

Table 6.6: Results for mean exchanger composition for all three tributaries and for all soil horizons; averaged over 5 soil pits per tributary

Source/Ion	Unit	O Layers	E horizon	Upper B	Lower B	C
AB Mean Ca	$Cmoles_c/kg$	1.60		0.06	0.06	
AB Mean Mg	$Cmoles_c/kg$	0.59		0.03	0.01	
AB Mean Na	$Cmoles_c/kg$	0.06		0.01	0.01	
AB Mean K	$Cmoles_c/kg$	0.60		0.03	0.01	
AB Mean Al	$Cmoles_c/kg$	13.2		4.2	1.0	
AB Mean H	$Cmoles_c/kg$	6.2		0.9	0.2	
BB Mean Ca	$Cmoles_c/kg$	4.44		0.15	0.07	0.02
BB Mean Mg	$Cmoles_c/kg$	1.12		0.10	0.03	0.01
BB Mean Na	$Cmoles_c/kg$	0.05		0.01	0.01	0.01
BB Mean K	$Cmoles_c/kg$	0.80		0.11	0.05	0.02
BB Mean Al	$Cmoles_c/kg$	6.8		8.3	4.2	1.3
BB Mean H	$Cmoles_c/kg$	6.0		1.8	0.3	2.01E-02
WB Mean Ca	$Cmoles_c/kg$	4.44	0.04	0.09	0.02	0.01
WB Mean Mg	$Cmoles_c/kg$	1.51	0.02	0.07	0.01	0.01
WB Mean Na	$Cmoles_c/kg$	0.09	0.01	0.01	3.55E-03	4.70E-03
WB Mean K	$Cmoles_c/kg$	0.69	0.03	0.06	0.02	0.02
WB Mean Al	$Cmoles_c/kg$	6.0	15.3	6.1	2.2	1.4
WB Mean H	$Cmoles_c/kg$	9.3	4.1	2.3	0.2	0

Table 6.7: Mean cation exchange capacity (CEC) for AB, BB, and WB soil horizons and for all mineral horizons; averaged over 5 soil pits per tributary

	AB mean CEC $Cmoles_c/kg$	BB mean CEC $Cmoles_c/kg$	WB mean CEC $Cmoles_c/kg$
O Layers	22.3	19.1	22.1
E horizon			19.5
Upper B	5.2	10.5	8.7
Lower B	1.3	4.7	2.4
C		1.4	1.5
Mean mineral horizons	3.3	5.5	8.0

AB shows the highest CEC in O-horizons, but cation exchange capacity decreases abruptly to minimal values in the upper B-horizon, as well as in the lower B-horizon.

Figures 6.17 to 6.19 show MEC for O-, B-, and C-horizons for all tributaries respectively and describe the shift of MEC with increasing soil depth.

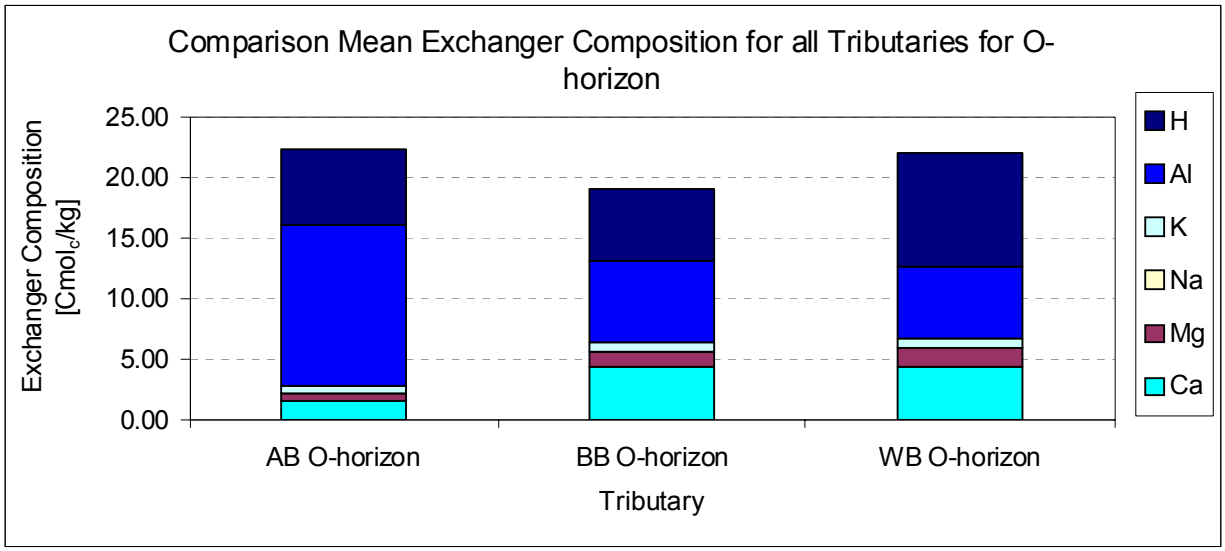

Figure 6.17: Comparison of MEC for all Biscuit Brook tributaries for O-horizon; averaged over 5 soil pits per tributary

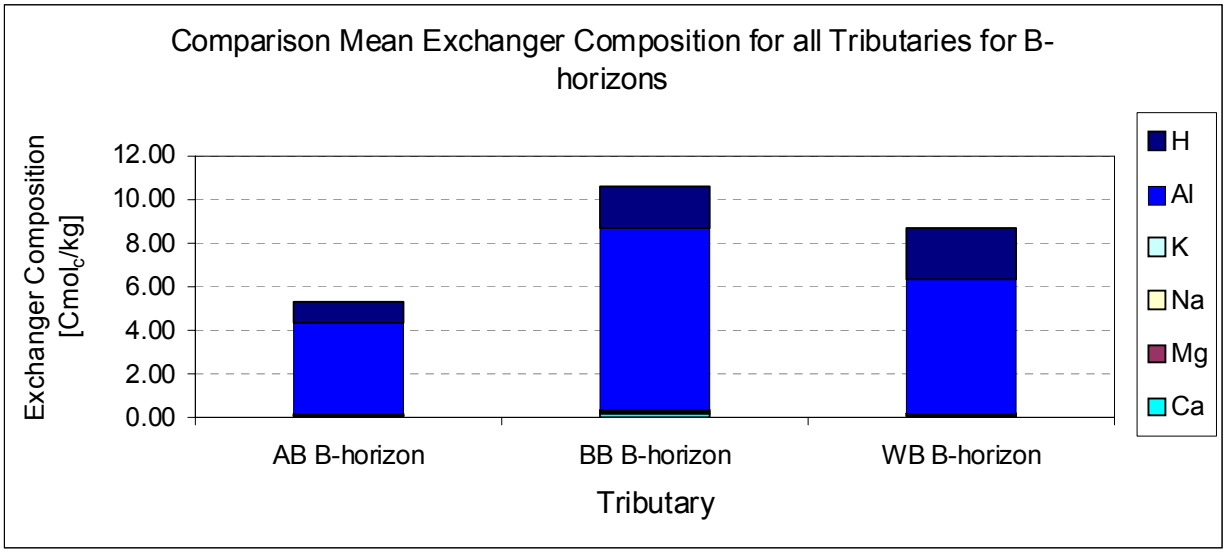

Figure 6.18: Comparison of MEC for all Biscuit Brook tributaries for B-horizon; averaged over 5 soil pits per tributary

In the organic horizon, base cations occupy a significant amount of exchanger sites, at least in BB and WB; the dominant exchangeable cation is H^+, closely followed by Al^{3+} and Ca^{2+}. In AB O-horizons, base cations make up only a minor part of MEC. In the B-horizons of all tributaries base cations are practically insignificant, and Al^{3+} gains importance as the dominant exchangeable cation, followed by H^+. In the C-horizon, solely Al^{3+} dominates the exchange sites. These results clearly show that no till layers were present in the chosen soil pits.

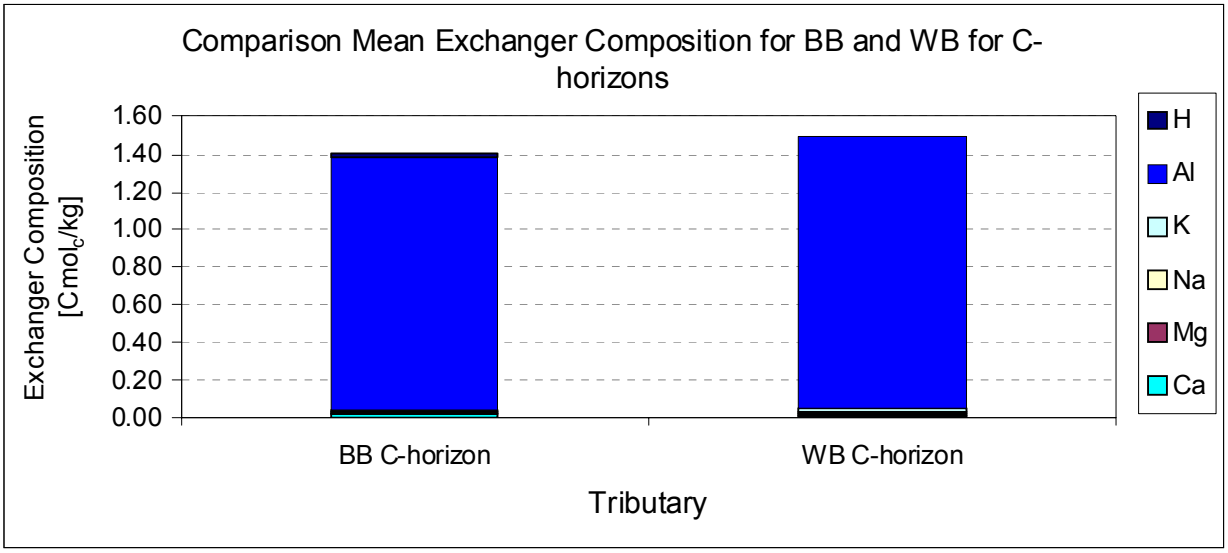

Figure 6.19: Comparison of MEC for BB and WB tributaries for C-horizon; averaged over 5 soil pits per tributary; no C-horizon sample from AB were available because of intrusion of groundwater

6.5 Conclusions

In the previous chapter sufficient evidence was shown to confirm the presence of different water types with different water chemistry and individual $\delta^{18}O$ signatures.

Generally, BB and WB are more basic, with pH-values between 6 and 7. Calcium concentrations are relatively high, and pCO_2 values are low. The more acidic tributary, AB, has pH-values < 5, with low Calcium concentrations, high Al^{3+} concentrations and high pCO_2 values. These discrepancies reflect different levels of acidification, which is also

supported by the respective mean exchanger composition and cation exchange capacity in each tributary.

Thus, our working hypothesis was that these different acidification levels are caused by variable buffer capacities, which originate from spatial variability of till depositions. These deposits are practically the only source of Calcite in the Catskills (COSTELLO-WALKER, 1995). Therefore, soil or till, respectively, acts as major buffer within Biscuit Brook, and not the bedrock.

Till depositions reflect the flow path of former glaciers during the last glaciation. Referring back to figure 2.3, it is noticeable that the headwaters of WB and AB, in contrast to BB, do not feature till deposits.

All these results were used to establish a simple, but powerful conceptual model for PHREEQC, which combines hydrology and geochemistry of Biscuit Brook.

7 Geochemical Model Biscuit Brook

7.1 Conceptual Model based on Field Measurements

The conceptual model is based on the hypothesis that the presence of Calcite or in other words a certain buffer capacity controls the aquatic chemistry in each tributary. But this Calcite is found in the soil and not in the bedrock; hence soil plays a major part in areas with till deposits. Thus, the presence or absence of Calcite controls level of acidification in each tributary: AB is chronically acidified, whereas WB and BB are only episodically acidified.

The concept model, as shown in figure 7.1, consists of 4 modules: (1.) a soil-infiltration module; (1a) a shallow subsurface flow module; (2) a groundwater flow module; (3) mixing of soilwater and groundwater in riparian zones.

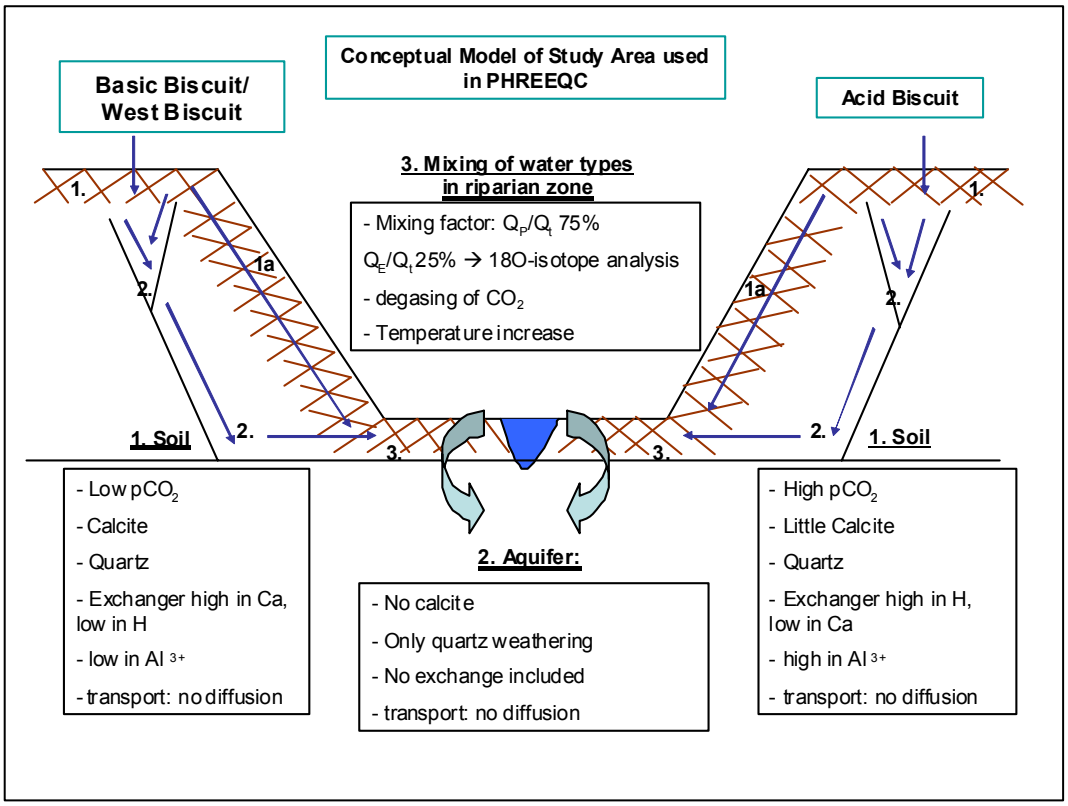

Figure 7.1: Conceptual model of study site used in PHREEQC: 1. Infiltration; 1a Shallow subsurface flow; 2. Groundwater flow; 3. Mixing of 1a and 2 in riparian zone

The model consists of two principle branches: 1. soilwater flow; 2. groundwater flow. The general approach of the model is:

Water enters the system as precipitation and infiltrates, whereat it gets transformed to soilwater by a sequence of chemical reactions (1.). This altered water enters then the groundwater system through a series of sub-vertical fractures and finally follows the flat-lying bedding plane towards the channel area (2.). The groundwater system is understood as chemically unreactive, so only minimal reactions are included. The second branch of the model, shallow subsurface flow (1a), is assumed to be located in the till at the interface of mineral soil and bedrock and is seen as chemically reactive with a sequence of buffering and exchange reactions. In the riparian zone the two principle branches meet again, where they are mixed and again altered through changes in the chemical environment (3.). Ultimately, the mixed water enters the channel and is then streamwater.

This approach was used for all three tributaries, where AB soil is assumed to be very much depleted of Calcite, which can be proved by the mean exchanger composition, in contrast to WB and BB that still have more Calcite in the soil.

7.2 General Modeling Approach

Figure 7.2 shows the general modeling sequence used in this study. First of all, hydrological and chemical data were collected to develop a conceptual model for the study site. Then data was assessed through various USGS sources and the measurement campaign was conducted to refine the established hypothesis. Afterwards, the PHREEQC model was established and complexity was added step by step. Then the model was calibrated with stream and seep water samples taken in June 2008. Since in the measurement campaign only water samples were taken and no hydrometric data was collected, the mixing factors for the confluence of all tributaries are unknown. Therefore, only a sensitivity analysis, and not a validation, was done. In the sensitivity analysis the influence of pCO_2 and CEC were explored further.

7.3 Model Development

Our working strategy was to increase complexity of transport calculations and chemical reactions step by step to explore the impact and necessity of each respective step. This is pointed out in figure 7.3, which shows the approach and sequence of chemical reactions included in the PHREEQC model. After each step Schoeller diagrams were created, and, additionally, objective functions were computed to test, if the respective step can explain the observed concentrations or not.

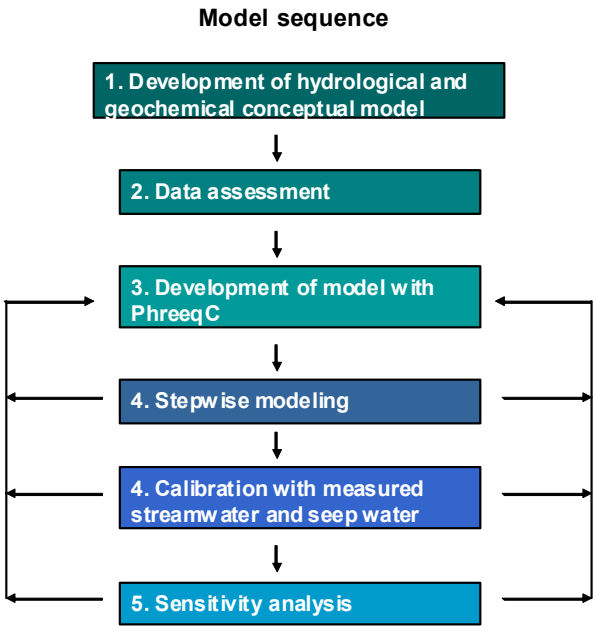

Figure 7.2: General modeling approach and sequence

If it can explain observed concentrations, all following steps are skipped up to cation exchange. Schoeller diagrams illustrate "related" water types, because concentrations are sorted and shown logarithmically. Thus, similar waters have corresponding curves. The objective function used is the square error (SE) meaning the square residues of observed (C_{obs}) and modeled concentrations (C_{mod}).

$$SE = (C_{obs} - C_{\mathrm{mod}})^2 \qquad \text{Eq.(7.1)}$$

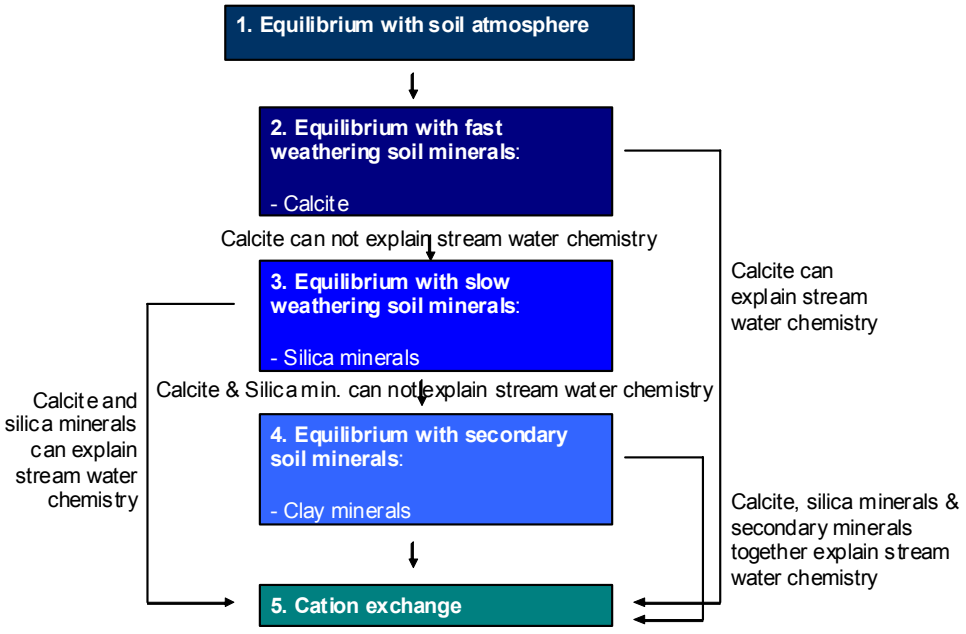

Figure 7.3: Sequence of chemical reactions included in stepwise modeling

Model Development

Model input is mean monthly precipitation chemistry from December 2007, measured at Slide Mt. weather station. This was the most recent

data available. The model starts with equilibrating infiltrating rain water with soil air, where soil pCO_2 ranges from $10^{-1.5}$ to $10^{-2.8}$ atm according to pCO_2 at the respective site after following scale: 10^{-3}: rock outcrop; $10^{-2.5}$ biologically inactive soil; $10^{-1.5}$ biologically active soil (Külls, 2008, personal communication). Then equilibrium reactions with fast weathering minerals, Calcite, are modeled. Target SI values were obtained from the respective stream and seepwater samples taken in June 2008. Here, a flexible approach was used meaning that either stream or seepwater SI were used according to the respective module and tributary. For the chemically reactive soil modules seepwater SI were generally used. For groundwater and mixing, streamwater SI values were used. After the fast weathering minerals, the slowly degradable minerals are included with equilibrium reactions and not with kinetics. Reasons were that SI values for quartz in streamwater were very close to zero, and the uptake of soil ions by soilwater, not the actual weathering process, are fast reactions (BUTTLE et al., 1997). Quartz weathering leads to formation of secondary clay minerals, like Gibbsite and Kaolinite, which both also occur in the study area. But some secondary minerals, like Chlorite, are primary minerals in Catskills, since bedrock is made up from sedimentary rocks. Finally, cation exchange was modeled with explicit exchanger composition, as measured in June 2008.

The mineral composition was altered during the stepwise modeling to explore which of the included minerals really needed to be in the model to explain measured ion concentrations.

7.4 PHREEQC Input

In this section input parameters and the respective PHREEQC inputfiles are described in detail.

7.4.1 PHREEQC Input Parameters

Table 7.1 summarizes general input parameters for the PHREEQC model. Firstly, the input variables for reaction calculations will be introduced. For any speciation or equilibrium calculation a temperature input is required, preferentially the water temperature. Here mean annual air temperature was used, since no water temperature for soil and groundwater was available. For equilibrium calculations the respective pCO_2 and target

saturation indices of included minerals are required. Partial pressure of CO_2 was calculated with the respective equilibrium constants and the temperature and pH dependency of CO_2 equilibria, as described in chapter 5. Target pCO_2 should be given in atm, but expressed as Log{ pCO_2 }. Target SI for the included minerals were obtained by a simple speciation calculation performed with PHREEQC from observed stream and seepwater samples. Cation exchange was calculated with the explicit exchanger composition in mol/L soilwater. This unit asks for some conversions, where inter alia CEC, grain size of Quartz, and porosities are involved. For modeling temperature changes the respective target water temperature is needed. Secondly, transport module input variables are described. The transport module used in PHREEQC is a 1D-disperion-only transport model. All soil parameters, needed for transport modeling, were obtained from the Natural Resources Conservation Service's (NRCS) Soil Survey Geographic database (SSURGO). Mean flow path length was calculated with the hydrology extension of GIS.

Table 7.1: Summary of input parameter required for PHREEQC reaction and transport calculation

Reactions	Input data
Equilibrium	pCO_2, pO_2, target SI for minerals
Cation Exchange	Exchanger composition in mo/L soilwater; porosity (**0.07** Aquifer, **0.34** O-horizon, **0.27** B-horizon); CEC; grain size Quartz
Temperature Increase	Water temperature
Transport	**Input data: 1-D-Dispersion Model, without diffusion**
Infiltration	soil depth (**1m**), velocity (**0.81m/d**), flow time (**1.25d**), CEC O- and B-horizon, porosity O- and B-horizon, dispersivity (**5m**), number of cells (**40**)
Shallow subsurface flow	flowpath length (**400m**), velocity (**3.33m/d**), flow time (**120d**), CEC O- and B-horizon, porosity O- and B-horizon, dispersivity (**5m**),number of cells (**80**)
Groundwater flow	flowpath length (**400m**), velocity (**1.10 m/d**), flow time (**365d)** CEC O-, B- and C-horizon, porosity O-, B- and aquifer, dispersivity (**5m**), number of cells (**80**)
Mixing	Contribution of event and preevent water (**25%, 75%**),Groundwater recharge (1**25mm/a**),porosity (**0.07** Aquifer, **0.34** O-horizon, **0.27** B-horizon)

Then, travel times of the respective water types were estimated. For infiltration, this was done by computations based on permeability of the given soil horizon. In the shallow soilwater module, travel time was estimated by the phase shifts of sine fittings for the analyzed events. Phase shifts were found to be between 3 and 6 months. Results (not shown) were not very satisfying, mainly due to an insufficient amount of data. However, they provide an estimate of the magnitude of travel time. For the groundwater module, results of BURNS et al. (1998) were used, who found groundwater residence times in an adjacent catchment to be between 6-22 months. Now velocities could be calculated. Dispersivities were calculated as in CARSTENS (2007), who estimated dispersivities with a method after KÄSS (2004). Minimal and maximal dispersion coefficients are calculated by means of velocity and distance, and converted into dispersivities. After CARSTENS (2007), a suitable number of cells for dispersive transport modeling with PHREEQC has to be at least two-digit.

Therefore, a cell number was chosen that was high enough, but the resulting calculating time, on the other hand, was not too long. Mean groundwater recharge was estimated after BURNS et al. (1998) to be 125 mm/yr. For the mixing of shallow soilwater and groundwater the mean contribution of event and preevent water was calculated using a two-component hydrograph separation with ^{18}O.

PHREEQC Inputfiles

Infiltration of Soilwater

Basic Biscuit: Table 7.2 presents input variables used in the infiltration module in PHREEQC for Basic Biscuit.

Table 7.2: SI and pCO_2 for equilibrium reactions after observed BB stream and seepwater, and exchanger composition as used in the infiltration module

- Equilibrium with soil air: pCO_2 -2.8

- Calcite: SI -3 → After LSEBB02/ LSTBB03

-Silica minerals:
- K-feldspar -4
- K-mica 5
- Albite -6
- Anorthite -6
- Quartz 0
- $Fe(OH)_3(a)$ 2

→ After LSEBB02/ LSTBB03

- Clay minerals:
- Chlorite (14A) -21
- Gibbsite 2
- Kaolinite 4
- Ca-Montmorillonite 1
- Illite -1

-Ion exchange: mol/L soilwater, averaged over top and mineral soil

CaX_2 1.2E-02	MgX_2 3.3E-03	KX 2.6E-03
NaX 2.0E-04	AlX_3 6.1E-02	HX 2.3E-02

For Basic Biscuit target saturation indices were averaged over seep and streamwater samples, since, generally, seep and stream concentrations were similar. Saturation indices of Al-bearing minerals, especially $SI_{K\text{-}mica}$, $SI_{Gibbsite}$, and $SI_{Kaolinite}$ have very high values, which are usually not observed in natural systems. Reasons may be correlated with the relatively high pH in BB and WB, which is high enough that there is no Aluminum in solution. Therefore, saturation indices are high, because at given BB and WB pH ranges Al^{3+} is insoluble.

West Biscuit: Table 7.3 presents input variables used in the infiltration module in PHREEQC for West Biscuit. Here target SI of LSEWB01, the seepwater sample, were used, since LSEWB01 concentrations were assumed to be more suitable for representing soilwater. It is noticeable, that the saturation indices mentioned above are again too high.

Table 7.3: SI and pCO_2 for equilibrium reactions after observed WB stream and seepwater, and exchanger composition as used in the infiltration module

- Equilibrium with soil air: pCO_2 -3

- Calcite: SI -2 → After LSEWB01/ LSTWB02

-Silica minerals:
- K-feldspar -3
- K-mica 5
- Albite -6
- Anorthite -5
- Quartz 0
- $Fe(OH)_3(a)$ 1

→ After LSEWB01/ LSTWB02

- Clay minerals:
- Chlorite (14A) -17
- Gibbsite 2
- Kaolinite 4
- Ca-Montmorillonite 1
- Illite -1

-Ion exchange: mol/L soilwater, averaged over top and mineral soil

CaX_2 2.5E-02	MgX_2 8.6E-03	KX 4.1E-03
NaX 5.4E-04	AlX_3 5.2E-02	HX 5.7E-02

Acid Biscuit: Table 7.4 presents input variables used in the infiltration module in PHREEQC for Acid Biscuit. In this tributary, the stream and seepwater samples were undersaturated in regard to every mineral, except Quartz.

Table 7.4: SI and pCO_2 for equilibrium reactions after observed AB stream and seepwater, and exchanger composition as used in the infiltration module

-Equilibrium with soil air: pCO_2 -2.5

- Calcite: SI -7 → after LSEAB01/ LSTAB03

-Silica minerals:
- K-feldspar -9
- K-mica -5
- Albite -11
- Anorthite -17
- Quart 0
- $Fe(OH)_3(a)$ -1

→ after LSEAB01/ LSTAB03

-Clay minerals:
- Chlorite (14A) -50
- Gibbsite -1
- Kaolinite -2
- Ca-Montmorillonite -6
- Illite -10

-Ion exchange: mol/L soilwater, averaged over top and mineral soil

CaX_2 6.5E-03	MgX_2 2.4E-03	KX 2.4E-03
NaX 3.0E-04	AlX_3 6.4E-02	HX 2.6E-02

Shallow subsurface flow

In this module the same minerals were included and the same saturation indices were used. Cation exchange was included, too. Only transport parameters were changed in the shallow soil flow module, as shown in table 7.1. Therefore input parameters are not shown again.

Groundwater Flow

For groundwater flow, it was assumed that all tributaries have the same input parameters. Calcite is not included in the equilibrium reactions, only Quartz is considered. Partial pressure of CO_2 and O_2 are kept constant, which is questionable, but no closed system was used to keep model structure as simple as possible. There is also no corresponding data available. No cation exchange was taken into consideration in the

groundwater module, because of the extremely low cation exchange capacities observed in the C-horizon of each respective tributary.

Mixing in Riparian Zone

The mixing factors were obtained by the ^{18}O two-component hydrograph separation. A temperature increase was included, where water temperature was increased form the mean annual air temperature to the actual streamwater temperature measured in June 2008. Finally, degasing of CO_2 was simulated according to the pCO_2 in the respective tributary, which was higher in AB and lower in BB and WB.

8 Modeling Results

This chapter presents modeling results for every module, as well as the outcome of a sensitivity analysis. With regard to the approach of stepwise modeling every one of the introduced steps was necessary to explain stream flow chemistry.

Results are shown as Schoeller diagrams to explore relationships between the different waters and to compare modeled with observed concentrations. In Schoeller diagrams concentrations are shown as Log(c), thus only positive absolute errors could be used as objective function in the graphs. But in the summary tables square errors (SE), mean square errors (MSE), absolute errors (AE), and mean absolute errors (MAE) are also listed. Fe concentrations are included for the sake of completeness.

8.1 Infiltration of Soilwater: Module 1

Figure 8.1 to 8.3 show results of modeled infiltrated soilwater for Acid, Basic and West Biscuit, respectively. Tables 8.1 to 8.5 compare modeled pH, temperature, ionic strength, charge, and percent error of charge for modeled soilwater of each tributary with measured stream and seepwater samples. Tables 8.2 to 8.6 introduce modeled soilwater concentrations, as well as observed stream and seepwater concentrations for each tributary. Also presented are used objective functions, SE, AE, MSE and MAE.

8.1.1 Acid Biscuit

Results are generally well, with MSE_{stream} of 3.4E-09 and MAE_{stream} of -9.2E-06 mol/L. In comparison, mean reporting limit was 2.1E-06 mol/L for observed stream and seepwater concentrations. Modeled soilwater has a percent error in charge of -0.3%, which is acceptable. A negative MAE indicates that the model underestimates modeled concentrations in average. In AB streamwater SI values from site LSTAB03 were used as target SI, since LSEAB01, the only seepwater sample from AB, had the lowest observed pH in AB. Therefore, it was not seen as suitable to represent soilwater. Problems occurred primarily with modeled HCO_3^- and NH_4^+ concentrations, which were significantly higher and lower, respectively, than the observed concentrations. For HCO_3^- this is due to a

higher pCO_2 in modeled soilwater than in observed streamwater (see table 8.1). In general, simulated NH_4^+ concentrations are to be regarded with precaution, since most NH_4^+ involving reactions are biotically controlled and thus kinetic reactions, which can not be considered in this work. However, it is well worth mentioning that NH_4^+ concentrations seem to be primarily controlled by exchange reactions, since after cation exchange NH_4^+ concentrations decrease significantly. Another explanation for this discrepancy of modeled and measured Ammonia concentrations could be the unrealistically high measured NH_4^+ concentrations, as for example at site LSEBB04, which is certainly not characteristic for the watershed (LAWRENCE & MCHALE, personal communication, 2009). Figure 8.2, as well as table 8.2, indicates an underestimation for both, Sulphate and Chloride concentrations. One possible reason could be that the chosen input, Slide Mt. December 2007 precipitation, does not quite correspond to observed streamwater in June 2008. But, as mentioned above, more recent precipitation data was not available. Modeled base cation concentrations, as well as Al^{3+} and Silica concentrations, fit well to observed concentrations. NO_3^- concentration also fits well to observed streamwater samples. Ionic strength of the simulated soilwater is underestimated in comparison with measured stream and seepwater, which could result from a shorter contact time of the modeled water. It only represents infiltrated soilwater, and not, like streamwater, a mixture of soil and groundwater with longer contact times. Noticeable is also that simulated soilwater has an opposite excess charge than observed streamwater samples. But remember that streamwater samples were adjusted to charge balance by modifying pCO_2. This also affects HCO_3 concentrations, and ultimately charge.

Table 8.1: Comparison of pH, temperature, ionic strength, charge and percent error of charge for modeled AB soilwater (solution 20) and measured stream (LSTAB03) and seepwater (LSEAB01) samples

	Units	Solution 20	LSTAB03	LSEAB01
pH	*pH units*	5.10	4.68	4.52
temp	*°C*	5.06	10.8	11.3
ionic strength	*eq/L*	5.09E-05	1.83E-04	1.66E-04
charge	*eq/L*	-3.00E-07	7.62E-12	6.7E-12
pct_err	*%*	-0.29	0.00E+00	0.00E+00

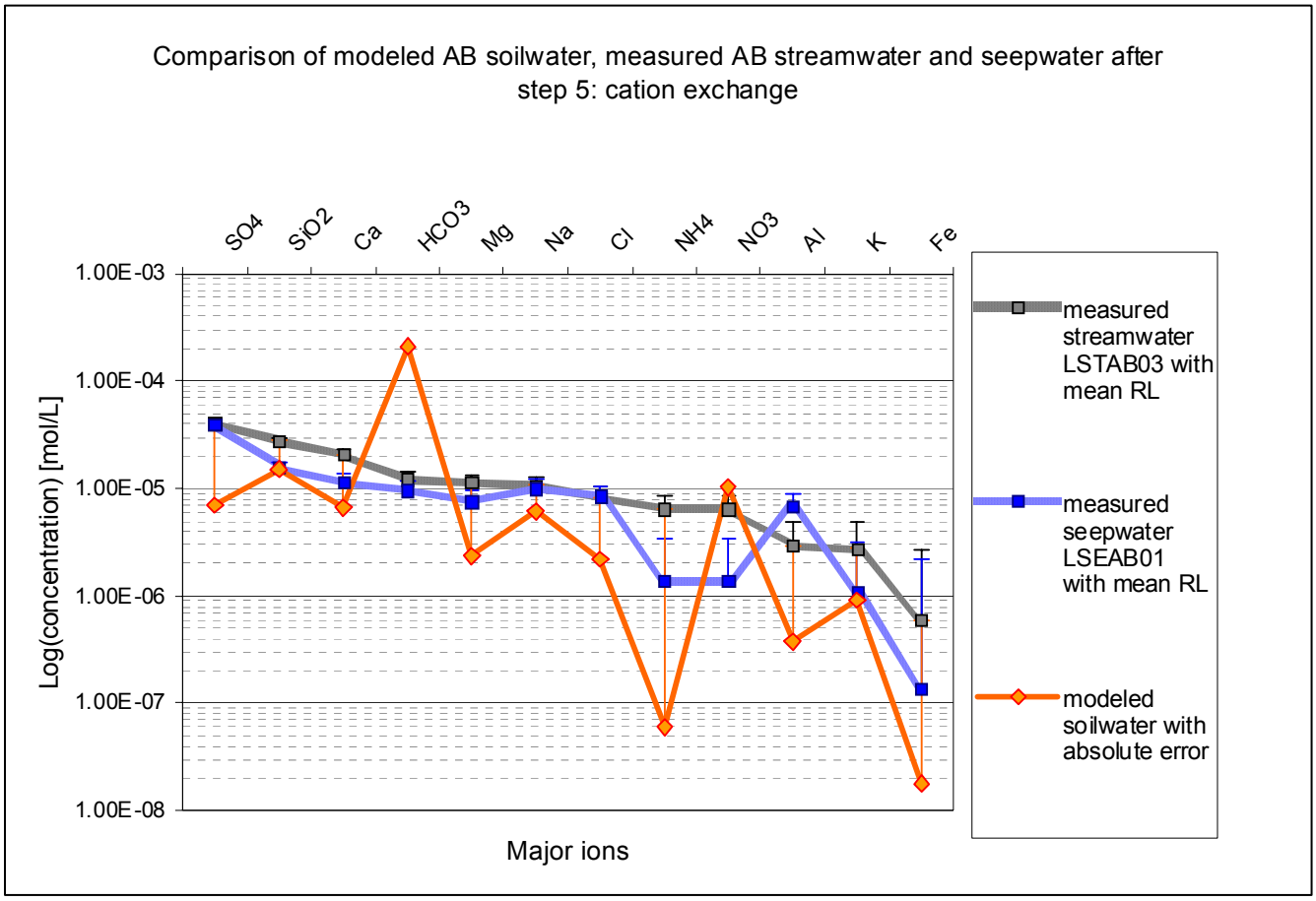

Figure 8.1: Results for modeled infiltrated soilwater in ACIC Biscuit in comparison with observed streamwater and seepwater samples; RL = reporting limit

Table 8.2: Compilation of modeled AB soilwater concentrations, observed streamwater/seepwater concentration; objective functions: SE and AE

		STREAM	SEEP	STREAM Square error	SEEP Square error	STREAM Absolute error
	Modeled	Measured 1	Measured 2	$(Qo_1\text{-}Qm)^2$	$(Qo_2\text{-}Qm)^2$	$(Qo_1\text{-}Qm)$
	mol	*mol*	*mol*			*mol*
SO_4	6.95E-06	4.04E-05	4.00E-05	1.12E-09	1.09E-09	3.34E-05
SiO_2	1.53E-05	2.79E-05	1.57E-05	1.60E-10	1.59E-13	1.27E-05
Ca	6.61E-06	2.08E-05	1.15E-05	2.03E-10	2.38E-11	1.42E-05
HCO_3	2.11E-04	1.21E-05	9.57E-06	3.94E-08	4.04E-08	-1.98E-04
Mg	2.35E-06	1.13E-05	7.56E-06	8.09E-11	2.72E-11	8.99E-06
Na	6.13E-06	1.07E-05	1.00E-05	2.06E-11	1.53E-11	4.54E-06
Cl	2.20E-06	8.39E-06	8.56E-06	3.83E-11	4.04E-11	6.19E-06
NH_4	5.95E-08	6.45E-06	1.38E-06	4.08E-11	1.75E-12	6.39E-06
NO_3	1.03E-05	6.45E-06	1.38E-06	1.49E-11	7.97E-11	-3.86E-06
Al	3.75E-07	2.92E-06	6.94E-06	6.50E-12	4.31E-11	2.55E-06
K	9.08E-07	2.76E-06	1.11E-06	3.44E-12	4.00E-14	1.85E-06
Fe	1.79E-08	5.96E-07	1.36E-07	3.34E-13	1.40E-14	5.78E-07
MSE/MAE				3.42E-09	3.48E-09	-9.24E-06

8.1.2 Basic Biscuit

Generally, Basic Biscuit follows the patterns observed in AB, but MSE_{stream} (5.2E-09) and MAE_{stream} (-1.7E-05) are slightly higher than in AB. Hence, the model also underestimates simulated concentration for Basic Biscuit. HCO_3^- concentrations are overestimated; NH_4^+, SO_4^{2-} and Cl^- concentrations are underestimated by the model. Reasons may be the same as in AB. Simulated BB soilwater also shows a slightly higher pH than observed stream and seepwater samples. Again, modeled base cation, Al^{3+} and Silica concentrations fit well to measured concentrations.

In contrast to AB, simulated ionic strength in BB is of the same order of magnitude than observed ionic strength in stream and seepwater samples. Again, simulated soilwater has a negative charge contrary to the positive charge in observed samples. But percent error of charge is with -0.04% much lower than in AB, probably because of the higher Calcite proportion in BB soils.

Table 8.3: Comparison of pH, temperature, ionic strength, charge and percent error of charge for modeled BB soilwater (solution 20) and measured stream (LSTBB03) and seepwater (LSEBB02) samples

	Units	Solution 20	LSTBB03	LSEBB02
pH	*pH units*	6.88	6.65	6.78
temp	*°C*	5.06	11.0	13.2
ionic strength	*eq/L*	4.12E-04	3.69E-04	4.52E-04
charge	*eq/L*	-2.61E-07	2.43E-10	3.0E-09
pct_err	*%*	-0.04	0.00E+00	0.00E+00

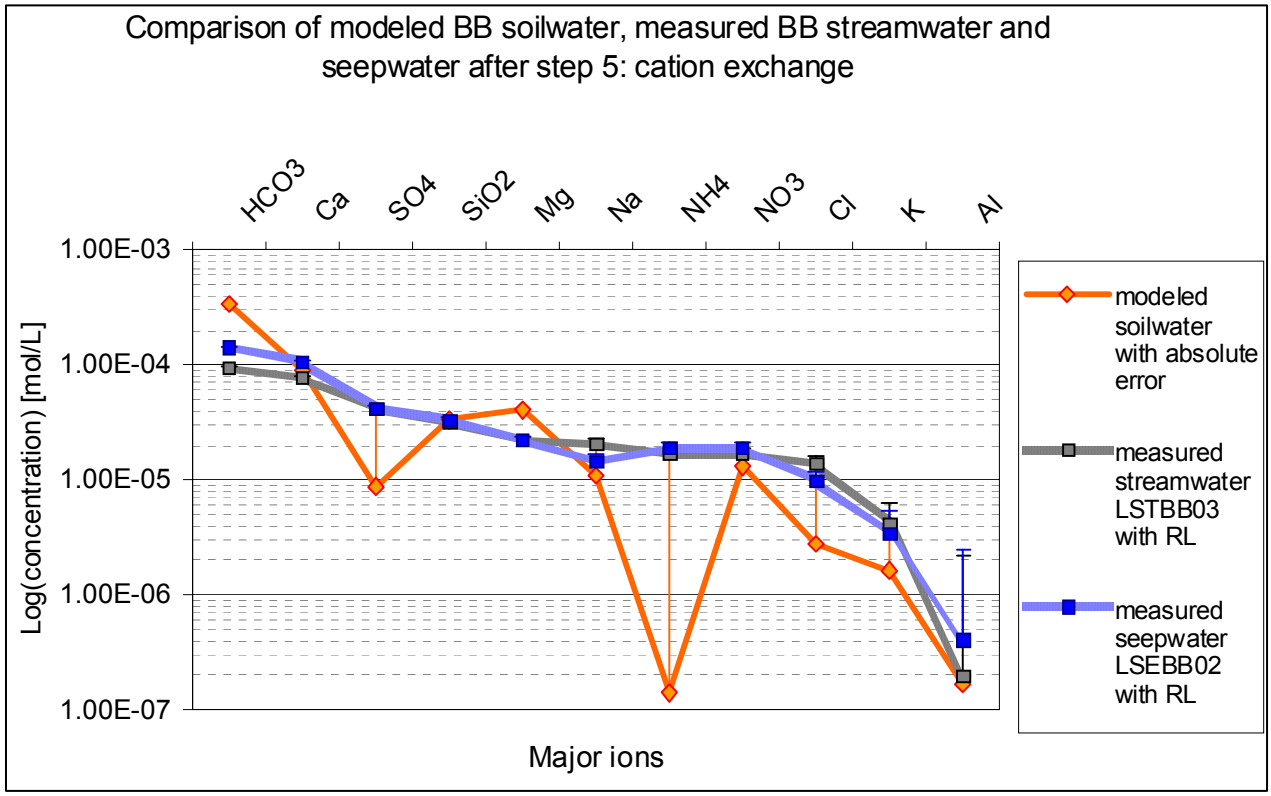

Figure 8.2: Results for modeled infiltrated soilwater in BASIC Biscuit in comparison with observed streamwater and seepwater samples; RL = reporting limit

Table 8.4: Compilation of modeled BB soilwater concentrations, observed streamwater/seepwater concentration; objective functions: SE and AE

		STREAM	SEEP	STREAM Square error	SEEP Square error	STREAM Absolute error
	Modeled	Measured 1	Measured 2	$(Qo_1\text{-}Qm)^2$	$(Qo_2\text{-}Qm)^2$	$(Qo_1\text{-}Qm)$
	mol	mol	mol			*mol*
HCO_3	3.42E-04	9.52E-05	1.43E-04	6.08E-08	3.95E-08	-2.47E-04
Mg	8.92E-05	7.74E-05	1.08E-04	1.40E-10	3.66E-10	-1.18E-05
SO_4	8.83E-06	4.23E-05	4.20E-05	1.12E-09	1.10E-09	3.34E-05
Ca	3.35E-05	3.20E-05	3.34E-05	2.26E-12	2.00E-15	-1.50E-06
SiO_2	4.10E-05	2.22E-05	2.23E-05	3.54E-10	3.52E-10	-1.88E-05
Na	1.10E-05	2.07E-05	1.47E-05	9.35E-11	1.37E-11	9.67E-06
NH_4	1.41E-07	1.70E-05	1.93E-05	2.85E-10	3.68E-10	1.69E-05
Cl	1.31E-05	1.70E-05	1.93E-05	1.54E-11	3.87E-11	3.92E-06
NO_3	2.79E-06	1.40E-05	9.89E-06	1.27E-10	5.04E-11	1.13E-05
K	1.63E-06	4.18E-06	3.42E-06	6.48E-12	3.19E-12	2.55E-06
Al	1.68E-07	1.95E-07	4.06E-07	7.44E-16	5.68E-14	2.73E-08
Fe	3.91E-07	4.46E-08		1.20E-13		-3.47E-07
MSE/MAE				5.24E-09	3.80E-09	-1.68E-05

8.1.3 West Biscuit

Results in WB show a slightly different pattern than as described for AB and BB, as shown in figure 8.3. Once again, HCO_3^- concentrations were overestimated by the model in comparison to observed Hydrogen-Carbonate concentrations, and NH_4^+ concentrations were underestimated. It is remarkable that simulated SO_4^{2-} and Cl^- concentrations fit better to the observed streamwater concentrations than to those in seepwater samples. Since these are seen as conservative ions, one possible explanation among others may be longer residence times in West Biscuit through a higher proportion of deep groundwater to stream flow. Therefore precipitation from December 2008 might represent stream flow in WB better than in AB and BB.

Table 8.5: Comparison of pH, temperature, ionic strength, charge and percent error of charge for modeled WB soilwater (solution 20) and measured stream (LSTWB02) and seepwater (LSEWB01) samples

	Units	Solution 20	LSTWB02	LSEWB01
pH	*pH units*	7.32	6.45	7.22
temp	*°C*	5.06	11.3	11.1
ionic strength	*eq/L*	6.90E-04	1.96E-04	6.52E-04
charge	*eq/L*	-1.80E-07	1.4E-11	1.7E-10
pct_err	*%*	-0.02	0.00E+00	0.00E+00

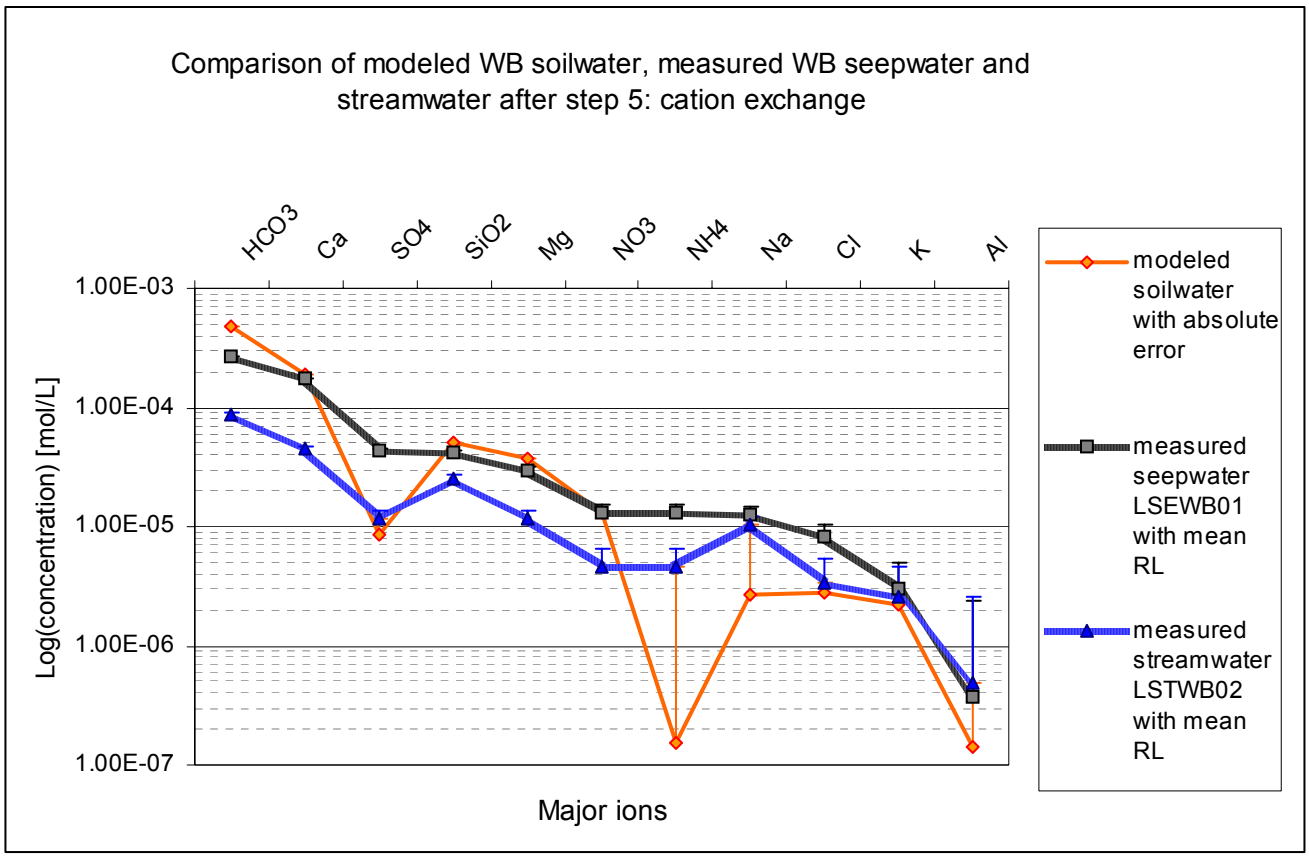

Figure 8.3: Results for modeled infiltrated soilwater in WEST Biscuit in comparison with observed streamwater and seepwater samples; RL = reporting limit

Target SI values in WB were taken from the seepwater sample LSEWB01. Therefore, MAE_{stream} (-5.0E-05) is slightly higher than in BB and AB. However, MSE_{stream} is with 4.7E-09 slightly smaller than in BB and AB. Results for objective functions are shown in table 8.4.

Simulated pH fits with a value of 7.3 well to measured seepwater pH (7.2), but is significantly higher than measured streamwater pH. Ionic strength follows this pattern. Charge is again negative, but lower than in BB. Percent error of charge is also lower and is with -0.02% the lowest in module 1 which is probably due to the higher Calcite proportion. Target $SI_{Calcite}$ was -2, which is closest to zero for all samples taken in Biscuit Brook in June 2008.

Table 8.6: Compilation of modeled WB soilwater concentrations, observed streamwater/seepwater concentration; objective functions: SE and AE

		SEEP	STREAM	SEEP Square error	STREAM Square error	STREAM Absolute error
	Modeled	Measured 1	Measured 2	$(Qo_1\text{-}Qm)^2$	$(Qo_2\text{-}Qm)^2$	$(Qo_1\text{-}Qm)$
	mol	*mol*	*mol*			*mol*
HCO_3	4.88E-04	2.65E-04	8.81E-05	4.98E-08	1.60E-07	-4.00E-04
Ca	1.88E-04	1.74E-04	4.50E-05	2.03E-10	2.06E-08	-1.43E-04
SO_4	8.72E-06	4.30E-05	1.17E-05	1.18E-09	8.80E-12	2.97E-06
SiO_2	5.12E-05	4.12E-05	2.54E-05	1.00E-10	6.67E-10	-2.58E-05
Mg	3.78E-05	2.95E-05	1.17E-05	6.82E-11	6.81E-10	-2.61E-05
NO_3	1.29E-05	1.31E-05	4.55E-06	2.05E-14	7.00E-11	-8.37E-06
NH_4	1.52E-07	1.31E-05	4.55E-06	1.67E-10	1.93E-11	4.39E-06
Na	2.65E-06	1.28E-05	1.03E-05	1.03E-10	5.84E-11	7.64E-06
Cl	2.76E-06	8.24E-06	3.39E-06	3.01E-11	3.94E-13	6.28E-07
K	2.21E-06	2.96E-06	2.54E-06	5.59E-13	1.11E-13	3.33E-07
Al	1.40E-07	3.76E-07	4.84E-07	5.57E-14	1.18E-13	3.44E-07
Fe	2.11E-08		5.57E-08		1.20E-15	3.47E-08
MSE/MAE				4.70E-09	1.52E-08	-4.89E-05

8.2 Shallow Subsurface Flow: Module 1a

8.2.1 Acid Biscuit

Here, observed patterns generally correspond to those described for simulated infiltrated soilwater, as shown in figure 8.4. The model still underestimates simulated soilwater concentrations in comparison to observed streamwater concentrations with a mean absolute error of -1.2E-05 (see table 8.8), which is slightly higher than the one calculated for solution 20 in module 1. According to the longer flow path and therefore longer contact time, ionic strength slightly increased in comparison to solution 20.

Table 8.7: Comparison of pH, temperature, ionic strength, charge and percent error of charge for modeled AB soilwater flow (solution 80) and measured stream (LSTAB03) and seepwater (LSEAB01) samples

	Units	Solution 80	LSTAB03	LSEAB01
pH	*pH units*	4.90	4.68	4.52
temp	*°C*	5.06	10.8	11.3
ionic strength	*eq/L*	6.70E-05	1.83E-04	1.66E-04
charge	*eq/L*	-2.91E-07	7.62E-12	6.7E-12
pct_err	*%*	-0.34	0.00E+00	0.00E+00

The model still overestimates simulated HCO_3^- concentrations in comparison to observed streamwater concentrations, and underestimates NH_4^+, SO_4^{2-} and Cl^- concentrations. But now base cation, Al^{3+} and silica concentrations are also underestimated by the model. This might also be caused by ion exchange reactions as described above. NO_3^- concentrations are again simulated well. It seems that the model can not explain water chemistry in AB as well as in BB and WB, probably because of the lower ionic strength resulting from a smaller Calcite proportion in AB.

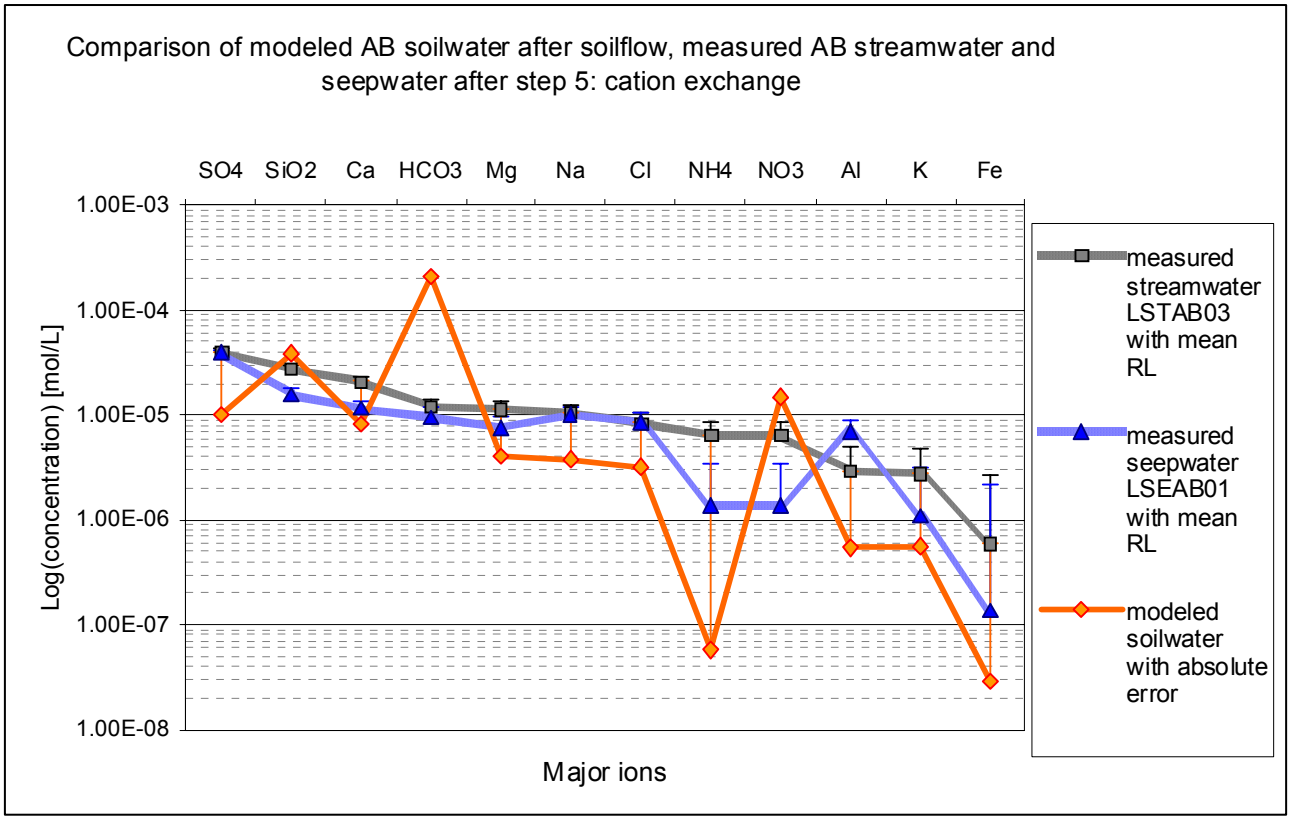

Figure 8.4: Results for modeled soilwater flow in ACID Biscuit in comparison with observed streamwater and seepwater samples; RL = reporting limit; SE = square error

Table 8.8: Compilation of modeled AB soilwater flow concentrations, observed streamwater/seepwater concentration; objective functions: SE and AE

		STREAM	SEEP	STREAM Square error	SEEP Square error	STREAM Absolute error
	Modeled	Measured 1	Measured 2	$(Qo_1-Qm)^2$	$(Qo_2-Qm)^2$	(Qo_1-Qm)
	mol	*mol*	*mol*			*mol*
SO_4	1.01E-05	4.04E-05	4.00E-05	9.16E-10	8.90E-10	3.03E-05
SiO_2	3.85E-05	2.79E-05	1.57E-05	1.12E-10	5.21E-10	-1.06E-05
Ca	8.18E-06	2.08E-05	1.15E-05	1.60E-10	1.09E-11	1.27E-05
HCO_3	2.08E-04	1.21E-05	9.57E-06	3.83E-08	3.93E-08	-1.96E-04
Mg	4.06E-06	1.13E-05	7.56E-06	5.30E-11	1.23E-11	7.28E-06
Na	3.80E-06	1.07E-05	1.00E-05	4.72E-11	3.90E-11	6.87E-06
Cl	3.21E-06	8.39E-06	8.56E-06	2.69E-11	2.86E-11	5.18E-06
NH_4	5.80E-08	6.45E-06	1.38E-06	4.08E-11	1.75E-12	6.39E-06
NO_3	1.50E-05	6.45E-06	1.38E-06	7.33E-11	1.86E-10	-8.56E-06
Al	5.40E-07	2.92E-06	6.94E-06	5.68E-12	4.10E-11	2.38E-06
K	5.63E-07	2.76E-06	1.11E-06	4.83E-12	2.97E-13	2.20E-06
Fe	2.91E-08	5.96E-07	1.36E-07	3.21E-13	1.15E-14	5.67E-07
MSE/MAE				3.31E-09	3.42E-09	-1.17E-05

8.2.2 Basic Biscuit

Basic Biscuit shallow subsurface flow chemistry also corresponds to BB soilwater in module 1. Results are presented in figure 8.5 and tables 8.9 and 8.10. The model still overestimates simulated HCO_3^- concentrations in comparison to observed streamwater concentrations, and underestimates NH_4^+, SO_4^{2-} and Cl^- concentrations. NO_3^- concentrations are modeled well. Base cation concentrations generally fit well to measured streamwater concentrations, except Mg^{2+} concentration which is overestimated. It could be proved with the stepwise modeling approach that cation exchange is responsible for significant increase in Mg^{2+} concentrations. Al^{3+} and silica concentrations also correspond well to respective measured concentrations.

Table 8.9: Comparison of pH, temperature, ionic strength, charge and percent error of charge for modeled BB soilwater flow (solution 80) and measured stream (LSTBB03) and seepwater (LSEBB02) samples

	Units	Solution 80	LSTBB03	LSEBB02
pH	*pH units*	6.72	6.65	6.78
temp	*°C*	5.06	11.0	13.2
ionic strength	*eq/L*	5.54E-04	3.69E-04	4.52E-04
charge	*eq/L*	-2.90E-07	2.4E-10	3.0E-09
pct_err	*%*	-0.04	0.0E+00	0.00E+00

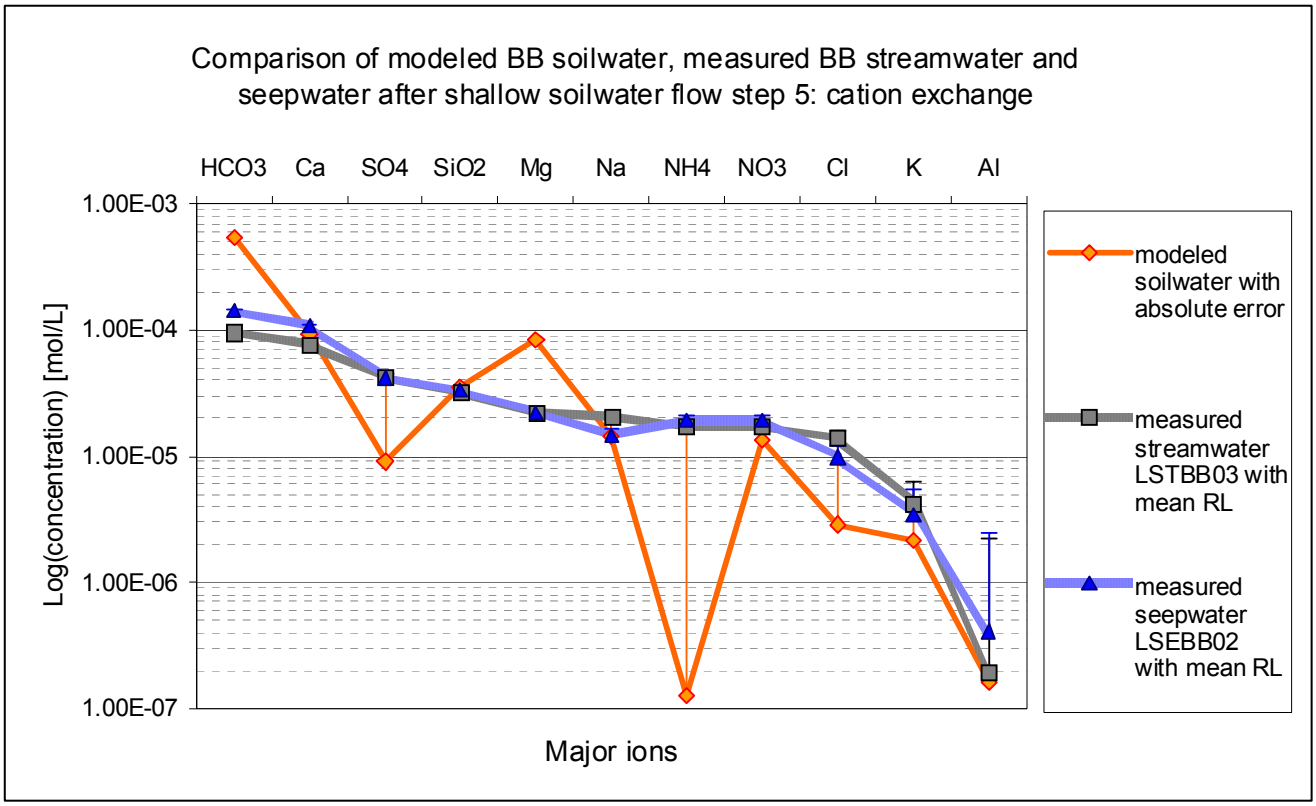

Figure 8.5: Results for modeled soilwater flow in BASIC Biscuit in comparison with observed streamwater and seepwater samples; RL = reporting limit

Table 8.10: Compilation of modeled BB soilwater flow concentrations, observed streamwater/seepwater concentration; objective functions: SE and AE

		STREAM	SEEP	STREAM Square error	SEEP Square error	STREAM Absolute error
	Modeled	Measured 1	Measured 2	$(Qo_1\text{-}Qm)^2$	$(Qo_2\text{-}Qm)^2$	$(Qo_1\text{-}Qm)$
	mol	mol	mol			*mol*
HCO_3	5.39E-04	9.52E-05	1.43E-04	1.97E-07	1.57E-07	-4.44E-04
Mg	9.28E-05	7.74E-05	1.08E-04	2.39E-10	2.40E-10	-1.55E-05
SO_4	9.04E-06	4.23E-05	4.20E-05	1.10E-09	1.09E-09	3.32E-05
Ca	3.45E-05	3.20E-05	3.34E-05	6.52E-12	1.20E-12	-2.55E-06
SiO_2	8.37E-05	2.22E-05	2.23E-05	3.78E-09	3.77E-09	-6.15E-05
Na	1.44E-05	2.07E-05	1.47E-05	3.94E-11	9.16E-14	6.27E-06
NH_4	1.27E-07	1.70E-05	1.93E-05	2.86E-10	3.69E-10	1.69E-05
Cl	1.34E-05	1.70E-05	1.93E-05	1.33E-11	3.53E-11	3.64E-06
NO_3	2.86E-06	1.40E-05	9.89E-06	1.25E-10	4.95E-11	1.12E-05
K	2.13E-06	4.18E-06	3.42E-06	4.18E-12	1.65E-12	2.04E-06
Al	1.60E-07	1.95E-07	4.06E-07	1.20E-15	6.03E-14	3.46E-08
Fe	5.16E-07	4.46E-08		2.22E-13		-4.71E-07
MSE/MAE				1.69E-08	1.48E-08	-3.75E-05

Simulated pH values fit well to measured pH in stream and seepwater, as well as ionic strength. Modeled soilwater still has a negative charge, but overall a very low percent error in charge with -0.04%, corresponding to the error in module 1. However, MSE and MAE increased in comparison to soilwater in module 1, because of the increase in Magnesia.

8.2.3 West Biscuit

As shown in figure 8.6 and tables 8.11 and 8.12, patterns of WB shallow subsurface flow correspond to those observed for simulated BB soilwater flow. Simulated HCO_3^- concentrations are still too high in comparison with observed streamwater concentrations, and the model underestimates NH_4^+, SO_4^{2-} and Cl^- concentrations. Simulated Sulphate and Chlorite concentrations fit well to streamwater concentrations, but are too low in comparison to seepwater. This phenomenon was already observed in module 1. Base cation concentrations generally fit well to measured streamwater concentrations, except Mg^{2+} concentration, which is too high. Here, cation exchange is again responsible for significant increase in Mg^{2+} concentrations, as proved by the stepwise modeling approach. Silica concentrations also correspond well to respective measured concentrations, but now Al^{3+} concentrations are underestimated by the model. Al^{3+} decrease is also due to cation exchange reactions. NO_3^- fits also well, as in all simulated waters.

Simulated pH values in shallow subsurface flow are lower than in the modeled soilwater in module 1, but still fit well to observed seepwater pH values. It slowly converges towards streamwater pH. According to the longer flow path, ionic strength also increased somewhat. It is interesting that simulated charge of soilwater in module 1a is now positive, probably due to the increase in Magnesia concentration. Therefore, the percent error is practically zero (see table 8.11).

Table 8.11: Comparison of pH, temperature, ionic strength, charge and percent error of charge for modeled WB soilwater flow (solution 80) and measured stream (LSTWB02) and seepwater (LSEWB01) samples

	Units	Solution 80	LSTWB02	LSEWB01
pH	*pH units*	7.04	6.45	7.22
temp	*°C*	5.06	11.3	11.1
ionic strength	*eq/L*	1.12E-03	1.96E-04	6.52E-04
charge	*eq/L*	2.01E-08	1.4E-11	1.7E-10
pct_err	*%*	0.00	0.0E+00	0.00E+00

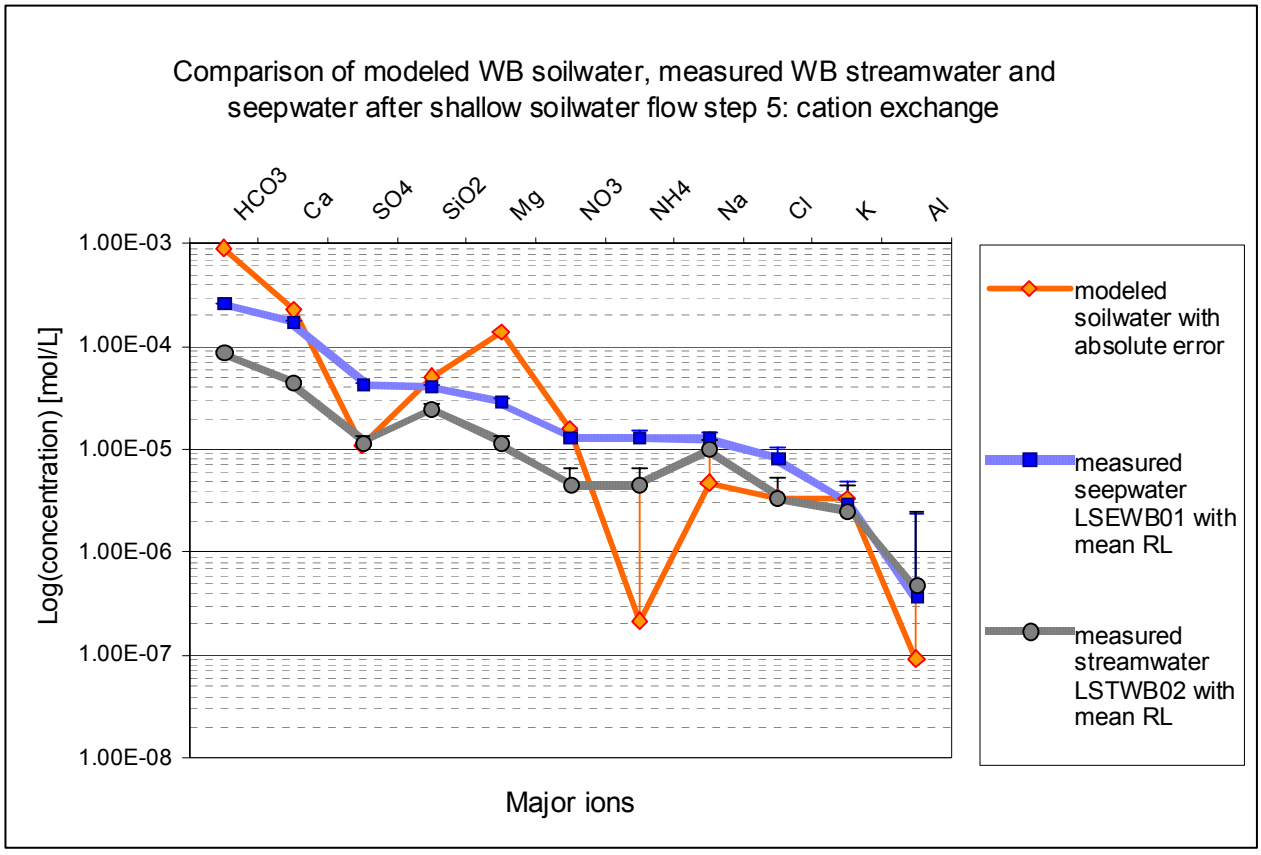

Figure 8.6: Results for modeled soilwater flow in WEST Biscuit in comparison with observed streamwater and seepwater samples; RL = reporting limit

Table 8.12: Compilation of modeled WB soilwater flow concentrations, observed streamwater/seepwater concentration; objective functions: SE and AE

		SEEP	STREAM	SEEP Square error	STREAM Square error	STREAM Absolute error
	Modeled *mol*	Measured 1 *mol*	Measured 2 *mol*	$(Qo_1\text{-}Qm)^2$	$(Qo_2\text{-}Qm)^2$	$(Qo_1\text{-}Qm)$ *mol*
HCO_3	9.05E-04	2.65E-04	8.81E-05	4.10E-07	6.67E-07	-8.17E-04
Ca	2.28E-04	1.74E-04	4.50E-05	2.87E-09	3.34E-08	-1.83E-04
SO_4	1.08E-05	4.30E-05	1.17E-05	1.04E-09	7.80E-13	8.83E-07
SiO_2	5.12E-05	4.12E-05	2.54E-05	9.96E-11	6.64E-10	-2.58E-05
Mg	1.40E-04	2.95E-05	1.17E-05	1.22E-08	1.64E-08	-1.28E-04
NO_3	1.60E-05	1.31E-05	4.55E-06	8.56E-12	1.31E-10	-1.14E-05
NH_4	2.19E-07	1.31E-05	4.55E-06	1.65E-10	1.87E-11	4.33E-06
Na	4.74E-06	1.28E-05	1.03E-05	6.48E-11	3.08E-11	5.55E-06
Cl	3.41E-06	8.24E-06	3.39E-06	2.33E-11	8.01E-16	-2.83E-08
K	3.35E-06	2.96E-06	2.54E-06	1.58E-13	6.59E-13	-8.12E-07
Al	9.28E-08	3.76E-07	4.84E-07	8.02E-14	1.53E-13	3.91E-07
Fe	3.07E-08		5.57E-08		6.27E-16	2.50E-08
MSE/MAE				3.87E-08	5.98E-08	-9.62E-05

MSE_{stream} and MAE_{stream} both increased in comparison to modeled soilwater in module 1, which makes sense, since the longer contact time in module 1a allows simulated weathering reactions to proceed completely.

8.3 Groundwater Flow: Module 2

Tables 8.13, 8.15, and 8.17 show results for simulated pH, temperature, ionic strength, charge, and percent error for each respective tributary. Figures 8.7 to 8.9 present Schoeller diagrams for AB, BB, and WB, respectively. Tables 8.14 to 8.18 summarize simulated concentrations and measured stream and seepwater concentrations, as well as MSE and MAE.

8.3.1 Acid Biscuit

Simulated AB groundwater concentrations show a different pattern as modeled AB soilwater concentrations, because only Quartz was included in the equilibrium reactions and cation exchange was not taken into consideration. HCO_3^- and SO_4^{2-} concentrations are still too high and low, respectively, in comparison with measured stream and seepwater concentrations, but now concentrations of all base cations are too low, as well as simulated Al^{3+} concentrations. The model therefore successfully simulates groundwater that is chemically more unreactive than the respective soilwater. It is also noticeable that NH_4^+ concentrations now fit much better to observed streamwater concentrations than in the modules described above, since no cation exchange was included. Even though simulated base cation concentrations have higher errors in the groundwater module, MSE and MAE are still the same as in module 1a, probably due to the better fit of NH_4^+ concentrations. Simulated pH and ionic strength for AB groundwater were lower as in the soilwater modules because of reasons mentioned above.

Table 8.13: Comparison of pH, temperature, ionic strength, charge and percent error of charge for modeled AB groundwater flow (solution 80) and measured stream (LSTAB03) and seepwater (LSEAB01) samples

	Units	Solution 80	LSTAB03	LSEAB01
pH	*pH units*	4.73	4.68	4.52
temp	*°C*	5.06	10.8	11.3
ionic strength	*eq/L*	5.06E-05	1.83E-04	1.66E-04
charge	*eq/L*	-2.23E-07	7.62E-12	6.7E-12
pct_err	*%*	-0.31	0.00E+00	0.00E+00

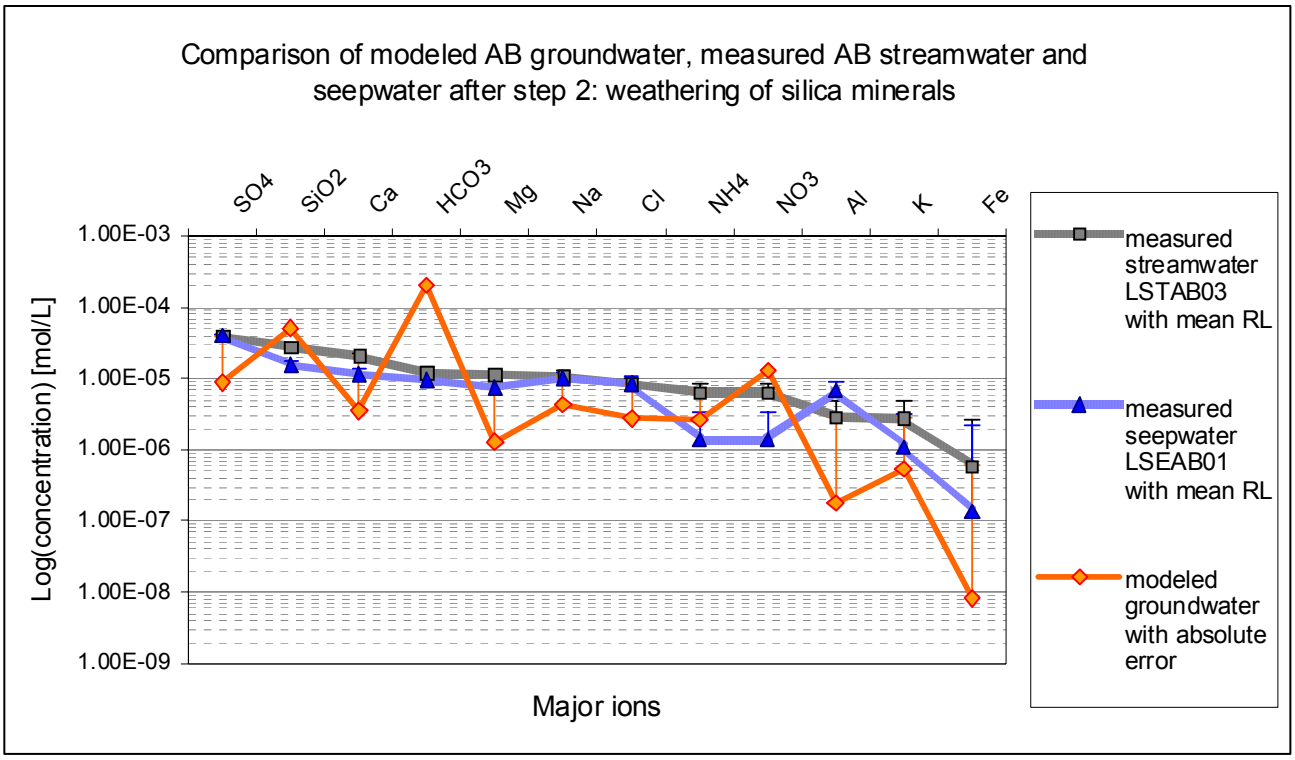

Figure 8.7: Results for modeled groundwater flow in ACID Biscuit in comparison with observed streamwater and seepwater samples; RL = reporting limit

Table 8.14: Compilation of modeled AB groundwater flow concentrations, observed streamwater/seepwater concentration

		STREAM	SEEP	STREAM SE	SEEP SE	STREAM AE
	Modeled	Measured 1	Measured 2	$(Qo_1\text{-}Qm)^2$	$(Qo_2\text{-}Qm)^2$	$(Qo_1\text{-}Qm)$
	mol	mol	mol	mol	mol	mol
SO_4	8.78E-06	4.04E-05	4.00E-05	1.00E-09	9.73E-10	3.16E-05
SiO_2	5.12E-05	2.79E-05	1.57E-05	5.40E-10	1.26E-09	-2.32E-05
Ca	3.53E-06	2.08E-05	1.15E-05	3.00E-10	6.32E-11	1.73E-05
HCO_3	2.06E-04	1.21E-05	9.57E-06	3.76E-08	3.86E-08	-1.94E-04
Mg	1.29E-06	1.13E-05	7.56E-06	1.01E-10	3.93E-11	1.01E-05
Na	4.26E-06	1.07E-05	1.00E-05	4.11E-11	3.34E-11	6.41E-06
Cl	2.78E-06	8.39E-06	8.56E-06	3.15E-11	3.34E-11	5.61E-06
NH_4	2.70E-06	6.45E-06	1.38E-06	1.41E-11	1.74E-12	3.75E-06
NO_3	1.30E-05	6.45E-06	1.38E-06	4.28E-11	1.35E-10	-6.54E-06
Al	1.80E-07	2.92E-06	6.94E-06	7.53E-12	4.57E-11	2.74E-06
K	5.46E-07	2.76E-06	1.11E-06	4.91E-12	3.16E-13	2.22E-06
Fe	8.29E-09	5.96E-07	1.36E-07	3.45E-13	1.63E-14	5.87E-07
MSE/MAE				3.31E-09	3.43E-09	-1.20E-05

8.3.2 Basic Biscuit

Modeled pH and ionic strength are significantly lower in the groundwater module than in the soil modules and in measured stream and seepwater. Thus, it was also possible to successfully model a more unreactive groundwater for BB. Because of the missing Calcite percent error in charge is with -0.2% much higher for the simulated groundwater than for the soilwater, but it is still an acceptable result. Surprisingly, calculated MSE and MAE are both significantly lower than in the simulated soilwater. Figure 8.8 makes clear why: HCO_3^- and NH_4^+ fit pretty well now, which results in lower errors. With regard to base cation concentrations, simulated BB groundwater follows the same pattern as AB groundwater. They are generally lower than in the soil modules and in stream and seepwater samples. But in contrast to AB, Al^{3+} concentrations still fit fairly well.

Table 8.15: Comparison of pH, temperature, ionic strength, charge and percent error of charge for modeled BB groundwater flow (solution 80) and measured stream (LSTBB03) and seepwater (LSEBB02) samples

	Units	Solution 80	LSTBB03	LSEBB02
pH	*pH units*	6.18	6.65	6.78
temp	*°C*	5.06	11.0	13.2
ionic strength	*eq/L*	1.99E-04	3.69E-04	4.52E-04
charge	*eq/L*	-4.38E-07	2.43E-10	3.0E-09
pct_err	*%*	-0.17	0.00E+00	0.00E+00

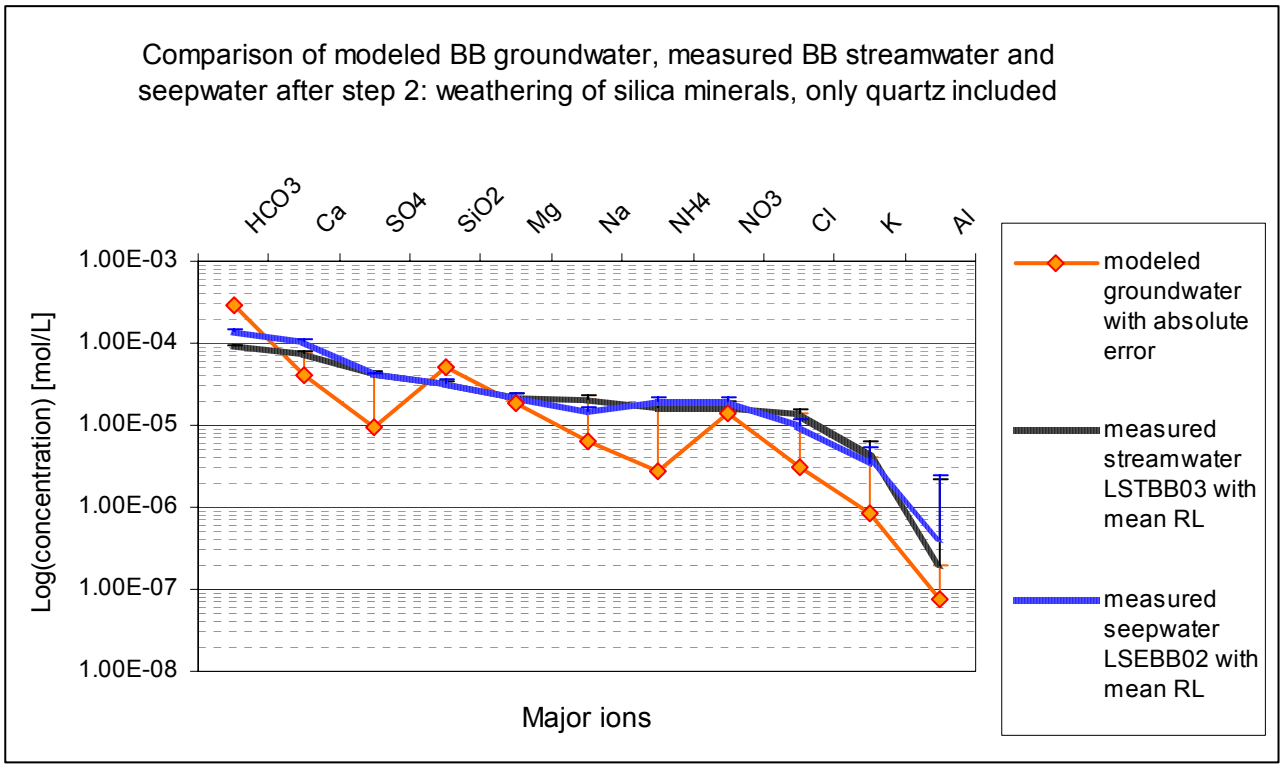

Figure 8.8: Results for modeled groundwater flow in BASIC Biscuit in comparison with observed streamwater and seepwater samples; RL = reporting limit

Table 8.16: Compilation of modeled BB groundwater flow concentrations, observed streamwater/seepwater concentration; objective functions: SE = square error and AE= absolute error

		STREAM	SEEP	STREAM SE	SEEP SE	STREAM AE
	Modeled	Measured 1	Measured 2	$(Qo_1-Qm)^2$	$(Qo_2-Qm)^2$	(Qo_1-Qm)
	mol	mol	mol			*mol*
HCO_3	2.97E-04	9.52E-05	1.43E-04	4.08E-08	2.38E-08	-2.02E-04
Mg	4.08E-05	7.74E-05	1.08E-04	1.34E-09	4.56E-09	3.66E-05
SO_4	9.47E-06	4.23E-05	4.20E-05	1.08E-09	1.06E-09	3.28E-05
Ca	5.12E-05	3.20E-05	3.34E-05	3.68E-10	3.14E-10	-1.92E-05
SiO_2	1.87E-05	2.22E-05	2.23E-05	1.20E-11	1.25E-11	3.47E-06
Na	6.41E-06	2.07E-05	1.47E-05	2.04E-10	6.88E-11	1.43E-05
NH_4	2.73E-06	1.70E-05	1.93E-05	2.04E-10	2.75E-10	1.43E-05
Cl	1.40E-05	1.70E-05	1.93E-05	8.98E-12	2.80E-11	3.00E-06
NO_3	2.99E-06	1.40E-05	9.89E-06	1.22E-10	4.76E-11	1.11E-05
K	8.64E-07	4.18E-06	3.42E-06	1.10E-11	6.51E-12	3.31E-06
Al	7.61E-08	1.95E-07	4.06E-07	1.41E-14	1.09E-13	1.19E-07
Fe	1.77E-07	4.46E-08		1.75E-14		-1.32E-07
MSE/MAE				3.68E-09	2.74E-09	-8.54E-06

8.3.3 West Biscuit

Simulated WB groundwater concentrations follow similar patterns than AB and WB groundwater concentrations. Modeled pH and ionic strength fit now perfectly to observed streamwater. The percent error in charge is higher than in the soil modules, since Calcite was excluded, but it is with -0.1% still low. Figure 8.9 shows how well modeled groundwater concentrations represent measured streamwater concentrations. Now, one can really see a great affinity between the shapes of the presented curves. Only Al^{3+} and Na^{+} are somewhat underestimated by the model, because of the exclusion of all other silica and clay minerals, except for Quartz.

Table 8.17: Comparison of pH, temperature, ionic strength, charge and percent error of charge for modeled BB groundwater flow (solution 80) and measured stream (LSTBB03) and seepwater (LSEBB02) samples

	Units	Solution 80	LSTWB02	LSEWB01
pH	*pH units*	6.45	6.45	7.22
temp	*°C*	5.06	11.3	11.1
ionic strength	*eq/L*	3.24E-04	1.96E-04	6.52E-04
charge	*eq/L*	-4.20E-07	1.4E-11	1.7E-10
pct_err	*%*	-0.10	0.00E+00	0.00E+00

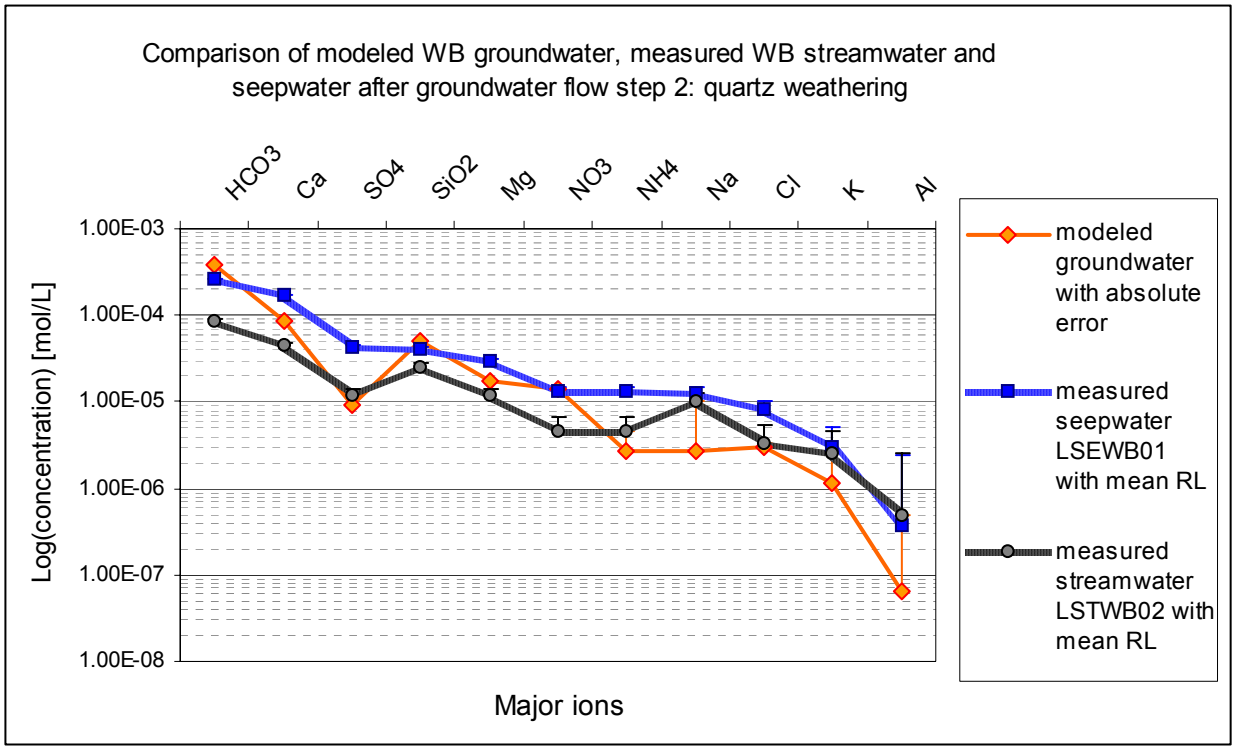

Figure 8.9: Results for modeled groundwater flow in WEST Biscuit in comparison with observed streamwater and seepwater samples; RL = reporting limit

Table 8.18: Compilation of modeled WB groundwater flow concentrations, observed streamwater/seepwater concentration; objective functions: SE = square error and AE= absolute error

		SEEP	STREAM	SEEP SE	STREAM SE	STREAM AE
	Modeled *mol*	Measured 1 *mol*	Measured 2 *mol*	$(Qo_1\text{-}Qm)^2$	$(Qo_2\text{-}Qm)^2$	$(Qo_1\text{-}Qm)$ *mol*
HCO_3	3.80E-04	2.65E-04	8.81E-05	1.33E-08	8.51E-08	-2.92E-04
Ca	8.55E-05	1.74E-04	4.50E-05	7.84E-09	1.65E-09	-4.06E-05
SO_4	9.42E-06	4.30E-05	1.17E-05	1.13E-09	5.17E-12	2.27E-06
SiO_2	5.12E-05	4.12E-05	2.54E-05	9.92E-11	6.63E-10	-2.58E-05
Mg	1.73E-05	2.95E-05	1.17E-05	1.50E-10	3.13E-11	-5.59E-06
NO_3	1.39E-05	1.31E-05	4.55E-06	7.80E-13	8.83E-11	-9.39E-06
NH_4	2.74E-06	1.31E-05	4.55E-06	1.06E-10	3.26E-12	1.81E-06
Na	2.63E-06	1.28E-05	1.03E-05	1.03E-10	5.88E-11	7.67E-06
Cl	2.98E-06	8.24E-06	3.39E-06	2.77E-11	1.66E-13	4.07E-07
K	1.13E-06	2.96E-06	2.54E-06	3.35E-12	2.00E-12	1.42E-06
Al	6.34E-08	3.76E-07	4.84E-07	9.77E-14	1.77E-13	4.21E-07
Fe	9.55E-09		5.57E-08		2.13E-15	4.62E-08
MSE/MAE				2.07E-09	7.30E-09	-2.99E-05

8.4 Mixing Groundwater and Soilwater: Module 3

Here the final modeling results are presented: simulated AB, BB, and WB streamwater. For an easier comprehension stock charts for modeled and measured streamwater concentrations in µeq/L were generated. The advantages of this type of graph are firstly that it is possible to see if the charge balance is even; and secondly it is a very easy to compare modeled and measured water.

8.4.1 Acid Biscuit

Stock charts for measured and modeled AB streamwater, as shown in figure 8.10, make clear that the model has problems explaining low ionic strength AB streamwater chemistry. Total anion concentrations in simulated streamwater are overestimated, whereas cation concentrations are underestimated. Measured streamwater has a positive charge excess, simulated concentration on the contrary a negative charge excess mainly due to the overestimated HCO_3^- concentration.

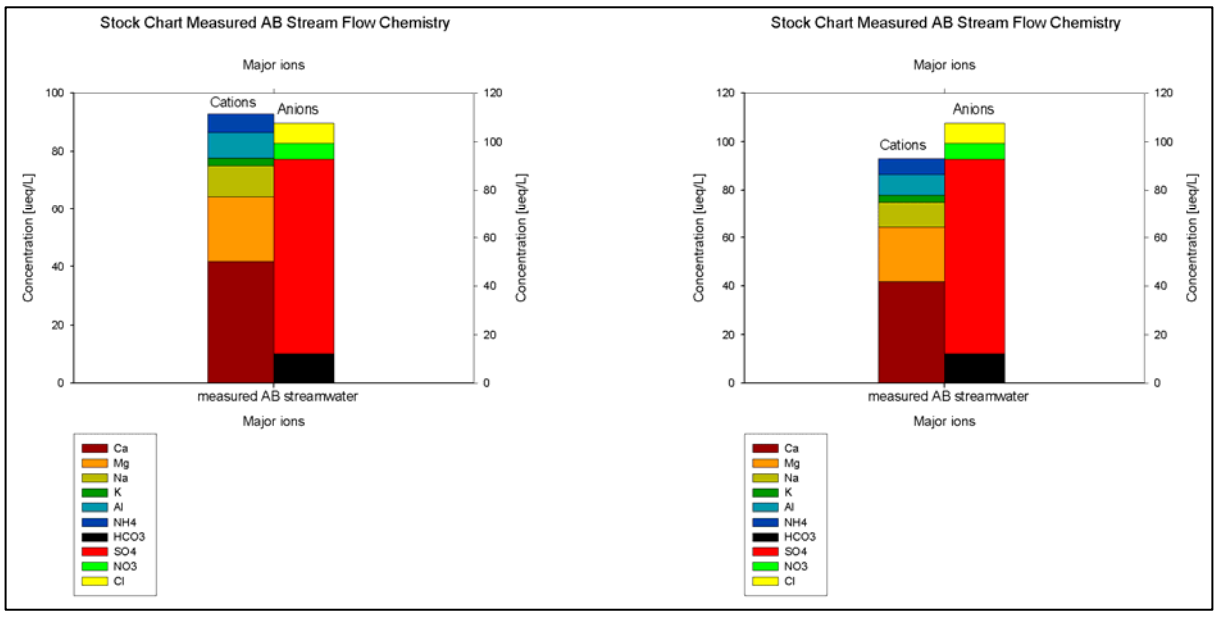

Figure 8.10: Stock charts for modeled and measured anion and cation streamwater concentrations in µeq/L for AB

It is also obvious that in simulated streamwater HCO_3^- is the most dominant anion, but in observed streamwater samples SO_4^{2-} has the highest proportion. These elevated Hydrogen-Carbonate concentrations might be partly caused by an overestimation of simulated pH, as shown in table 8.19.

The underestimation of modeled base cation concentrations is mainly caused by a Calcium concentration that is much too low. But as shown in figure 8.11, all base cation concentrations are slightly underestimated by the model. Simulated cation concentrations follow the pattern: Ca^{2+}> Na^{+}> Mg^{2+}> K^{+}, in contrast to measured concentration, where Ca^{2+}> Mg^{2+} > Na^{+}> K^{+}.

Overall, the results for AB are still acceptable with a percent error in charge of -0.3%, and, as shown in table 20, with a MSE and a MAE of 2.2E-09 and -8.7E-06, respectively.

Table 8.19: Comparison of pH, temperature, ionic strength, charge and percent error of charge for modeled AB streamwater (solution 80) and measured stream (LSTAB03) and seepwater (LSEAB01) samples

	Units	Solution 80	LSTAB03	LSEAB01
pH	*pH units*	4.77	4.68	4.52
temp	*°C*	11	10.8	11.3
ionic strength	*eq/L*	5.44E-05	1.83E-04	1.66E-04
charge	*eq/L*	-2.30E-07	7.62E-12	6.7E-12
pct_err	*%*	-0.30	0.00E+00	0.00E+00

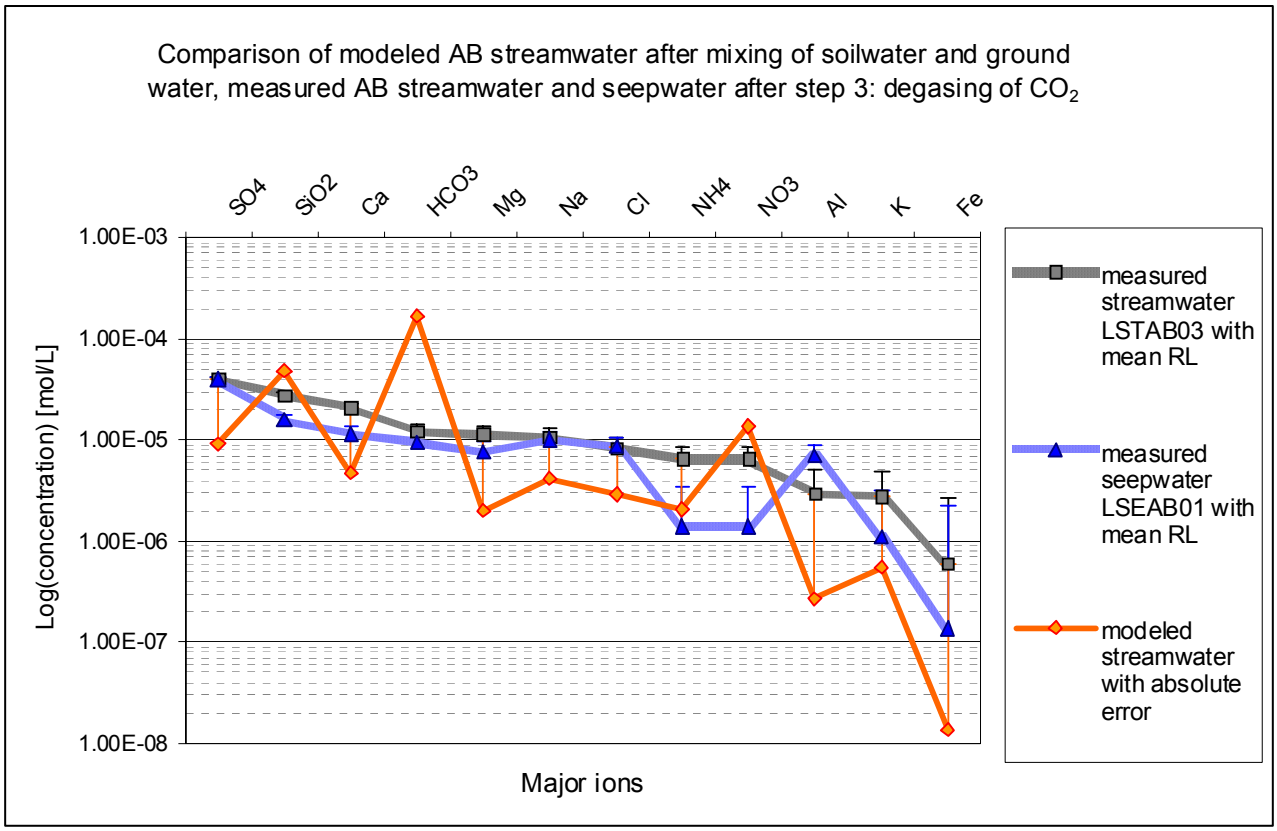

Figure 8.11: Results for modeled streamwater in ACID Biscuit in comparison with observed streamwater and seepwater samples; RL = reporting limit

Table 8.20: Compilation of modeled AB streamwater concentrations, observed streamwater/seepwater concentration; objective functions: SE = square error and AE= absolute error

		STREAM	SEEP	STREAM SE	SEEP SE	STREAM AE
	Modeled	Measured 1	Measured 2	$(Qo_1\text{-}Qm)^2$	$(Qo_2\text{-}Qm)^2$	$(Qo_1\text{-}Qm)$
	mol	mol	mol	mol	mol	mol
SO_4	9.11E-06	4.04E-05	4.00E-05	9.79E-10	9.52E-10	3.13E-05
SiO_2	4.80E-05	2.79E-05	1.57E-05	4.04E-10	1.05E-09	-2.01E-05
Ca	4.69E-06	2.08E-05	1.15E-05	2.61E-10	4.61E-11	1.62E-05
HCO_3	1.68E-04	1.21E-05	9.57E-06	2.43E-08	2.51E-08	-1.56E-04
Mg	1.98E-06	1.13E-05	7.56E-06	8.76E-11	3.11E-11	9.36E-06
Na	4.15E-06	1.07E-05	1.00E-05	4.26E-11	3.48E-11	6.53E-06
Cl	2.89E-06	8.39E-06	8.56E-06	3.03E-11	3.21E-11	5.50E-06
NH_4	2.04E-06	6.45E-06	1.38E-06	1.94E-11	4.34E-13	4.41E-06
NO_3	1.35E-05	6.45E-06	1.38E-06	4.97E-11	1.47E-10	-7.05E-06
Al	2.70E-07	2.92E-06	6.94E-06	7.04E-12	4.45E-11	2.65E-06
K	5.50E-07	2.76E-06	1.11E-06	4.89E-12	3.11E-13	2.21E-06
Fe	1.35E-08	5.96E-07	1.36E-07	3.39E-13	1.50E-14	5.82E-07
MSE/MAE				2.18E-09	2.28E-09	-8.68E-06

8.4.2 Basic Biscuit

Figure 8.12 shows that modeled HCO_3^- concentrations are again too high, whereas simulated SO_4^{2-}, NH_4^+, and Cl^- concentrations are underestimated by the model. Ca^{2+} and Mg^{2+} concentrations fit pretty well, but Na^+ and K^+, as well as Al^{3+}, concentrations are slightly underestimated. But overall, the Schoeller curve for the simulated streamwater resembles the curve of the observed streamwater concentrations.

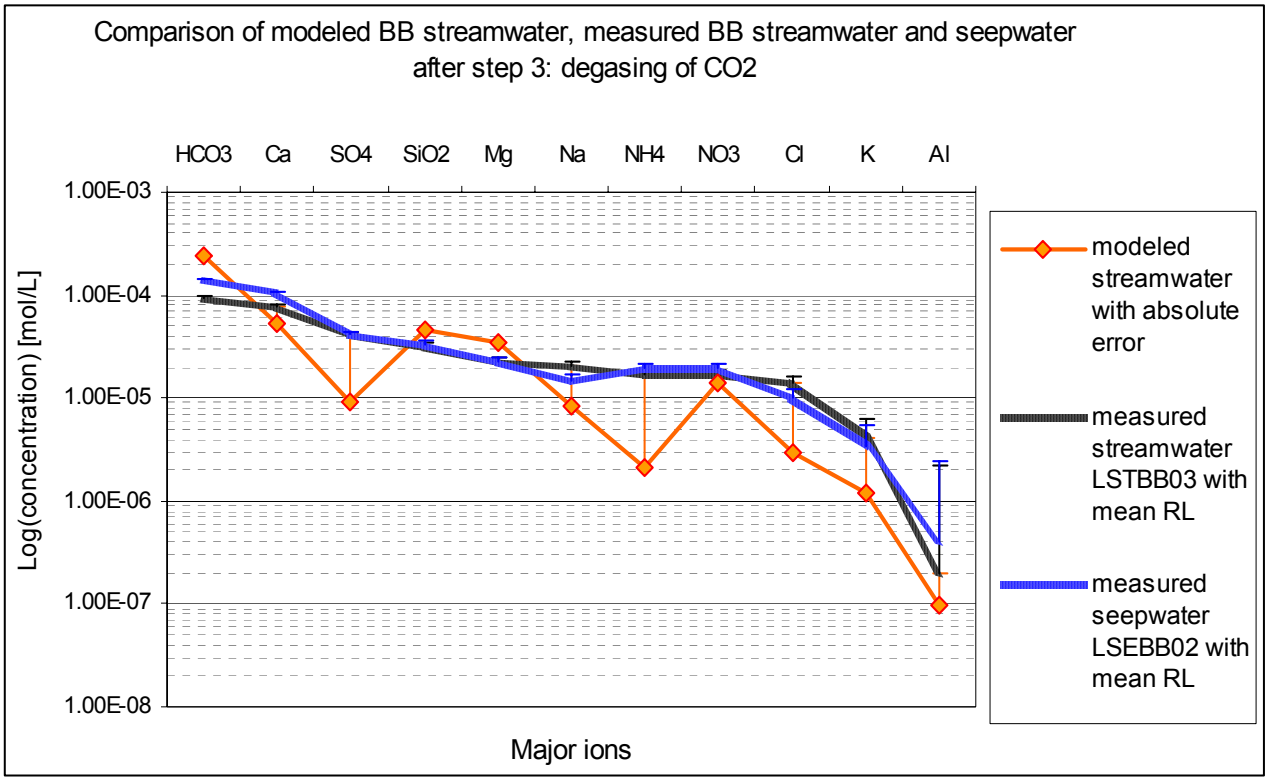

Figure 8.12: Results for modeled streamwater in BASIC Biscuit in comparison with observed streamwater and seepwater samples; RL = reporting limit

Corresponding to the results presented in figure 8.12, stock charts in figure 8.13 follow the same patterns. It is clearly visible that the model underestimates total anion concentration and underestimates total cation concentration. As in AB, the simulated dominant anion is HCO_3^-, but the dominant anion in observed BB streamwater is SO_4^{2-}, closely followed by HCO_3^-. It is also clearly obvious that modeled and observed streamwaters have opposite charge balances. Simulated BB streamwater has a negative excess charge, whereas measured streamwater features a positive excess

charge, which is also shown in table 8.21. Simulated pH and ionic strength, on the other hand, fit very well to observed values.

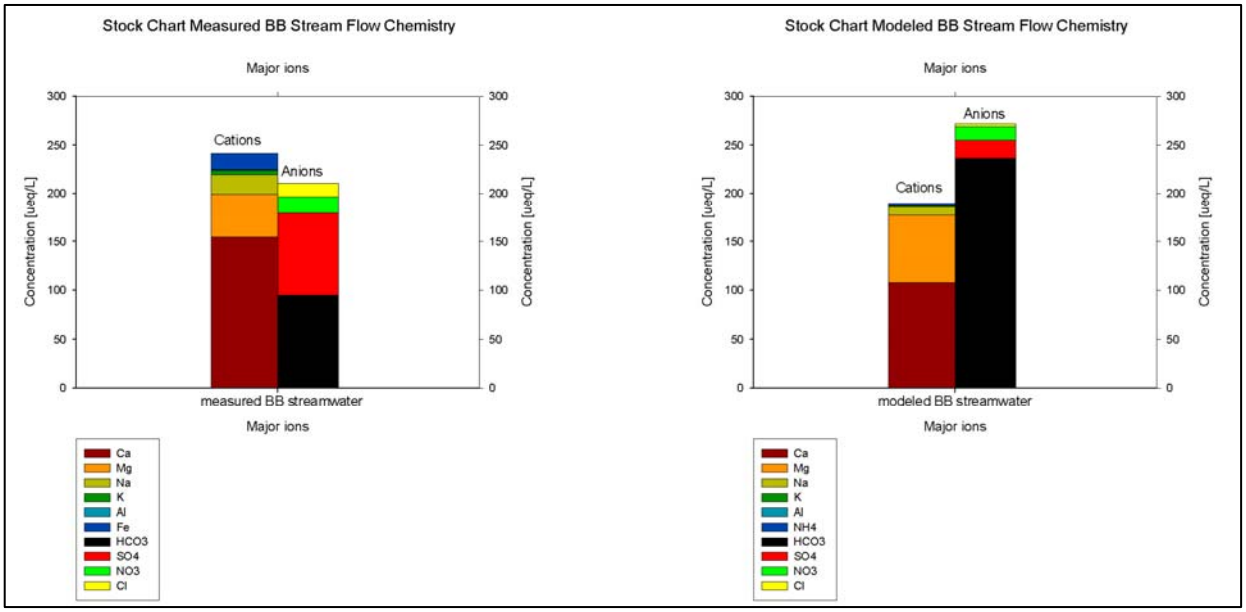

Figure 8.13: Stock charts for modeled and measured anion and cation streamwater concentrations in µeq/L for BB

Table 8.21: Comparison of pH, temperature, ionic strength, charge and percent error of charge for modeled BB streamwater (solution 80) and measured stream (LSTBB03) and seepwater (LSEBB02) samples

	Units	Solution 80	LSTBB03	LSEBB02
pH	*pH units*	6.72	6.65	6.78
temp	*°C*	11	11.0	13.2
ionic strength	*eq/L*	2.87E-04	3.69E-04	4.52E-04
charge	*eq/L*	-4.99E-07	2.43E-10	3.0E-09
pct_err	*%*	-0.13	0.00E+00	0.00E+00

Generally, results for BB are better than those for AB, as obvious from table 8.22. MSE and MAE are with 1.9E-09 and -5.7E-06 mol/L lower than in Acid Biscuit. The mean absolute error is only slightly higher than the mean reporting limit (2.0E-06) for observed concentrations.

Table 8.22: Compilation of modeled BB streamwater concentrations, observed streamwater/seepwater concentration; objective functions: SE = square error and AE= absolute error

		STREAM	SEEP	STREAM SE	SEEP SE	STREAM AE
	Modeled	Measured 1	Measured 2	$(Qo_1-Qm)^2$	$(Qo_2-Qm)^2$	(Qo_1-Qm)
	mol	mol	mol			*mol*
HCO_3	2.37E-04	9.52E-05	1.43E-04	2.01E-08	8.82E-09	-1.42E-04
Mg	5.38E-05	7.74E-05	1.08E-04	5.55E-10	2.97E-09	2.36E-05
SO_4	9.36E-06	4.23E-05	4.20E-05	1.08E-09	1.06E-09	3.29E-05
Ca	4.70E-05	3.20E-05	3.34E-05	2.26E-10	1.84E-10	-1.50E-05
SiO_2	3.50E-05	2.22E-05	2.23E-05	1.62E-10	1.61E-10	-1.27E-05
Na	8.41E-06	2.07E-05	1.47E-05	1.50E-10	3.96E-11	1.23E-05
NH_4	2.08E-06	1.70E-05	1.93E-05	2.23E-10	2.97E-10	1.49E-05
Cl	1.39E-05	1.70E-05	1.93E-05	1.01E-11	3.00E-11	3.18E-06
NO_3	2.96E-06	1.40E-05	9.89E-06	1.23E-10	4.81E-11	1.11E-05
K	1.18E-06	4.18E-06	3.42E-06	8.97E-12	5.00E-12	3.00E-06
Al	9.71E-08	1.95E-07	4.06E-07	9.59E-15	9.54E-14	9.79E-08
Fe	2.62E-07	4.46E-08		4.72E-14		-2.17E-07
MSE/MAE				1.88E-09	1.24E-09	-5.72E-06

8.4.3 West Biscuit

Results for WB are shown as Schoeller diagrams in figure 8.14. Again modeled HCO_3^- concentration is overestimated and NH_4^+ concentration is too low. But now, Sulphate and Chloride concentrations fit well to observed streamwater concentrations. Calcium and Magnesia concentrations are significantly higher than in observed streamwater. Simulated Na^+ and K^+ concentrations, however, fit well. Aluminum concentrations are slightly underestimated by the model. One possible reason for the overestimation of Ca and Mg is the chosen target SI, which was taken from a seepwater sample. Observed streamwater seems to have a lower saturation status for Calcite and Mg bearing minerals. Overall cation and anion concentrations are obviously overestimated by the model, as shown in the stock charts in figure 8.15.

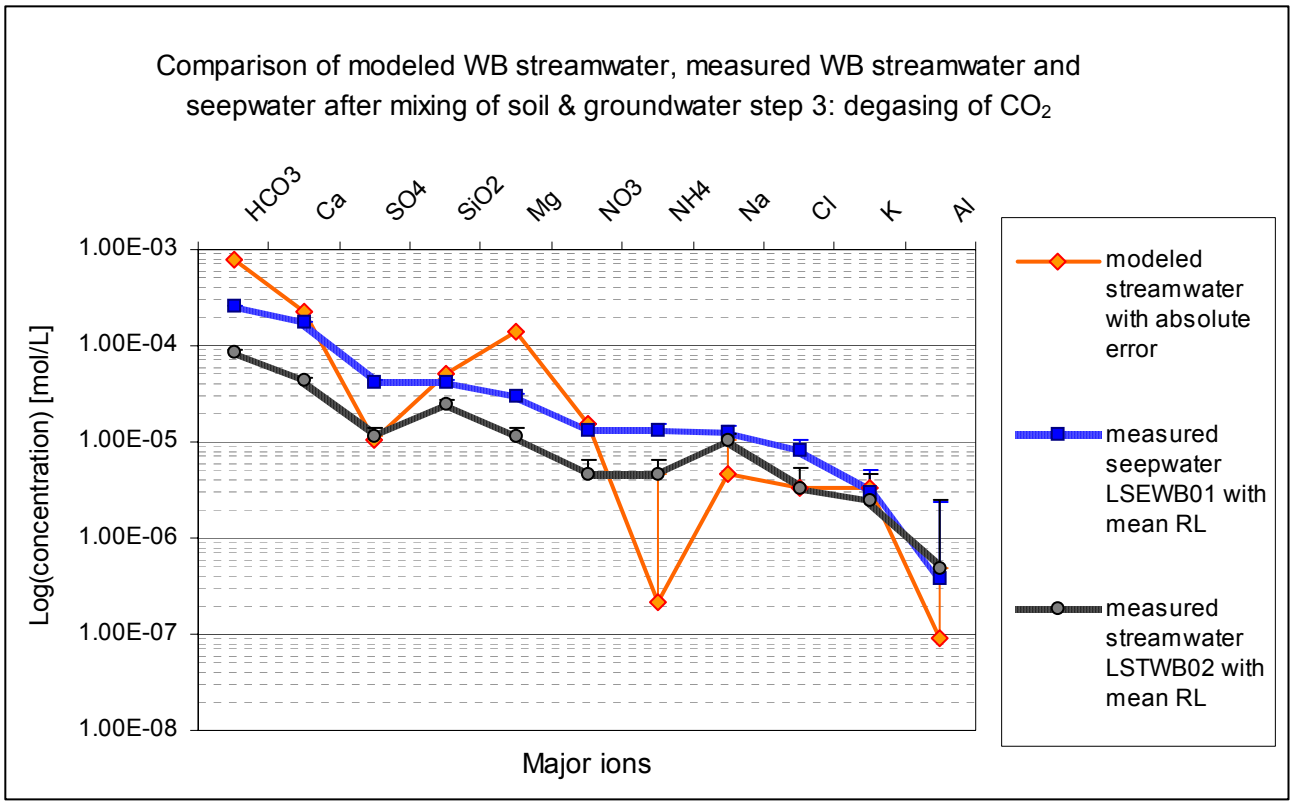

Figure 8.14: Results for modeled streamwater in WEST Biscuit in comparison with observed streamwater and seepwater samples; RL = reporting limit; objective functions: SE = square error and AE= absolute error

This overestimation is mainly due to the high Calcium, Magnesia, and HCO_3^-concentrations. As in BB and AB, also in WB, the simulated most dominant anion is HCO_3^-, but in observed streamwater it is SO_4^{2-}.

Simulated pH is significantly higher than that measured in WB streamwater, as presented in table 8.23, which also results from the target SI chosen for Calcite and other Mg bearing minerals. Following the overestimation of overall concentrations, simulated ionic strength is also one order of magnitude higher than in observed streamwater.

All this leads to higher MSE and MAE with values of -2.6E-08 and -8.6 mol/L, which is approximately one order of magnitude higher than in BB and AB (see table 8.24). This indicates that the flexible approach of choosing the target SI values might not have been appropriate.

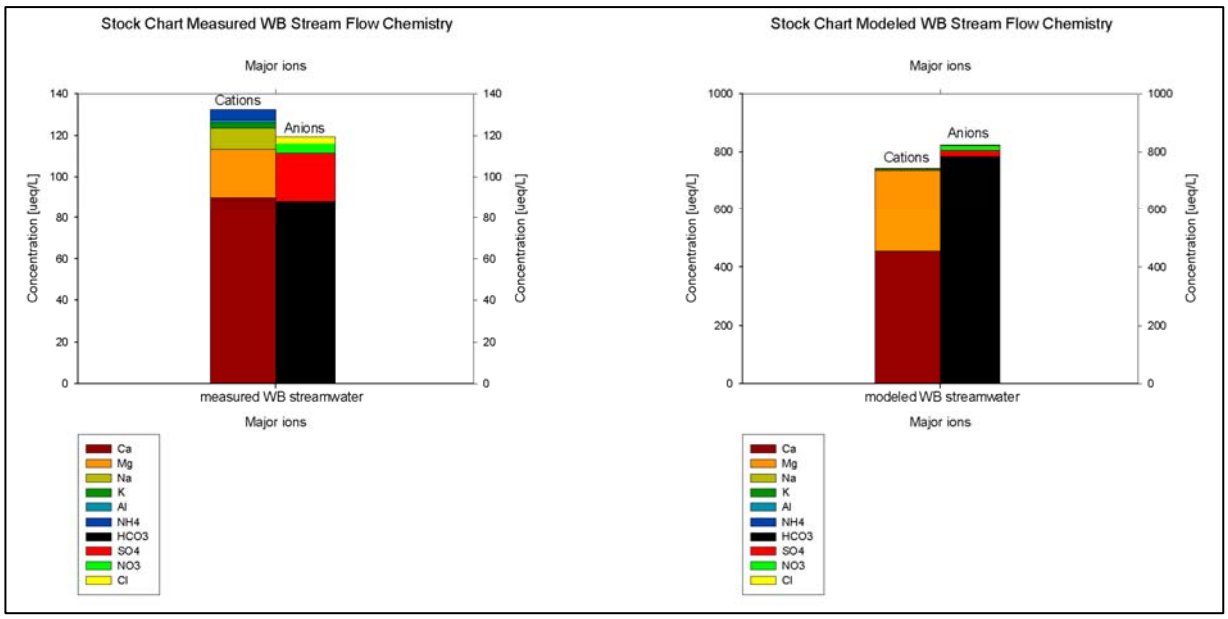

Figure 8.15: Stock charts for modeled and measured anion and cation streamwater concentrations in µeq/L for BB

Table 8.23: Comparison of pH, temperature, ionic strength, charge and percent error of charge for modeled WB streamwater (solution 80) and measured stream (LSTWB02) and seepwater (LSEWB01) samples

	Units	Solution 80	LSTWB02	LSEWB01
pH	*pH units*	7.37	6.45	7.22
temp	*°C*	11	11.3	11.1
ionic strength	*eq/L*	1.12E-03	1.96E-04	6.52E-04
charge	*eq/L*	-2.94E-07	1.4E-11	1.7E-10
pct_err	*%*	-0.02	0.00E+00	0.00E+00

Table 8.24: Compilation of modeled WB streamwater concentrations, observed streamwater/seepwater concentration; objective functions: SE = square error and AE= absolute error

		SEEP	STREAM	SEEP SE	STREAM SE	STREAM AE
	Modeled	Measured 1	Measured 2	$(Qo_1-Qm)^2$	$(Qo_2-Qm)^2$	(Qo_1-Qm)
	mol	*mol*	*mol*			*mol*
HCO_3	7.85E-04	2.65E-04	8.81E-05	2.71E-07	4.85E-07	-6.97E-04
Ca	2.28E-04	1.74E-04	4.50E-05	2.89E-09	3.34E-08	-1.83E-04
SO_4	1.06E-05	4.30E-05	1.17E-05	1.05E-09	1.26E-12	1.12E-06
SiO_2	5.12E-05	4.12E-05	2.54E-05	1.00E-10	6.65E-10	-2.58E-05
Mg	1.40E-04	2.95E-05	1.17E-05	1.22E-08	1.64E-08	-1.28E-04
NO_3	1.57E-05	1.31E-05	4.55E-06	6.73E-12	1.23E-10	-1.11E-05
NH_4	2.19E-07	1.31E-05	4.55E-06	1.65E-10	1.87E-11	4.33E-06
Na	4.74E-06	1.28E-05	1.03E-05	6.48E-11	3.09E-11	5.56E-06
Cl	3.34E-06	8.24E-06	3.39E-06	2.41E-11	2.58E-15	5.08E-08
K	3.35E-06	2.96E-06	2.54E-06	1.55E-13	6.54E-13	-8.09E-07
Al	9.28E-08	3.76E-07	4.84E-07	8.02E-14	1.53E-13	3.91E-07
Fe	3.07E-08		5.57E-08		6.27E-16	2.50E-08
MSE/MAE				2.61E-08	4.47E-08	-8.62E-05

8.5 Conclusions

In general, the model could explain streamwater chemistry better in the more basic tributaries, BB and WB, which is probably connected with the lower ionic strength in AB due to a smaller proportion of Calcite. Results also indicate that modeled cation concentrations generally fit better to observed streamwater concentrations than simulated anion concentrations. Problems occurred especially with simulated Hydrogen-Carbonate, Sulphate, and Chloride concentrations, where the first was overestimated and the two latter were underestimated even after degasing of CO_2 in the mixing module. Overestimation of HCO_3^- could be

caused by an actual underestimation of observed alkalinity in Biscuit Brook, because of CO_2 degasing after sampling (COSTELLO-WALKER, 1995). Since SO_4^{2-}, but especially Cl^- are considered as conservative ions, it is questionable if the chosen model input, mean Biscuit Brook precipitation from December 2007, really represents streamwater of June 2008. But there was no more recent precipitation data available. NH_4 concentrations were generally much too low in comparison with observed streamwater concentrations. After LAWRENCE (2009; personal communication) observed Ammonia concentrations might be overestimated, since they are somewhat higher than usually reported for headwater streams in the Neversink River basin.

9 Sensitivity Analyses

As mentioned in the previous chapter, sensitivity analyses were conducted to explore affects of hydrological and model internal parameters, mineral composition, pCO_2 and exchanger composition.

9.1 Affect of Mineral Composition

Many different combinations of possible minerals and target SI were tried in the course of this work. But with the stepwise modeling approach it could be proved that all minerals that are included now are needed to explain streamwater chemistry. This is shown in figures 9.1 to 9.3, for AB subsurface flow for Ca^{2+}, Mg^{2+}, and Al^{3+} and for all 5 subsequent steps.

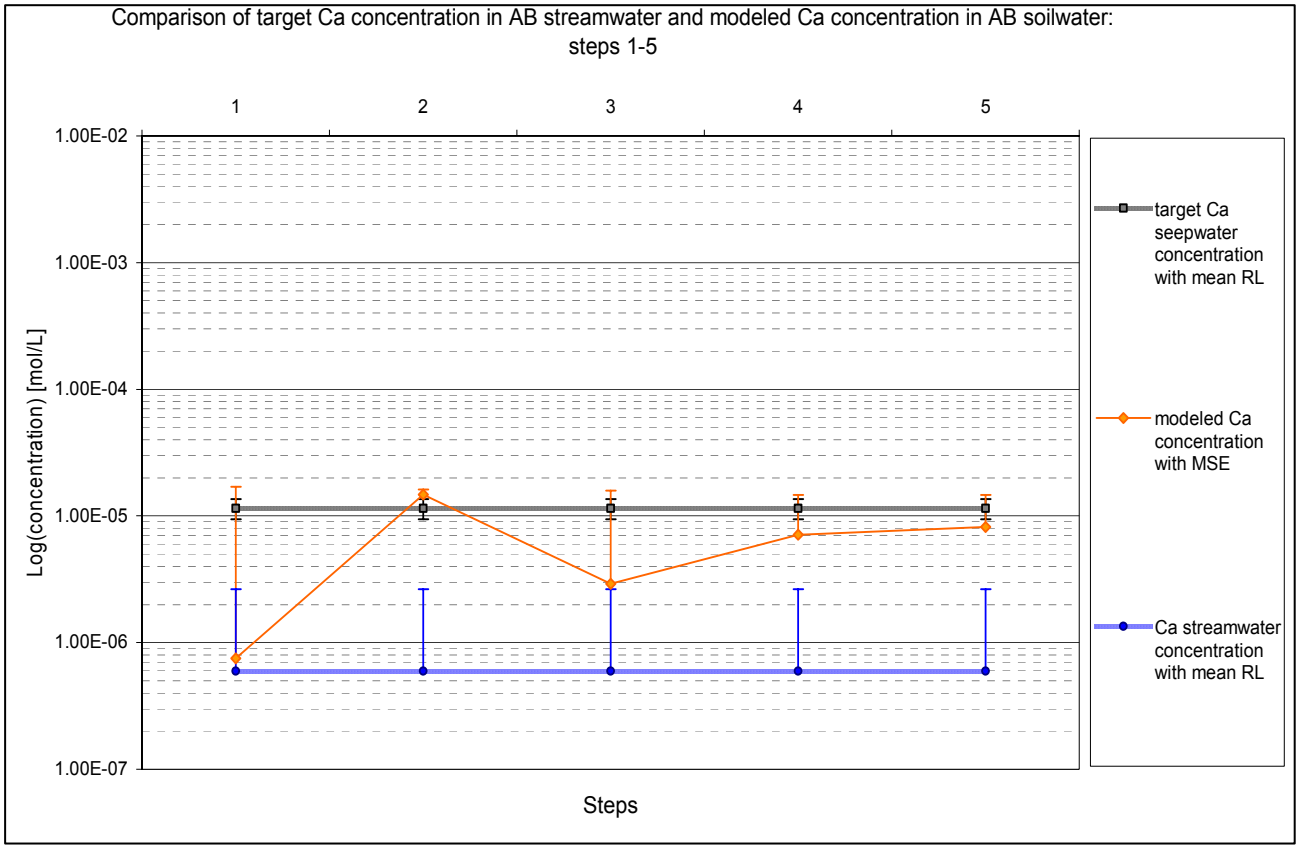

Figure 9.1: Evolution of Calcium concentrations in simulated AB subsurface flow for every subsequent step; Step 1 = Equilibria with soil air; Step 2 = Weathering of Calcite; Step 3 = Weathering of Silica minerals; Step 4 = Dissolution and formation of clay minerals; Step 5 = cation exchange

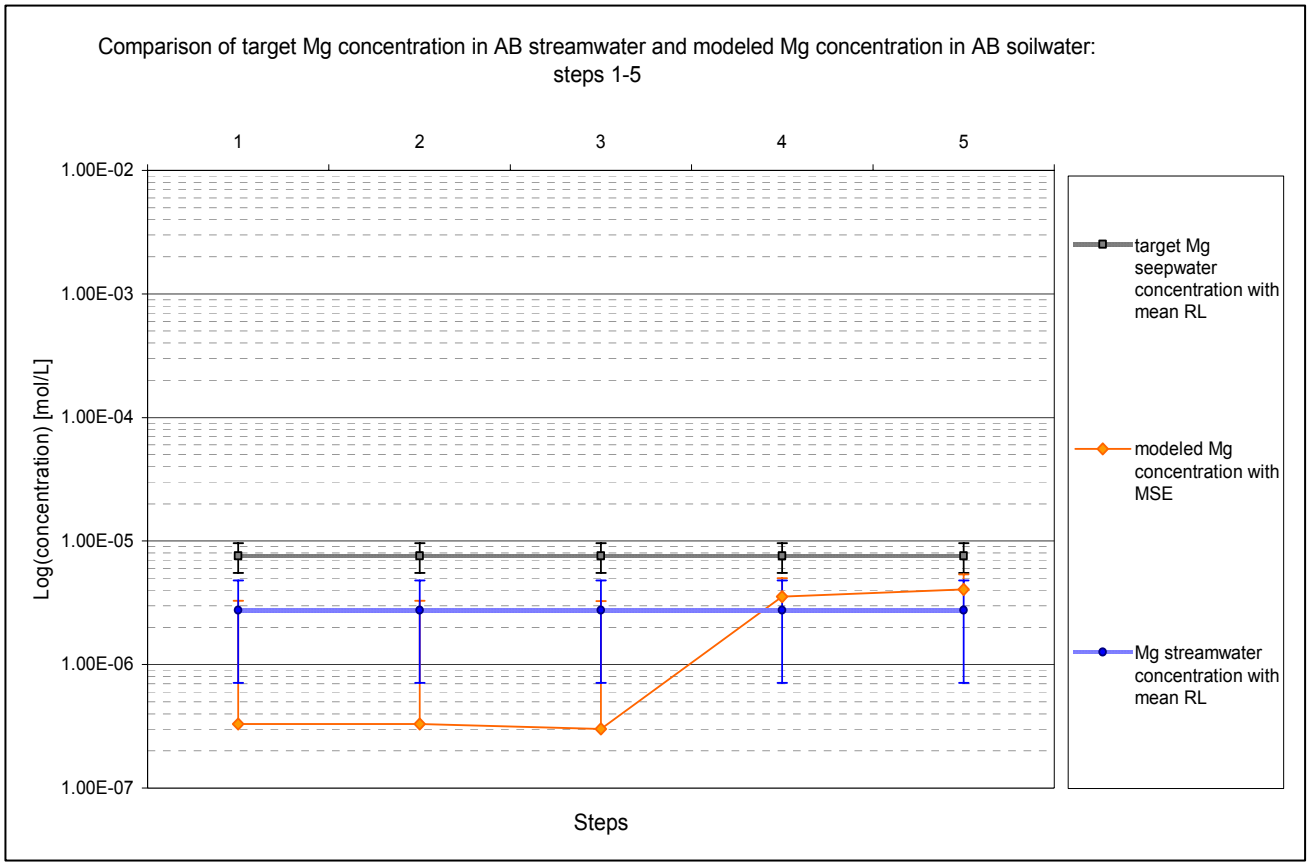

Figure 9.2: Evolution of Magnesia concentrations in simulated AB subsurface flow for every subsequent step; Step 1 = Equilibria with soil air; Step 2 = Weathering of Calcite; Step 3 Weathering of Silica minerals; Step 4 = Dissolution and formation of clay minerals; Step 5 = cation exchange

Of course, all these minerals were detected in the Catskills (see chapter 2). It could be shown that Chlorite had to be included because of the Mg^{2+} concentrations, and Kaolinite and Gibbsite had to be in the model to adjust the Al^{3+} concentrations after weathering of silica minerals. It was also proven that streamwater chemistry in Acid Biscuit can not be explain if Calcite was completely excluded from the soil modules. As mentioned in the previous part of this chapter, it is questionable if our flexible approach for the target SI really worked, since BB and WB streamwater seem not to be influenced so much by seepwater chemistry. This can be best seen in West Biscuit if you look at the seep sample LSEWB01 with the highest pH and the highest Calcium concentration, but just some 100m downstream, at LSTWB02, streamwater chemistry is different, with a much lower pH and lower base cation concentrations. For future work, it would be very

helpful to have real thin sections so that not only qualitative but also quantitative conclusions about mineral composition can be made.

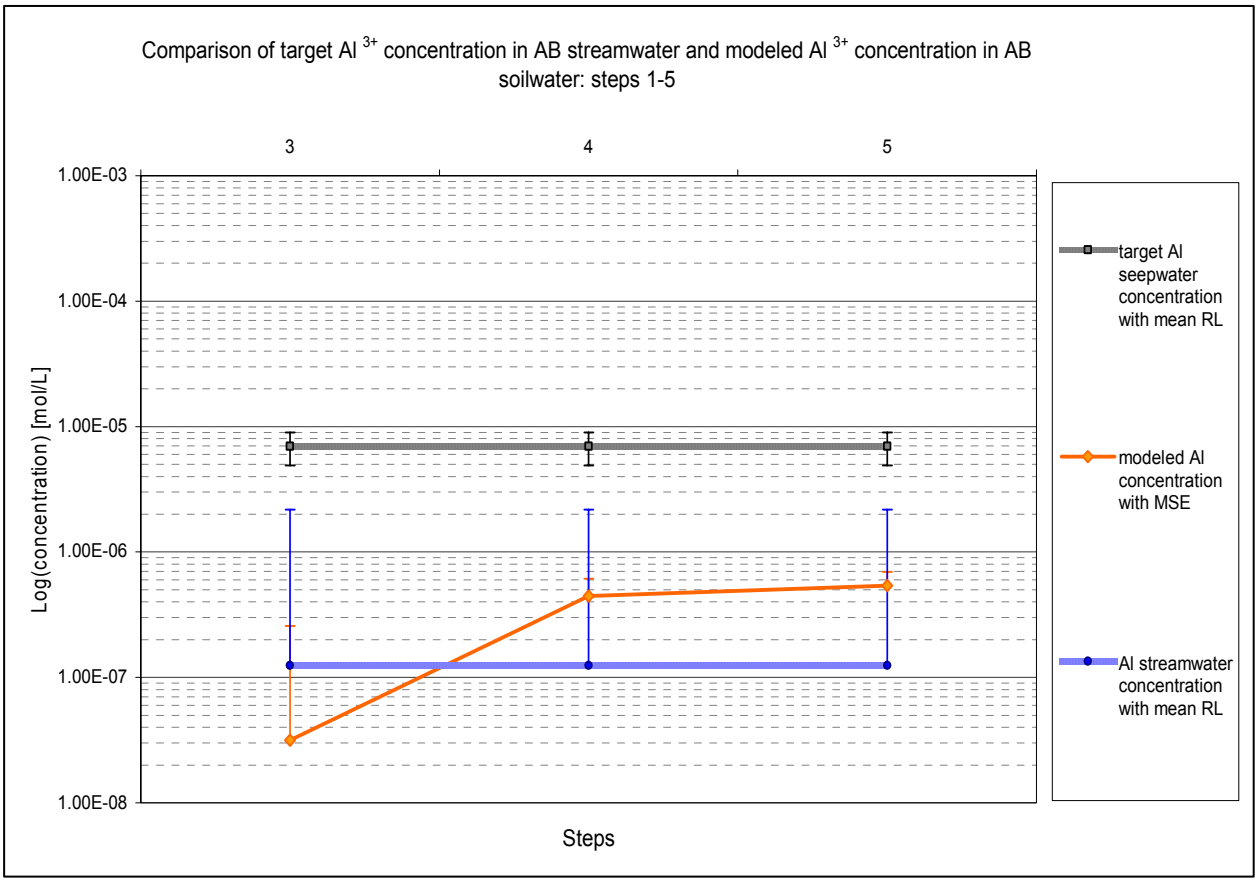

Figure 9.3: Evolution of Aluminum concentrations in simulated AB subsurface flow for every subsequent step; Step 1 = Equilibria with soil air; Step 2 = Weathering of Calcite; Step 3 Weathering of Silica minerals; Step 4 = Dissolution and formation of clay minerals; Step 5 = cation exchange

9.2 Affect of Dispersivity, Velocity and Cell Size

Here different scenarios of possible combinations of dispersivity and velocity were run. Objective functions were the Peclet number, P_e, and the Courant number, C_0. P_e helps with the definition of the cell size, and is recommended to be <2. The Courant number assures that transport of a particle is calculated within at least one time step per cell and it should be <1. Results indicate that the combination of mean velocity and minimal dispersivity satisfies these terms best. Therefore, this combination was used for all transport modules.

9.3 Affect of pCO_2

Here partial pressure of carbon dioxide was changed to represent low ($10^{-3.0}$), medium ($10^{-2.5}$), and high pCO_2 ($10^{-1.5}$), where naturally results for low and medium pCO_2 were closer together than for medium and high pCO_2. Figures 9.4 to 9.6 compare these results for each respective tributary. Tables 9.1 to 9.6 summarize simulated concentrations and MSE as well as MAE.

9.3.1 Acid Biscuit

The sensitivity analysis for pCO_2 truly uncovers the model's disability to simulate AB streamwater realistically. As shown in figure 9.4, the greatest impact of pCO_2 is naturally seen on HCO_3^- concentrations, where concentrations significantly increase with increasing pCO_2, since the amount of CO_2(aq) determines the amount of HCO_3^- in the solution. On the one hand, modeled streamwater with a Log(pCO_2) of -1.5 shows maximal Hydrogen-Carbonate concentrations, and has thus the highest MSE, MAE, and percent error in charge, as shown in table 9.2. But on the other hand simulated pH and ionic strength fit very well to measured AB seep and streamwater, as presented in table 9.1. Simulated streamwater with Log(pCO_2) -3.0 has the lowest MSE and MAE, as well as the lowest percent error. But then ionic strength is underestimated and pH is somewhat overestimated. Interestingly, the solution with the lowest pCO_2 has not as expected the highest pH, but simulated soilwater with medium pCO_2. This could be caused by superposition effects of the different chemical reactions. All this leads to the conclusion that for Acid Biscuit an important chemical process was not considered within the model.

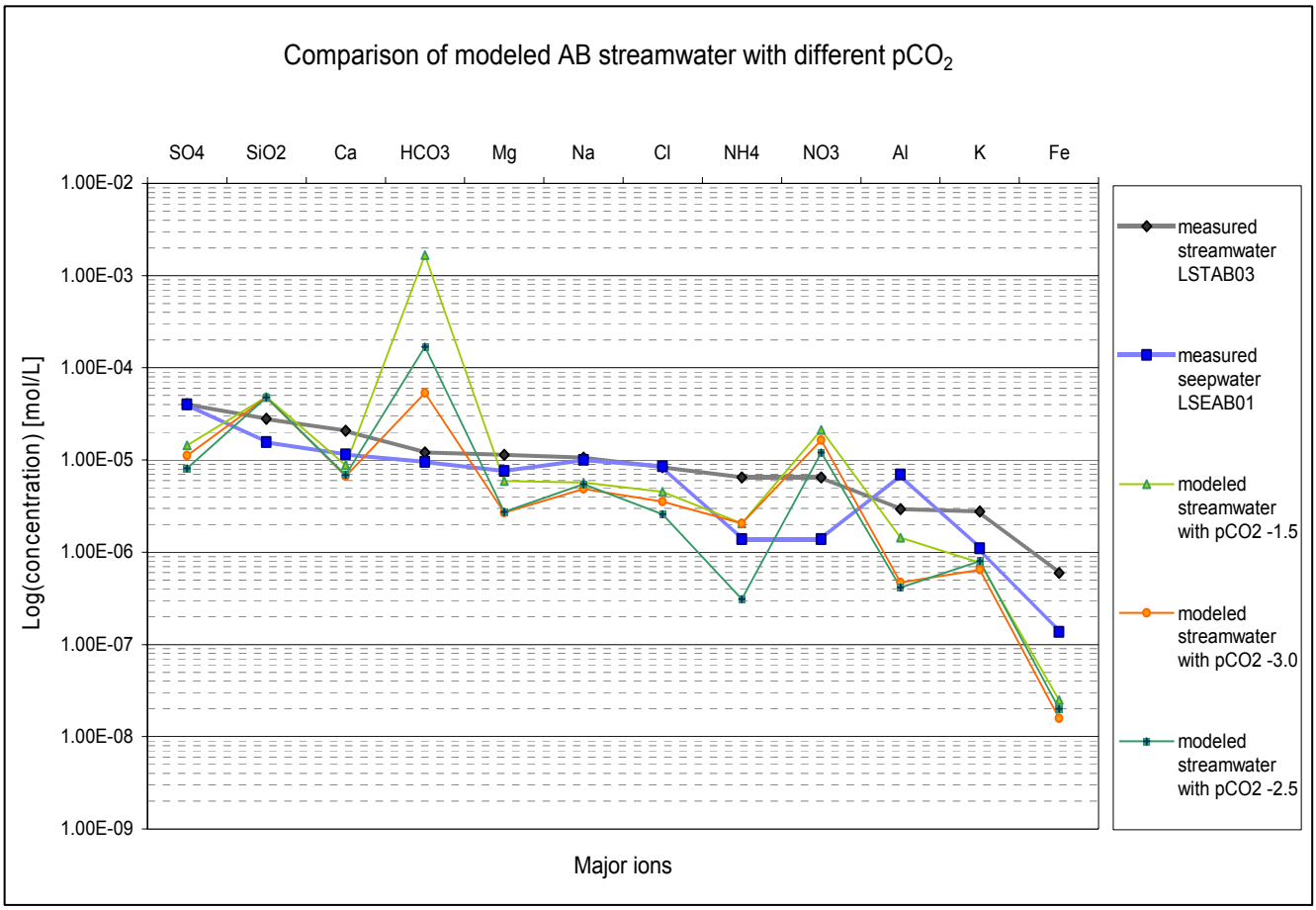

Figure 9.4: Comparison of streamwater in ACID Biscuit with low, medium and high pCO2 and with observed stream and seepwater samples

Table 9.1: Comparison of pH, temperature, ionic strength, charge and percent error of charge for modeled AB streamwater (solution 80) with high, medium and low pCO_2 and measured stream (LSTAB03) and seepwater (LSEAB01) samples

		pCO2 -1.5	pCO2 -2.5	pCO2 -3.0	pCO2 -1.7	pCO2 -1.7
	Units	Solution 80	Solution 80	Solution 80	LSTAB03	LSEAB01
pH	*pH units*	4.51	5.01	4.80	4.68	4.52
temp	*°C*	11	11	11	10.8	11.3
ionic strength	*eq/L*	1.06E-04	5.55E-05	6.51E-05	1.83E-04	1.66E-04
charge	*eq/L*	-4.49E-07	-2.21E-07	-5.41E-08	7.62E-12	6.7E-12
pct_err	*%*	-0.31	-0.30	-0.06	0.00E+00	0.00E+00

One explanation could be that calculated pCO_2 in measured streamwater was overestimated because of the contribution of an unconsidered substance to charge balance, which could be DOC for example. DOC was not included in the model, since no information about charge and

speciation of dissolved organic carbon was available. But after Külls (2008), personal communication, DOC mainly occurs as uncharged macro molecules. Another reason might be the increasing anion adsorption with decreasing pH in soils (SCHEFFER & SCHACHTSCHABEL, 2002).

Unclear is also the presence and the impact of redox reactions, since signs of redoxiemorphosis were found in AB soil profiles, and AB streamwater also showed the highest dissolved iron concentrations measured in Biscuit Brook. Another interesting, but unclear point is that Ammonia concentrations were significantly affected by varying pCO_2. Medium pCO_2 streamwater has the lowest simulated NH_4^+ concentrations in AB. This must be connected with pH and exchange reactions.

Al^{3+} concentrations are naturally affected by variation of pCO_2 since all these reactions are strongly pH dependent. Therefore, simulated streamwater with highest pCO_2 has the highest simulated Al^{3+} concentration. Calcium concentrations are hardly affected by variation of pCO_2, since Calcite content in Acid Biscuit is generally low. Thus, increasing Calcite solubility with increasing pCO_2 does not apply.

Table 9.2: Compilation of modeled AB streamwater with low, medium and high pCO_2 in comparison with observed streamwater/seepwater concentration; objective functions: SE = square error and AE= absolute error

pCO_2	3.0	2.5	1.5	3.0 SE	3.0 AE	2.5 SE	2.5 AE	1.5 SE	1.5 AE
	Modeled	Modeled	Modeled	$(Qo_1\text{-}Qm)^2$	$(Qo_1\text{-}Qm)$	$(Qo_1\text{-}Qm)^2$	$(Qo_1\text{-}Qm)$	$(Qo_1\text{-}Qm)^2$	$(Qo_1\text{-}Qm)$
	mol	mol	mol	mol	mol	mol	mol	mol	mol
SO_4	1.1E-05	9.1E-06	1.4E-05	8.6E-10	2.9E-05	9.8E-10	3.1E-05	6.8E-10	2.6E-05
SiO_2	4.8E-05	4.8E-05	4.8E-05	4.0E-10	-2.0E-05	4.0E-10	-2.0E-05	4.2E-10	-2.0E-05
Ca	6.7E-06	4.7E-06	8.8E-06	2.0E-10	1.4E-05	2.6E-10	1.6E-05	1.4E-10	1.2E-05
HCO_3	5.3E-05	1.7E-04	1.7E-03	1.7E-09	-4.1E-05	2.4E-08	-1.6E-04	2.7E-06	-1.7E-03
Mg	2.7E-06	2.0E-06	5.9E-06	7.5E-11	8.7E-06	8.8E-11	9.4E-06	2.9E-11	5.4E-06
Na	4.9E-06	4.1E-06	5.7E-06	3.4E-11	5.8E-06	4.3E-11	6.5E-06	2.5E-11	5.0E-06
Cl	3.5E-06	2.9E-06	4.6E-06	2.4E-11	4.9E-06	3.0E-11	5.5E-06	1.5E-11	3.8E-06
NH_4	2.0E-06	2.0E-06	2.1E-06	1.9E-11	4.4E-06	1.9E-11	4.4E-06	1.9E-11	4.4E-06
NO_3	1.7E-05	1.4E-05	2.1E-05	1.0E-10	-1.0E-05	5.0E-11	-7.1E-06	2.2E-10	-1.5E-05
Al	4.7E-07	2.7E-07	1.4E-06	6.0E-12	2.5E-06	7.0E-12	2.7E-06	2.2E-12	1.5E-06
K	6.5E-07	5.5E-07	7.7E-07	4.5E-12	2.1E-06	4.9E-12	2.2E-06	4.0E-12	2.0E-06
Fe	1.6E-08	1.3E-08	2.5E-08	3.4E-13	5.8E-07	3.4E-13	5.8E-07	3.3E-13	5.7E-07
MSE/MAE				2.8E-10	8.9E-08	2.2E-09	-8.7E-06	2.3E-07	-1.4E-04

9.3.2 Basic Biscuit

Again, HCO_3^- concentrations significantly increase with increasing pCO_2, as shown in figure 9.5. In BB simulated streamwaters with a high pCO_2 of -

1.5 and with a low pCO_2 of -3.0 have the lowest percent error in charge with a value of -0.02%, as presented in table 9.3. It is surprising that both streamwaters have negative errors, since the first has the highest and the latter the lowest HCO_3^- concentrations.

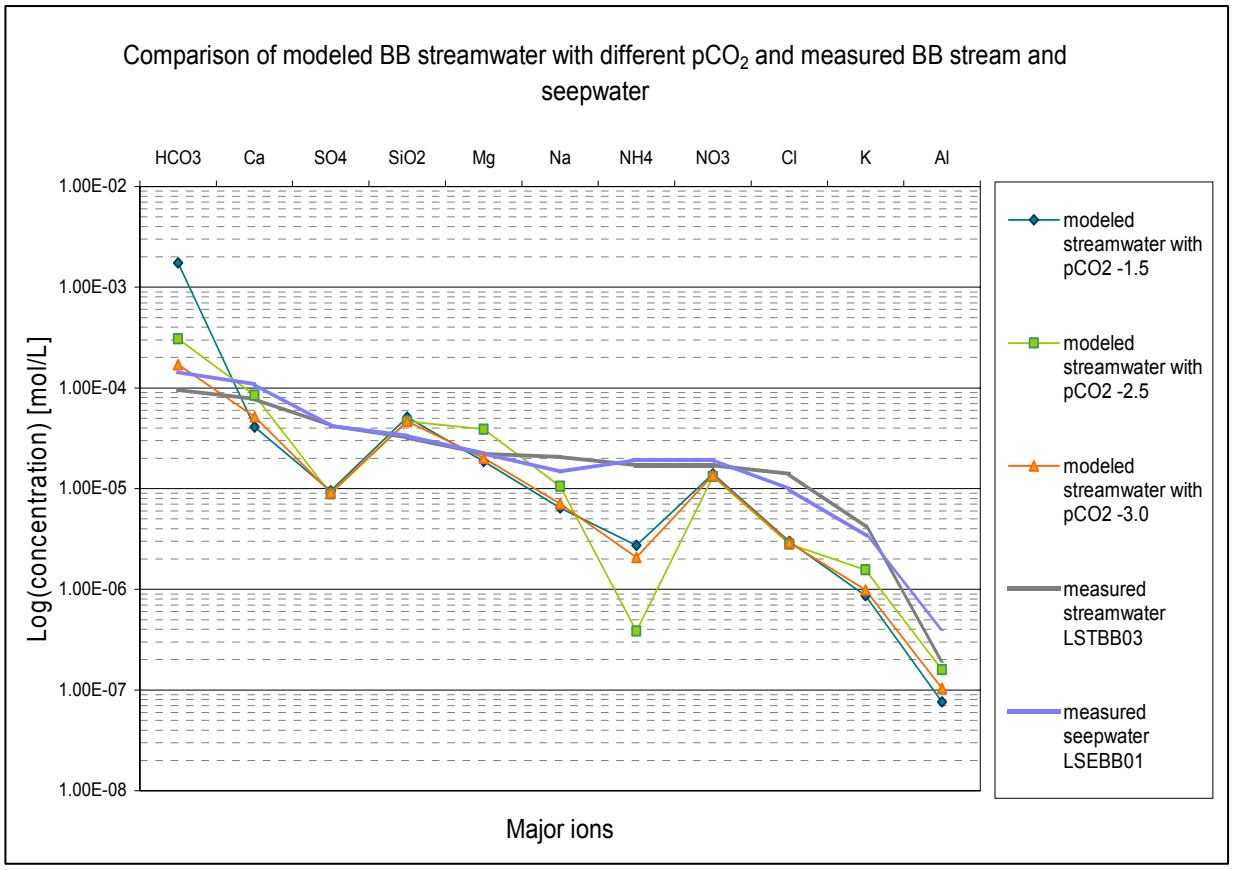

Figure 9.5: Comparison of streamwater in BASIC Biscuit with low, medium and high pCO2 and with observed stream and seepwater samples

Table 9.3: Comparison of pH, temperature, ionic strength, charge and percent error of charge for modeled BB streamwater (solution 80) with high, medium and low pCO_2 and measured stream (LSTBB03) and seepwater (LSEBB02) samples

		pCO2 -1.5	pCO2 -2.5	pCO2 -3.0	pCO2 -2.9	pCO2 -2.8
	Units	Solution 80	Solution 80	Solution 80	LSTBB03	LSEBB02
pH	*pH units*	5.23	6.88	6.81	6.65	6.78
temp	*°C*	11	11	11	11.0	13.2
ionic strength	*eq/L*	2.04E-04	3.91E-04	2.34E-04	3.69E-04	4.52E-04
charge	*eq/L*	-5.92E-08	5.43E-07	-7.48E-08	2.43E-10	3.0E-09
pct_err	*%*	-0.02	0.10	-0.02	0.00E+00	0.00E+00

The model overestimates HCO_3^- concentrations in streamwater with pCO_2 -1.5, and it underestimates Ca^{2+}, Na^+, K^+, NH_4^+ and Al^{3+} concentrations.

Actually, simulated Calcium concentrations are lowest of all modeled streamwaters, which is untypical, since Calcite solubility should increase with higher pCO_2 (APPELO & POSTMA, 2005). The underestimation of Aluminum is also remarkable, because streamwater with pCO_2 -1.5 has the lowest pH and thus expected Al^{3+} concentrations should be higher. These irregularities could be caused by cation exchange reactions. In the streamwater with pCO_2 -3.0, the negative charge balance is not caused by overestimation of simulated anion concentrations but by underestimation of cation concentrations, such as Ca^{2+}, Na^+, K^+, NH_4^+ and Al^{3+}. Lower Calcium concentrations are here caused by decreasing Calcite solubility with decreasing pCO_2. The simulated streamwater with medium pCO_2 has the highest percent of error in charge with -0.1%, but this is still a good result. Positive charge balance is here caused by overestimation of mainly NH_4^+, but also Mg^{2+}. Unexpectedly, simulated Calcium concentrations are highest for streamwater with medium pCO_2 (-2.5).

Streamwaters with pCO_2 -2.5 and -1.5 have the highest MSE, but streamwater with pCO_2 -1.5 has the highest absolute error, as shown in table 9.4.

Table 9.4: Compilation of modeled BB streamwater with low, medium and high pCO_2 and observed streamwater/seepwater concentration; objective functions: SE = square error and AE= absolute error

pCO_2	3.0	2.5	1.5	3.0	2.5	1.5	3.0	2.5	1.5
				SE	SE	SE	AE	AE	AE
	Modeled	Modeled	Modeled	$(Qo_1\text{-}Qm)^2$	$(Qo_1\text{-}Qm)^2$	$(Qo_1\text{-}Qm)^2$	$(Qo_1\text{-}Qm)$	$(Qo_1\text{-}Qm)$	$(Qo_1\text{-}Qm)$
	mol	*mol*	*mol*				*mol*	*mol*	*mol*
HCO_3	1.71E-04	3.08E-04	1.87E-03	5.75E-09	3.16E-06	3.16E-06	-7.58E-05	-2.13E-04	-1.78E-03
Mg	5.15E-05	8.46E-05	8.46E-05	6.69E-10	5.28E-11	5.28E-11	2.59E-05	-7.26E-06	-7.26E-06
SO_4	9.16E-06	8.89E-06	8.89E-06	1.10E-09	1.11E-09	1.11E-09	3.31E-05	3.34E-05	3.34E-05
Ca	4.66E-05	4.68E-05	4.68E-05	2.13E-10	2.19E-10	2.19E-10	-1.46E-05	-1.48E-05	-1.48E-05
SiO_2	2.02E-05	3.89E-05	3.89E-05	4.15E-12	2.79E-10	2.79E-10	2.04E-06	-1.67E-05	-1.67E-05
Na	7.07E-06	1.06E-05	1.06E-05	1.85E-10	1.03E-10	1.03E-10	1.36E-05	1.01E-05	1.01E-05
NH_4	2.07E-06	3.86E-07	3.86E-07	2.24E-10	2.77E-10	2.77E-10	1.50E-05	1.66E-05	1.66E-05
Cl	1.36E-05	1.32E-05	1.32E-05	1.21E-11	1.48E-11	1.48E-11	3.48E-06	3.85E-06	3.85E-06
NO_3	2.89E-06	2.81E-06	2.81E-06	1.24E-10	1.26E-10	1.26E-10	1.12E-05	1.12E-05	1.12E-05
K	9.83E-07	1.56E-06	1.56E-06	1.02E-11	6.87E-12	6.87E-12	3.19E-06	2.62E-06	2.62E-06
Al	1.04E-07	1.59E-07	1.59E-07	8.27E-15	1.30E-15	1.30E-15	9.09E-08	3.60E-08	3.60E-08
Fe	2.14E-07	3.71E-07	3.71E-07	2.88E-14	1.06E-13	1.06E-13	-1.70E-07	-3.26E-07	-3.26E-07
MSE/MAE				6.90E-10	2.63E-07	2.63E-07	1.41E-06	-1.45E-05	-1.45E-04

9.3.3 West Biscuit

Here, HCO_3^-, Mg^{2+}, and NH_4^+ concentrations differ significantly, whereas all other concentrations are pretty close, as presented in figure 9.6. Hydrogen-Carbonate follows the same pattern as described for BB and AB. Magnesia concentrations were highest for modeled streamwater with pCO_2 -1.5, but are still overestimated in streamwater with pCO_2 -2.5.

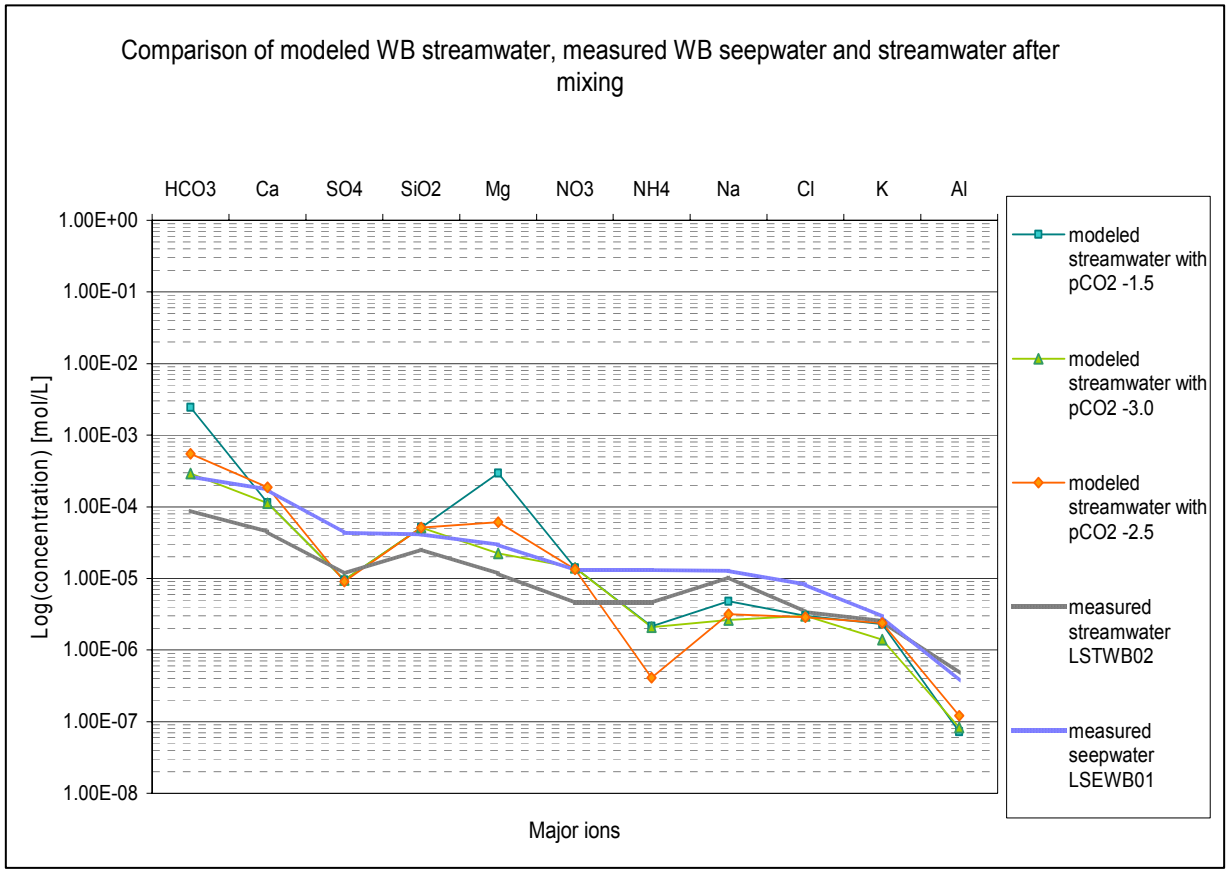

Figure 9.6: Comparison of streamwater in WEST Biscuit with low, medium and high pCO2 and with observed stream and seepwater samples

Table 9.5: Comparison of pH, temperature, ionic strength, charge and percent error of charge for modeled WB streamwater (solution 80) with high, medium and low pCO_2 and measured stream (LSTWB02) and seepwater (LSEWB01) samples

		pCO2 -1.5	pCO2 -2.5	pCO2 -3.0	pCO2 -2.7	pCO2 -3.0
	Units	Solution 80			LSTWB02	LSEWB01
pH	*pH units*	6.12	7.19	7.10	6.45	7.22
temp	*°C*	11	11	11	11.3	11.1
ionic strength	*eq/L*	1.24E-03	7.59E-04	4.17E-04	1.96E-04	6.52E-04
charge	*eq/L*	-4.38E-06	1.38E-06	-5.13E-07	1.4E-11	1.7E-10
pct_err	*%*	-0.27	0.14	-0.09	0.00E+00	0.00E+00

Ammonia concentrations are strongly underestimated in streamwater with pCO_2 -2.5, whereas streamwaters with pCO_2 -1.5 and -3.0 had very similar NH_4^+ concentrations that were closer to observed streamwater concentrations.

Expectedly, simulated pH is lowest in streamwater with pCO_2 -1.5, and, unexpectedly, highest in streamwater with pCO_2 -2.5, as shown in table 9.5. PH and ionic strength of streamwater with pCO_2 -2.5 fits very well to the observed seepwater sample, but simulated pCO_2 is too high in comparison with the calculated pCO_2 of the seepwater sample. The observed streamwater sample has with -2.7 a very similar pCO_2 than streamwater with pCO_2 -2.5, but then pH values differ significantly.

The lowest percent error in charge, as well as the lowest MSE and MAE, has streamwater with a pCO_2 of -3.0, which are presented in table 9.6. The negative charge balance is here caused by an underestimation of base cation concentrations, but most of all by an underestimation of NH_4^+ and Al^{3+} concentrations. Streamwater with a pCO_2 of -2.5 has the highest mean absolute error, whereas Streamwater with a pCO_2 of -1.5 has the highest MSE.

Table 9.6: Compilation of modeled WB streamwater with low, medium and high pCO_2 and observed streamwater/seepwater concentration; objective functions: SE = square error and AE= absolute error

pCO_2	3.0	2.5	1.5	3.0 SE	2.5 SE	1.5 SE	3.0 AE	2.5 AE	1.5 AE
	Modeled *mol*	Modeled *mol*	Modeled *mol*	$(Qo_1\text{-}Qm)^2$	$(Qo_1\text{-}Qm)^2$	$(Qo_1\text{-}Qm)^2$	$(Qo_1\text{-}Qm)$ *mol*	$(Qo_1\text{-}Qm)$ *mol*	$(Qo_1\text{-}Qm)$ *mol*
HCO_3	2.90E-04	2.44E-03	5.50E-04	4.09E-08	2.14E-07	5.53E-06	-2.02E-04	-4.62E-04	-2.35E-03
Ca	1.12E-04	1.13E-04	1.88E-04	4.45E-09	2.05E-08	4.65E-09	-6.67E-05	-1.43E-04	-6.82E-05
SO_4	9.53E-06	9.53E-06	9.07E-06	4.66E-12	6.84E-12	4.66E-12	2.16E-06	2.62E-06	2.16E-06
SiO_2	5.12E-05	5.12E-05	5.12E-05	6.65E-10	6.65E-10	6.64E-10	-2.58E-05	-2.58E-05	-2.58E-05
Mg	2.25E-05	2.96E-04	6.12E-05	1.16E-10	2.45E-09	8.06E-08	-1.08E-05	-4.95E-05	-2.84E-04
NO_3	1.41E-05	1.41E-05	1.34E-05	9.08E-11	7.84E-11	9.09E-11	-9.53E-06	-8.86E-06	-9.53E-06
NH_4	2.10E-06	2.14E-06	4.13E-07	5.98E-12	1.71E-11	5.76E-12	2.44E-06	4.13E-06	2.40E-06
Na	2.64E-06	4.82E-06	3.17E-06	5.86E-11	5.08E-11	2.99E-11	7.66E-06	7.12E-06	5.47E-06
Cl	3.01E-06	3.01E-06	2.87E-06	1.39E-13	2.66E-13	1.39E-13	3.73E-07	5.16E-07	3.73E-07
K	1.40E-06	2.31E-06	2.39E-06	1.30E-12	2.29E-14	5.45E-14	1.14E-06	1.51E-07	2.33E-07
Al	8.26E-08	7.21E-08	1.21E-07	1.61E-13	1.32E-13	1.70E-13	4.01E-07	3.63E-07	4.12E-07
Fe	1.24E-08	2.41E-08	2.24E-08	1.88E-15	1.11E-15	1.00E-15	4.33E-08	3.34E-08	3.17E-08
MSE/MAE				3.86E-09	1.98E-08	4.68E-07	-2.51E-05	-5.62E-05	-2.27E-04

9.3.4 Conclusions

One possible reason for the significant overestimation of Hydrogen-Carbonate concentrations in all modules could be the underestimation of measured alkalinity in Biscuit Brook. COSTELLO-WALKER (1995) found that alkalinity is generally underestimated in the headwaters of the Neversink River due to CO_2 degasing after sampling. Therefore, pH values measured not in the field must be naturally underestimated, too. So, the real HCO_3^- concentrations in Biscuit Brook streamwater might be higher than calculated in the present study, as explained in chapter 5.

9.4 Affect of CEC

To explore the impact of exchanger composition and CEC, two different scenarios were simulated: a high CEC and a low CEC range were used. The high CEC range was represented by Basic Biscuit and the West Biscuit exchanger composition respectively, the low CEC was represented by AB exchanger composition.

Results for AB can not be shown since the model could not find a numerical solution for AB with BB exchanger composition in the cation exchange module.

9.4.1 Basic Biscuit

As apparent from figure 9.7, results for both CEC ranges are very similar. The most remarkable difference between streamwater with AB and BB CEC are Ammonia concentrations, where the model underestimates NH_4^+ much more in the modeled streamwater with BB CEC. Slight differences can be seen for all base cations, where streamwater with CEC as in AB has lower concentrations.

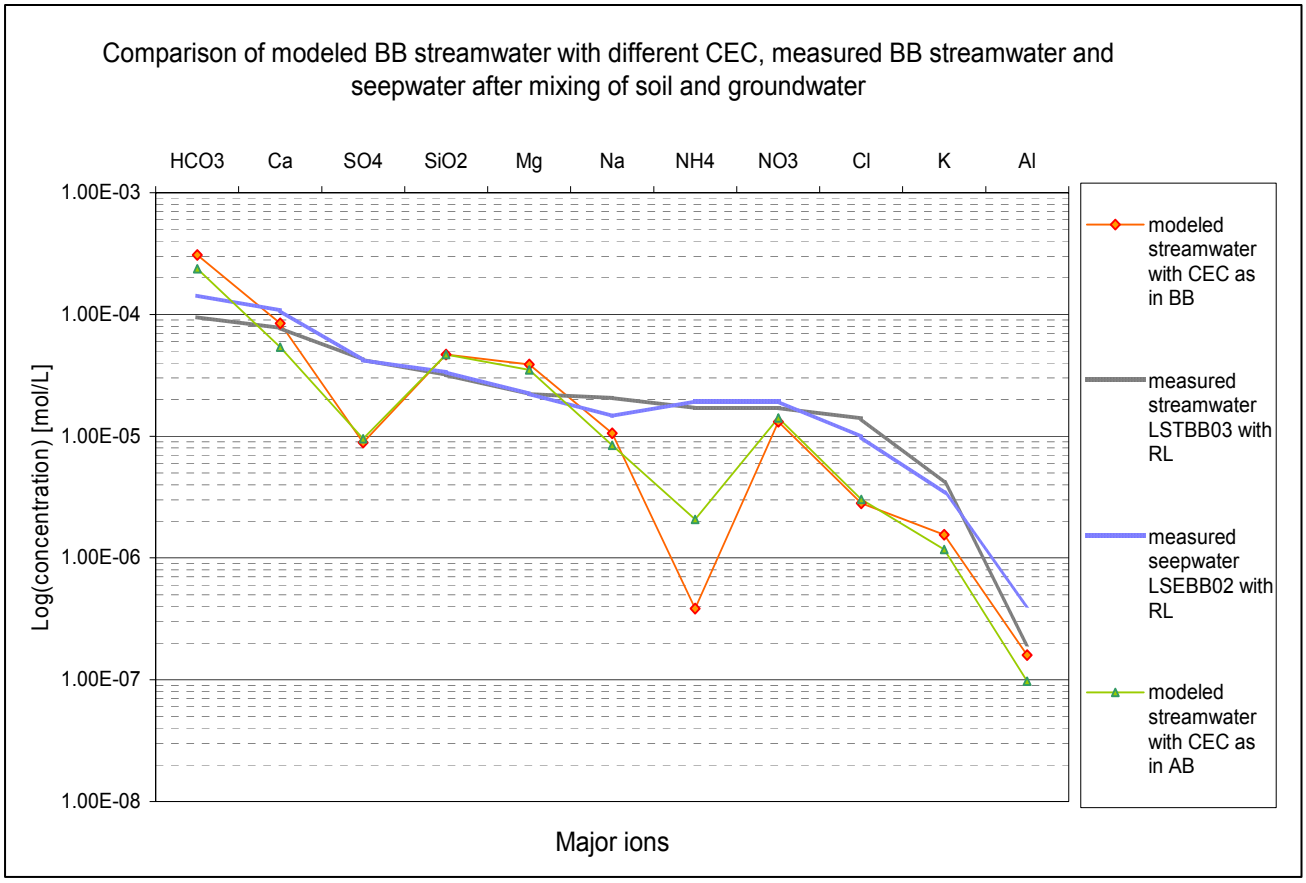

Figure 9.7: Comparison of streamwater in BASIC Biscuit with low and high CEC and with observed stream and seepwater samples

As presented in table 9.7, simulated pH was lower for CEC as in BB, but both values fitted well to observed streamwater. Simulated ionic strength is slightly lower for streamwater with CEC as in BB, but again both values are similar and fit well to observed stream and seepwater samples. Streamwater with AB CEC has a negative charge balance, in contrast to streamwater with BB CEC and observed stream and seepwater samples, which have a positive charge balance. This negative charge balance, as well as the higher percent error in charge, probably results from the slight underestimation of base cation concentrations.

Table 9.7: Comparison of pH, temperature, ionic strength, charge and percent error of charge for modeled BB streamwater (solution 80) with high, medium and low pCO_2 and measured stream (LSTBB03) and seepwater (LSEBB02) samples

Solution	Units	CEC AB	CEC BB	LSTBB03	LSEBB02
pH	*pH units*	6.72	6.88	6.65	6.78
temp	*°C*	11.0	11.0	11.0	13.2
ionic strength	*eq/L*	2.88E-04	3.91E-04	3.69E-04	4.52E-04
charge	*eq/L*	-6.22E-07	5.43E-07	2.43E-10	3.0E-09
pct_err	*%*	-0.16	0.10	0.00	0.00

Table 9.8: Compilation of modeled BB streamwater with low and high CEC and observed streamwater/seepwater concentration

	CEC AB	CEC BB	CEC AB SE	CEC AB AE	CEC BB SE	CEC BB AE
	Modeled	Modeled	$(Qo_1\text{-}Qm)^2$	$(Qo_1\text{-}Qm)$	$(Qo_1\text{-}Qm)^2$	$(Qo_1\text{-}Qm)$
	mol	mol		*mol*		*mol*
HCO_3	2.37E-04	2.37E-04	2.01E-08	-1.42E-04	2.01E-08	-1.42E-04
Mg	5.40E-05	5.38E-05	5.48E-10	2.34E-05	5.55E-10	2.36E-05
SO_4	9.54E-06	9.36E-06	1.07E-09	3.27E-05	1.08E-09	3.29E-05
Ca	4.70E-05	4.70E-05	2.26E-10	-1.50E-05	2.26E-10	-1.50E-05
SiO_2	3.51E-05	3.50E-05	1.66E-10	-1.29E-05	1.62E-10	-1.27E-05
Na	8.41E-06	8.41E-06	1.50E-10	1.23E-05	1.50E-10	1.23E-05
NH_4	2.08E-06	2.08E-06	2.23E-10	1.49E-05	2.23E-10	1.49E-05
Cl	1.42E-05	1.39E-05	8.28E-12	2.88E-06	1.01E-11	3.18E-06
NO_3	3.02E-06	2.96E-06	1.22E-10	1.10E-05	1.23E-10	1.11E-05
K	1.18E-06	1.18E-06	8.97E-12	3.00E-06	8.97E-12	3.00E-06
Al	9.71E-08	9.71E-08	9.59E-15	9.79E-08	9.59E-15	9.79E-08
Fe	2.62E-07	2.62E-07	4.72E-14	-2.17E-07	4.72E-14	-2.17E-07
MSE/MAE			1.88E-09	-5.79E-06	1.88E-09	-5.72E-06

9.4.2 West Biscuit

Figure 9.8, and tables 9.9 and 9.10 show the same patterns for West Biscuit than described as in the previous section for Basic Biscuit. But surprisingly, streamwater with CEC as in AB has lower percent error in charge than streamwater with CEC as in WB, as well as a lower MSE and MAE. The higher errors in streamwater with CEC as in WB result probably from the much lower Ammonia concentrations.

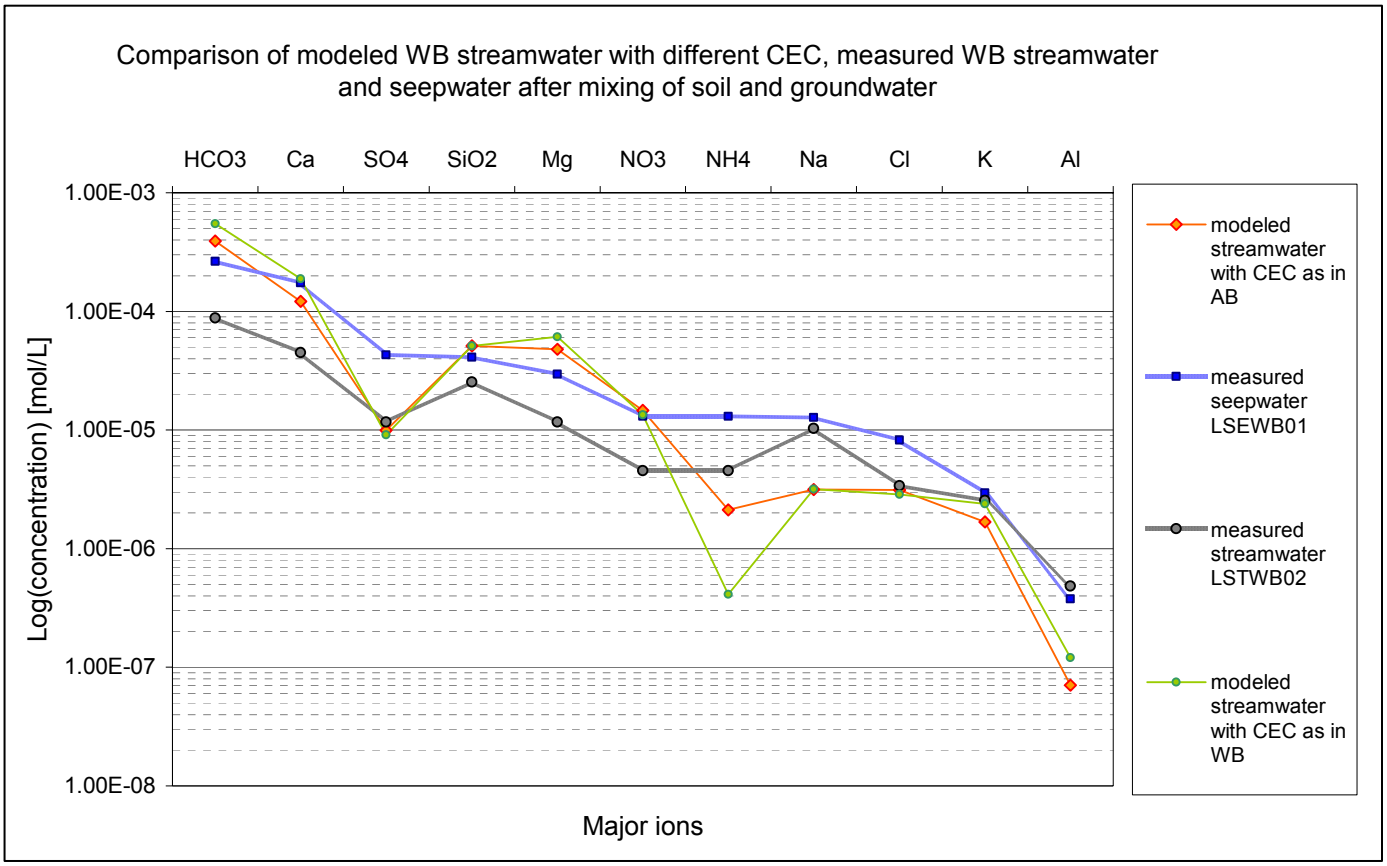

Figure 9.8: Comparison of streamwater in WEST Biscuit with low and high CEC and with observed stream and seepwater samples

Table 9.9: Comparison of pH, temperature, ionic strength, charge and percent error of charge for modeled BB streamwater (solution 80) with high, medium and low pCO_2 and measured stream (LSTBB03) and seepwater (LSEBB02) samples

Solution	Units	CEC AB	CEC WB	LSTWB02	LSEWB01
pH	*pH units*	7.02	7.19	6.45	7.22
temp	*°C*	11.0	11.0	11.3	11.1
ionic strength	*eq/L*	5.24E-04	7.59E-04	1.96E-04	6.52E-04
charge	*eq/L*	-4.56E-07	1.38E-06	1.39E-11	1.7E-10
pct_err	*%*	-0.07	0.14	0.00	0.00

Table 9.10: Compilation of modeled WB streamwater with low and high CEC and observed streamwater/seepwater concentration

	CEC AB	CEC WB	CEC AB SE	CEC AB AE	CEC WB SE	CEC WB AE
	Modeled *mol*	Modeled *mol*	$(Qo_2-Qm)^2$	(Qo_1-Qm) *mol*	$(Qo_2-Qm)^2$	(Qo_1-Qm) *mol*
HCO_3	3.91E-04	7.85E-04	9.17E-08	-3.03E-04	4.85E-07	-6.97E-04
Ca	1.22E-04	2.28E-04	5.86E-09	-7.66E-05	3.34E-08	-1.83E-04
SO_4	9.91E-06	1.06E-05	3.17E-12	1.78E-06	1.26E-12	1.12E-06
SiO_2	5.12E-05	5.12E-05	6.65E-10	-2.58E-05	6.65E-10	-2.58E-05
Mg	4.80E-05	1.40E-04	1.32E-09	-3.63E-05	1.64E-08	-1.28E-04
NO_3	1.47E-05	1.57E-05	1.02E-10	-1.01E-05	1.23E-10	-1.11E-05
NH_4	2.12E-06	2.19E-07	5.90E-12	2.43E-06	1.87E-11	4.33E-06
Na	3.16E-06	4.74E-06	5.09E-11	7.14E-06	3.09E-11	5.56E-06
Cl	3.13E-06	3.34E-06	6.42E-14	2.53E-07	2.58E-15	5.08E-08
K	1.69E-06	3.35E-06	7.34E-13	8.56E-07	6.54E-13	-8.09E-07
Al	7.08E-08	9.28E-08	1.71E-13	4.13E-07	1.53E-13	3.91E-07
Fe	1.48E-08	3.07E-08	1.67E-15	4.09E-08	6.27E-16	2.50E-08
MSE/MAE			8.31E-09	-3.66E-05	4.47E-08	-8.62E-05

10 Conclusions

Generally, results were well with mean errors of the same order of magnitude than the reporting limit for the observed stream and seepwater samples. Percent error in charge ranged between 0.0 and 0.34%. However, several problems occurred, which will be discussed in the following.

10.1 Soilwater Modules

Module 1 and 1a are discussed together, since chemical parameters were remained constant, and only hydrological parameters, flow path length, travel time and velocity, were altered. Since no soilwater data were available for Biscuit Brook, some transfers had to be undertaken in the soilwater modules, based on soilwater samples from Shelter Creek, an adjacent watershed with very similar geology and soils. Our working approach was, firstly, that soilwater should be higher ionized than streamwater and it should also feature a higher pH, because of a higher buffer capacity in the unsaturated zone than in saturated zone. Secondly, it should have a higher pCO_2 due to biological activity. It could be shown that the model is able to simulate soilwater with higher ionic strength, higher pCO_2 and higher pH than in observed streamwater samples for the more basic tributaries, BB and WB. Problems occurred in the more acidic tributary, AB, were base cation and Al^{3+} concentrations were underestimated. Simulated AB soilwater also has the highest percent error in charge, whereas both, BB and WB, have very low charge errors. Interestingly, NH_4^+ concentrations are underestimated by the soil model in all three subcatchments, and this seems to be controlled by cation exchange reactions, since, as shown by the stepwise modeling approach, the Ammonia concentrations only dropped significantly after step 5 (cation exchange). This could be due to an overestimation of measured Ammonia concentrations especially in some seepwater samples, which feature unrealistically high NH_4^+ concentrations, e.g. LSEBB04, which are not characteristic for Catskill waters (LAWRENCE, 2009; personal communication). The simulated Sulphate and Chloride concentrations were systematically underestimated by the model. Since these compounds are considered as conservative, this leads to the conclusion that the input

signal, mean monthly Biscuit Brook precipitation from December 2007, does not represent measured Biscuit Brook streamwater from June 2008. In general, modeled soilwater in the infiltration module still underestimates ionic strength, pH, and base cation concentrations, since flow path length and, therefore, contact times are shorter than in the soilwater flow model. For certain substances, like Al^{3+} and partly Mg^{2+}, K^{+}, Na^{+}, cation exchange seems to have degraded the results. Therefore, it remains uncertain if PHREEQC' approach of modeling cation exchange is appropriate for Biscuit Brook.

10.2 Groundwater Module

In this module certain simplifying assumptions had to done, because no groundwater data was available for the study site. Diffusion was not included, which is probably not correct, especially if you consider the base flow conditions during the measurement campaign in June 2008. In reality, groundwater flow systems in the Catskills are in all likelihood dual porosity systems with a mobile flow system in the fissures and an immobile flow system in the matrix of the sandstone aquifer. Another simplification was the assumption of an open system in regard to CO_2. Typically, the saturated zone is considered as a closed system, where CO_2 is supplied by the root zone along the flow path (APPELO & POSTMA, 2005). But since no data about additional supply of CO_2 by the root zone was available, pCO_2 of soilwater was retained. This approach is clearly not precise, but it was seen as the best alternative, since modeling a simple CO_2 consumption would lead to even bigger uncertainties.

For the groundwater module, our working hypothesis was that the saturated zone is almost chemically unreactive with very low buffer capacity, since the bedrock contains 80% Quartz (WAY, 1972). Also, cation exchange was excluded, since we assumed groundwater flow to be only in fractures. This shows in simulated NH_4^{+} concentrations in groundwater of all three tributaries, which fit much better to observed streamwater concentrations now. It could be proved that the model was able to model groundwater with lower ionic strength, lower pH and lower base cation concentrations successfully for all three subcatchment. After our approach pH in simulated groundwater should be lower than in observed streamwater, which was achieved for BB and WB, but not in AB.

10.3 Streamwater Module

The approach in the mixing model was that a soilwater with higher pH and higher base cation concentrations, as well as a higher pCO_2, mixed with a groundwater with a low ionization and a lower pH should result in the respective measured streamwater. But even after degasing of CO_2 simulated stream flow in AB and WB has HCO_3^- concentrations that are significantly higher than the respective target streamwater concentrations. This could be partly caused by the open pCO_2 system used in the groundwater module, since the relatively high pCO_2 in simulated groundwater could result in an overestimation of HCO_3^- concentration in simulated groundwater. Another explanation is the overestimation of pH in simulated streamwater of both tributaries, since activity of CO_2 species is pH dependent, and between pH values of 6 and 10 HCO_3^- is the dominant CO_2 species (STUMM & MORGAN, 1997).

One other problem that occurred for simulated streamwater in AB was that simulated streamwater chemistry resembles much more modeled groundwater chemistry than observed in measured AB streamwater. These findings support results from BURNS et al. (1998), who found that the contribution of deep groundwater is much smaller in Acid Biscuit than in West and Basic Biscuit respectively. It also has to be considered that the estimated mean preevent contribution has to be regarded as a maximal preevent proportion, as explained in section 6.3.2. Thus, mean groundwater contribution could be overestimated. For BB and WB modeling results were generally closer to observed streamwater at the respective sites than in AB. This proves on the one hand, that BB and WB must have a higher contribution of deeper groundwater. This proportion must be maximal in BB, since BB seep and streamwater samples showed less variability than in WB. But on the other hand, it leads also to the conclusion that water with higher ionization and higher Calcite proportion is easier to model with the established PHREEQC model, which is also supported by the smaller charge error for BB and WB.

In WB, target SI for equilibrium reactions in the soilwater modules were taken from measured seepwater samples. But as showed, this approach led to an overestimation of Calcium and Magnesia in simulated streamwater, since observed West Biscuit streamwater (LSTWB02) seems not to be affected by the more basic seepwater sampling site (LSEWB01),

which is just some tens of meters upstream with no other significant tributary downstream of LSEWB01.

However, it could be proved that streamwater chemistry is mainly controlled by the presence or absence of Calcite, which is coupled with pCO_2. Figure 10.1 shows a topographic map of Biscuit Brook with all sampling points and a superposition of the surficial geology showing the spatial distribution of till, which is the only source of Calcite in the Catskills (ETHRIDGE, 1977; COSTELLO-WALKER, 1995). This map shows that the majority of sampling points are taken within the area with till deposits.

But it has to be considered that these deposits vary in depth, with thinner till layers on slopes and till accumulation in the valley bottoms. Typically, groundwater springs are found at the base of steep slopes in the Catskills (SHAMAN et al., 2004), but in Biscuit Brook some can be found along the slopes where till deposits are much shallower or even eroded. Thus, these spring waters would be less buffered, since spring water does not pass trough a till layer during recharge and discharge. This could possibly explain variations in chemistry and isotope signature of seep and streamwater in Biscuit Brook. These internal variations were not considered in the model.

Thus, the discrepancy between precipitation and streamwater chemistry in Biscuit Brook, and probably throughout the Catskills, is caused by the spatial variability of till and hence a variable buffer capacity of the soils. This leads to acidification of tributaries like AB, where till deposits are rare, because soils without a till layer and bedrock in this region are inherently acid sensitive. The presence or absence of Calcite is also reflected in the respective pCO_2, where sites with a lower pCO_2 have a higher Calcite proportion in the mineral composition of the till layer according to the pH dependent speciation of CO_2 species (APPELO & POSTMA, 2005). If the three observed tributaries are compared, a sequence of acidification degrees can be established: Basic Biscuit is well buffered, West Biscuit can be called medium-well buffered, and Acid Biscuit is poorly buffered, as shown by the measured exchange composition and the longitudinal streamwater chemistry profiles.

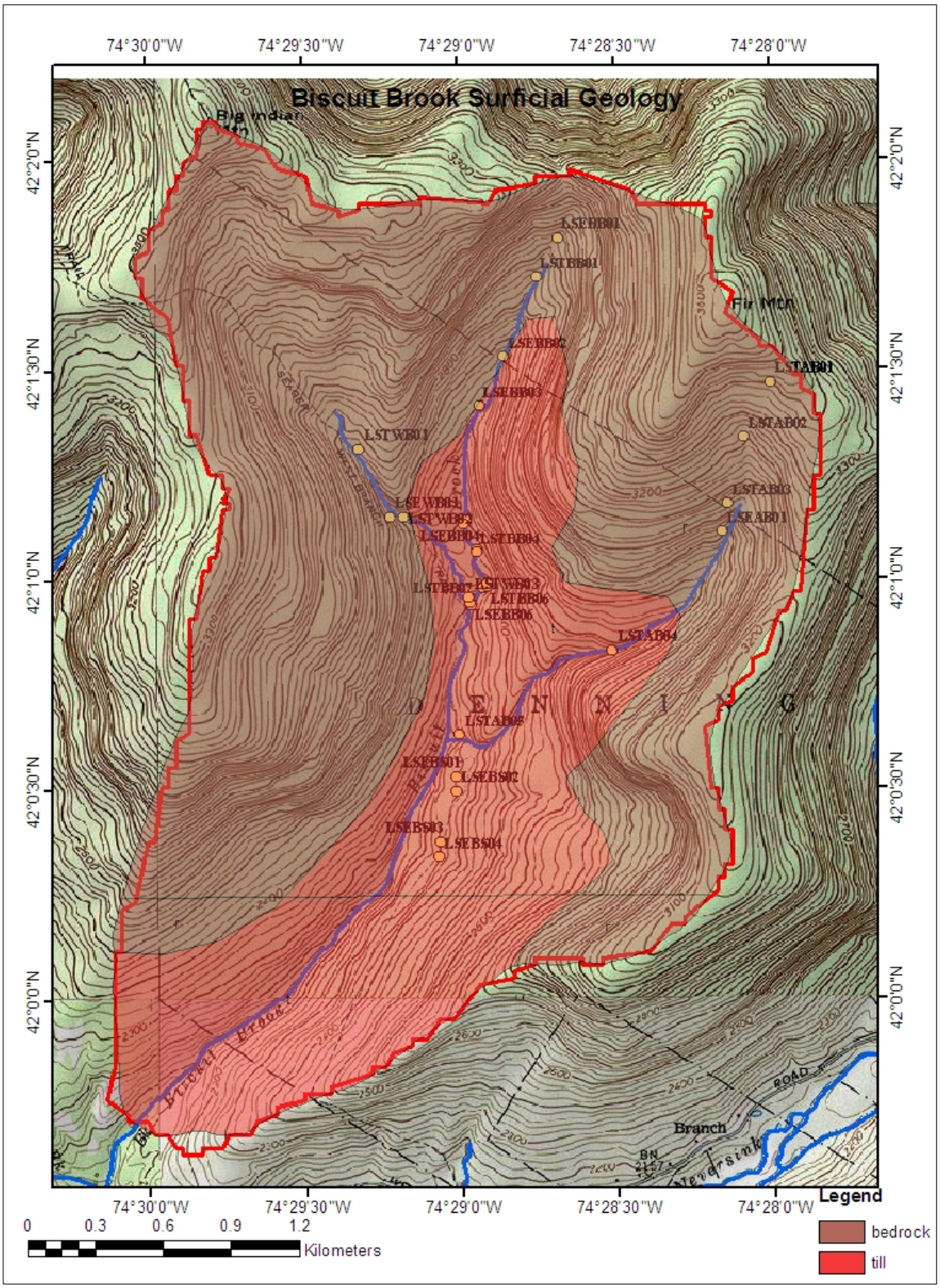

Figure 10.1: Topographic map of Biscuit Brook with superposition of surficial geology showing sampling points

Mixing of these different water types, even though two are generally basic with pH values close to 7, leads to a pH at the catchment outlet, which is closer to 6.

If no drastic changes in environmental politics are made, tributaries like BB and WB will develop towards AB over time, since the Calcite buffer in the till layer will be depleted.

Concluding, in naturally acid sensitive areas, recovery from anthropogenic acidification is not easily achieved, since soils are not able to buffer the acid entering the system. One possible amelioration practice could be liming, which is done routinely in German forest management, but it is labor and cost intensive.

10.4 Sensitivity Analysis

In the following, detected significant chemical reactions with regard to acidification are discussed. The most important reactions are buffering reactions, where the presence of Calcite is controlling stream pH. This confirms the results of COSTELLO-WALKER (1995), which are described in detail in chapter 3. But it could be shown that the source of alkalinity not only in Basic and West Biscuit, but also in Acid Biscuit must be Calcite, since Calcite had to be included to explain measured Ca^{2+} concentrations. Generally, buffering reactions were modeled well within the established PHREEQC equilibrium model and followed this weathering sequence:

1. Calcite weathering
2. Weathering of silica minerals: Quartz, K-feldspar, K-mica, Albite, Anorthite
3. Formation/ weathering of clay minerals: Gibbsite, Kaolinite, Ca-Montmorillonite, Chlorite, Illite

Calcite weathering was needed to explain Calcium concentration, silica minerals had to be included because of K^+, Na^+, SiO_2 and Al^{3+} concentrations. Clay minerals with positive saturation indices in measured streamwater samples, like Gibbsite and Kaolinite, are assumed to precipitate, whereas clay minerals with negative SI, Chlorite, are assumed to dissolve in simulated waters. Typically, clay minerals are seen as secondary minerals that are formed as weathering products of silica minerals. But in the Catskills some clay minerals, like Chlorite and Illite,

are primary minerals, since the Catskill region consists of sedimentary rocks. Gibbsite and Kaolinite were needed to adjust Al^{3+} concentrations, and Chlorite had to be included to explain Mg^{2+} concentrations, even though $SI_{chlorite}$ was very low in all observed streamwater and seepwater samples respectively. It was tried to use Biotite instead of Chlorite to adjust modeled Magnesia concentrations, since there are reports that this mineral occurs in the Catskills (WAY, 1972), but results showed very high charge errors and therefore Biotite was excluded from the equilibrium model.

Overall, the model was able to successfully simulate fast, but also slow weathering processes through equilibrium reactions, and not by using kinetic reactions by using saturation indices which were unequal to zero and which were obtained from the stream and seepwater samples taken in June 2008.

An important affect on streamwater chemistry has pCO_2, which is of course strongly correlated with pH and Calcite weathering. One possible reason for the significant overestimation of Hydrogen-Carbonate concentrations in all modules could be the underestimation of measured alkalinity in Biscuit Brook, since pH significantly drops if CO_2 degases from the sample bottles (COSTELLO-WALKER, 1995).

It could be proven that cation exchange is not the dominant process in Biscuit Brook, since the exchange model showed no specific sensitivity. Simulated streamwater concentrations with high and low CEC are not significantly different.

10.5 Model Limitations

It is obvious that various assumptions and approximations had to be made to establish the coupled hydrological and geochemical model. But especially the hydrology domain of the model could be improved. One problem in the subsurface flow module is that water volume and water level remain constant in each cell, whereas in natural hillslopes water level and water volume would increase downslope. Rising water levels could lead to anaerobe conditions, or soilwater chemistry can be altered just by mixing processes. Another approximation had to be made in the groundwater flow module, where diffusion was not considered. But it would have been more precise to include a double porosity system, since

bedrock in Biscuit Brook is mainly fissured sandstone. Especially during low flow conditions water stored in the porous matrix could contribute a significant proportion to streamflow. If you consider that the measurement campaign in June 2008 was conducted during low flow, this could also partly explain discrepancies between modeled streamwater and measured stream and seepwater. Another unrealistic assumption in the groundwater flow module is that only one set of flow path length, velocity, travel time and dispersivities was used. Better would have been to include an exponential model, which simulates travel times between zero and infinity. But our approach was to keep the model as simple as possible and also to minimize uncertainties.

Another weakness of the model is the total exclusion of flora, where especially nutrient uptake and cycling affects water chemistry.

11 Outlook

Although, there have been two geological and lithologic studies conducted in the Catskill region in the 1970s, it would be helpful for future studies to make thin sections for every site of interest. This could deliver valuable spatial and quantitative information about the mineral composition in the Neversink River watershed and could shed light on some of the uncertainties in the former studies.

For future large scale studies working with PHREEQC it would be interesting to couple PHREEQC with a hydrological model like Topmodel, which uses the so called topographic index to determine the given water saturation status of the respective cell. This would make spatially distributed reactive transport modeling possible.

Another interesting approach would be the combination of PHREEQC and an ecohydological model, like PnET, which would allow modeling comprehensive element and nutrient cycling, as well as geochemical reactions.

12 Acknowledgment

First of all, I want to thank my supervisor in the United States, Mike McHale from the USGS office in Troy, NY, who not only supported and helped me throughout this study, but who also went out of his way to make this cooperation of a German University and the USGS office in New York possible.

Then I have to thank my German supervisor, Christoph Külls, for his support and his help with the mass spectrometric isotope analyses.

I also want to thank Doug Burns, Greg Lawrence and Pete Murdoch, who also provided me with helpful information. During the field work I was supported by Mike McHale, Jason Siemon, Doug Burns, and Greg Lawrence.

Special thanks have to go to the USGS scientists that work in the laboratory in Troy, NY, where the taken water samples were analyzed for major ions.

I also want to thank my friends, family and my husband for their support and their love. A special thanks for Maria Friderich, who printed and bound my thesis in Germany.

I also want to thank Prof. Markus Weiler, who allowed me to actually finish this work in the United States.

13 References

Appelo, C.A.J., Postma, D. (2005): Geochemistry, Groundwater and Pollution. A.A. Balkema Publishers, Leiden, 2nd edition, ISBN: 04 1536 428 0, 590 pages

Baldigo, B.P., Murdoch, P.S., Burns, D.A. (2005): Stream acidification and mortality of brook trout (Salvelinus fontinalis) in response to timber harvest in small Catskill Mountain watersheds, New York, USA. Canadian Journal of Fishery and Aquatic Science Vol. 62, p. 1168-1183

Blume, L.J., Schumacher, B.A., Schaffer, P.W., Cappo, K.A., Papp, M.L., Van Remortel, R.D., Coffey, D.S., Johnson, M.G., Chaloud D.J. (1990): Handbook of methods for acid deposition studies laboratory analyses for soil chemistry. U.S. EPA, Environmental Monitoring Systems Laboratory, Las Vegas, NV EPA/600/4-90/023

Brown, V.A., McDonnell, J.J., Burns, D.A., Kendall, C. (1999): The role of event water, a rapid shallow soil flow component, and catchment size in summer stormflow. Journal of Hydrology, Vol. 217, p. 171-190

Burns, D.A., Murdoch, P.S., Lawrence, G.B., Michel, R.L. (1998a): The effect of ground-water springs on NO3- concentrations during summer in Catskill Mountain streams. Water Resource Research, Vol. 34, p. 187-196

Burns, D.A. (1998b): Retention of NO3- in an upland stream environment: A mass balance approach. Biogeochemistry, Vol. 40, p. 73-96

Burns, D. A., Lovett, G. M., Murdoch, P. S. (2004): The Relative Effects of Hydrology, Ecology, and Climate on Temporal Trends and Spatial Patterns

of Stream Nitrate Concentrations in the Catskill Mountains, New York, USA. American Geophysical Union, Fall Meeting 2004, abstract #H53F-01

Burns, D.A., Riva-Murray, K., Bode, R.W., Passy, S. (2008): Changes in stream chemistry and biology in response to reduced levels of acid deposition during 1987-2003 in the Neversink River Basin, Catskill Mountains. Ecological Indicators, Vol. 8, p. 191-203

Buttle, J.M., Peters, D.L. (1997): Inferring Hydrological Processes in a Temperate Basin Using Isotopic and Geochemical Hydrograph Separation: A Re-evaluation. Hydrological Processes, Vol. 11, p. 557-573

Carstens, D. (2007): Modellierung von Adsorption und Transport von Schwermetallen in der gesättigten Zone mit PHREEQC. Diplom Thesis IHF at Albert-Ludwigs-Universität Freiburg, unpublished

Charlet, L., Chakraborty, S., Appelo, C.A.J., Roman-Ross, G., Nath, B., Ansari, A.A., Lanson, M., Chatterjee, D., Mallik, S.B. (2007): Thermodynamics of an arsenic "hotspot" in a West Bengal aquifer: A field and reactive transport modeling study. Applied Geochemistry, Vol. 22, p. 1273-1292

Clark, I.D., Fritz, P., (1997): Environmental Isotopes in Hydrogeology. Lewis Publishers, New York, 290 p.

Costello-Walker, C. (1995): Surface Water Alkalinity in the Neversink Basin, Catskill Mountains, New York. Master Thesis Lehigh University, New York, 108 p.

Cronan, C.S., Grigal, D.F. (1995): Use of Calcium /Aluminum Ratios as Indicators of Stress in Forest Ecosystems. Journal of Environmental Quality, Vol. 24, p. 209-226

Dise, N.B., Matzner, E., Armbruster, M., MacDonald, J. (2001): Aluminum Output Fluxes from Forest Ecosystems in Europe: a Regional Assessment. Journal of Environmental Quality, Vol. 30, p. 1747-1756

Dunne, T. (1978): Field Studies of Hillslope processes, In: Kirkby, M.J. (Ed.): Hillslope Hydrology. Wiley, Chichester, p. 227-293

Ethridge, F.G. (1977): Petrology, Transport and Environment in Isochronous Upper Devonian Sandstone and Siltstone Units, New York. Journal of Sedimentary Petrology, Vol. 47, p. 53-65

Firda, G.D., Lumia, R., Murray, P.M., Flanary, E.A. (1996): Water Resources Data, New York – Water Year 1995, Vol. 1. Eastern New York excluding Long Island. US Geological Survey Water Data Report NY-95-1, Troy, New York, p. 434

Hoeg, S., Uhlenbrook, S., Leibundgut, Ch. (2000): Hydrograph Separation in a Mountainous Catchment- Combining Hydrochemical and Isotopic Tracers. Hydrological Processes, Vol. 14, p. 1199-1216

Jenkins, A., Ferrier, R.C., Harriman, R., Ogunkoya, Y.O. (1994): A case Study in Catchment Hydrochemistry: Conflicting Interpretations from Hydrological and Chemical Observations. Hydrological Processes, Vol. 8, p. 335-349

Kaeser, A.J., Sharpe, W.E. (2001): The Influence of Acidic Runoff Episodes on Slimy Sculpin Reproduction in Stone Run. Transactions of the American Fisheries Society, Vol. 130, p. 1106-1115

Käss, W. (2004): Geohydrologische Makierungstechnik. Lehrbuch der Hydrogeologie. Band 9. Gebrüder Borntraeger, Berlin, 2nd edition, ISBN 3-443-01050-4

Lawrence, G.B., Lincoln, T.A., Horan-Ross, D.A., Olson, M., Waldron, L.A. (1995a): Analytical Methods of the US Geological Survey's New York District Water-analysis Laboratory. USGS Open File Report 95-416, p.78

Lincoln, T.A., Horan-Ross, D.A., Olson, M.L., Lawrence, G.B. (1995b): Quality Assurance Data for Routine Water-Analyses by the U.S. Geological Survey Laboratory in Troy, New York. USGS Open File Report 96-167

Lawrence, G.B., David, M.B., Lovett, G.M., Murdoch, P.S., Burns, D.A., Stoddard, J.L., Baldigo, B.P., Porter, J.H., Thompson, A.W. (1999): Soil Calcium Status and the Response of Stream Chemistry to Changing Acidic Deposition Rates. Ecological Applications, Vol. 9, p. 1059-1072

Lincoln, T.A., Horan-Ross, D.A., McHale, M.R., Lawrence, G.B. (1995b): Quality Assurance Data for Routine Water-Analyses by the U.S. Geological Survey Laboratory in Troy, New York. USGS Open File Report 2004-1327, p. 23

Lynch, J.A., Bowersox, V.C., Grimm, J.W. (2000): Acid Rain reduced in eastern United States. Environmental Sciences & Technology, Vol. 34, p. 940-949

Machado, C.J.F., Santiago, M.M.F., Mendonca, L.A.R., Frischkorn, H., Filho, J.M. (2007): Hydrochemical and Flow Modeling of Aquitard Percolation in the Cariri Valley- Northeast Brazil. Aquatic Geochemistry, Vol. 13, p. 187-196

Mahlknecht, J., Garfias-Solis, J., Aravena, R., Tesch, R. (2006): Geochemical and isotopic investigations on groundwater residence time and flow in the Independence Basin, Mexico. Journal of Hydrology, Vol. 324, p. 283-300

McHale, M.R., Burns, D.A., Lawrence, G.B., Murdoch, P.S., (2007): Factors controlling soilwater and streamwater aluminum concentrations after a clearcut in a forested watershed with calcium-poor soils. Biogeochemistry, Vol. 84, p. 311-331

Merkel, B.J., Planer-Friedrich, B. (2005): Groundwater Geochemistry. A Practical Guide to Modeling of Natural and Contaminated Aquatic Systems. Springer-Verlag, Berlin, ISBN 3-540-24195-7, 181 p.

Murdoch, P.S. (1991): Chemical budgets and stream-chemistry dynamics of a headwater stream in the Catskill Mountains of New York, October 1, 1983 through September 30, 1985. U. S. Geological Survey Water Resources Investigation Report 88-4035, 66 p.

Murdoch, P.S., Stoddard, J.L. (1993): The Role of Nitrate in the Acidification of Streams in the Catskill Mountains of New York. Water Resources Research, Vol. 28, p. 2707-2720

Murdoch, P. S., Stoddard, J. L. (1993): Chemical Characteristics and Temporal Trends in Eight Streams of the Catskill Mountains, New York. Water, Air, and Soil Pollution, Vol. 67, p. 367-395

Murdoch, P.S., Shanley, J.B. (2006): Detection of water quality trends at high, median, and low flow in a Catskill Mountain stream, New York, through a new statistical method. Water Resources Research, Vol. 42, W08407

Parker, G.G., Hely, A.G., Keighton, W.B., Olmstead, F.H. (1964): Water Resources of the Delaware River Basin. U.S. Geological Survey Professional Paper 381, 200 p.

Parkhurst, D.L., Thorstenson, D.C., Plummer, L.N. (1980): PHREEQE- A Computer Program for Geochemical Calculations: U.S. Geological Survey Water-Resources Investigations Report 80-96, 195 p.

Parkhurst, D.L., Appelo, C.A.J. (1999): User's Guide to PHREEQC (version 2)- A Computer Program for Speciation, Batch-Reaction, One-dimensional Transport and Inverse Geochemical Calculations. Water-Resources Investigations Report 99-4259

Reuss, J.O., Johnson, D.W. (1985): Effect of soil processes on the acidification of water by acid deposition. Journal Environmental Quality, Vol. 14, p. 26-31

Reuss, J.O., Johnson, D.W. (1986): Acid deposition and the acidification of soils and waters. Ecological Studies 59. Springer-Verlag, New York

Scheffer, F., Schachtschabel, P., Blume, H.P. (2002): Lehrbuch der Bodenkunde. Spektrum Akademischer Verlag, Heidelberg, Berlin, 15th edition, ISBN: 3-8274-1324-9

Shaman, J., Stieglitz, M., Burns, D. (2004): Are big basins just the sum of small catchments? Hydrological Processes, Vol. 18, p. 3195-3206

Stoddard, J.L., Murdoch, P.S. (1991): In: Acid Deposition and Aquatic Ecosystems: Regional Case Studies. Charles, D.F. (ed.), Springer-Verlag, New York, 237 p.

Stumm, W., Morgan, J.J. (1996): Aquatic Chemistry. Chemical Equilibria and Rates in Natural Waters. 3rd edition, John Wiley & Sons, Inc., New York, ISBN: 0-471-51184-6

Way, J.H. (1972): A More Detailed Discussion of the Depositional Environmental Analysis Middle and Upper Devonian Sedimentary Rocks Catskill Mountain Area, New York. Ph D. Dissertation Rensselaer Polytechnic Institution, 136 p.

Winner (2006): Trend Analyses in Streamwater, Soilwater and Precipitation in the Neversink River Basin, New York, U.S. Geological Survey in Troy, New York Poster, unpublished

URL1: last check 02/05/08

http://www.chromatography-online.org/topics/ion/chromatography.htm

URL 2: last check 02/05/08

http://www.chemistry.nmsu.edu/Instrumentation/IC.html

Appendix

Table 0.1: All data from longitudinal sampling campaign in June 2008 in Biscuit Brook, highlighted pH values had to be calculated with a regression; values in brackets show gfw; table is continued up to page 147

Source	Date and Time	Temp	pH	ANC*	SC**	DOC***	Cl (35.453)	Ca (40.078)	Fe (55.845)	Mg (24.305)	K (39.0983)	Si (28.0855)
				µeq/L	µS/cm²	µeq/L	mg/L	mg/L	mg/L	mg/L	mg/L	mg/L
LSEAB01	04.06.2008 11:15	11.3	4.52	-30.3	20.5	259.2	0.3	0.5	7.6E-03	0.2	0.0	0.4
LSEBB01	12.06.2008 14:10	8.1	6.98			79.4	0.4	9.2	3.0E-02	0.6	0.3	1.0
LSEBB02	12.06.2008 14:50	13.2	6.78			96.8	0.4	4.3	0	0.5	0.1	0.9
LSEBB03	12.06.2008 15:00	13.2	5.71			145.8	0.4	3.4	1.9E-03	0.5	0.0	0.9
LSEBB04	03.06.2008 13:38	11.3	6.53	90.6	24.7	226.2	0.5	3.4	3.4E-02	0.8	0.4	0.9
LSEBB05	03.06.2008 13:54	11.3	6.81	80.9	22.7	110.9	0.3	2.8	0	0.7	0.1	1.0
LSEBB06	03.06.2008 14:20	11.3	7.05	184.5	30.2	189.3	0.3	3.8	8.5E-03	0.9	0.0	1.3
LSEBB07	04.06.2008 14:35	10.5	6.86	88.0	23.3	100.7	0.3	3.2	3.2E-03	0.7	0.1	1.0
LSEBS01	03.06.2008 09:30	11.2	5.84	26.8	15.7	136.4	0.2	1.5	1.8E-02	0.4	0.1	0.7
LSEBS02	03.06.2008 09:20	11.1	6.24	29.2	17.8	107.8	0.4	1.9	3.0E-03	0.6	0.1	0.9
LSEBS03	03.06.2008 09:00	10.6	5.56	5.8	16.3	118.6	0.3	0.8	0	0.3	0.0	1.0
LSEBS04	03.06.2008 09:15	10.4	5.07	-0.4	16.8	83.8	0.3	1.4	0	0.4	0.0	1.0
LSEWB01	03.06.2008 12:44	11.1	7.22	289.0	41.1	79.8	0.3	7.0	0	0.7	0.1	1.2
LSTAB01	04.06.2008 12:10	10.5	4.78	-6.5	25.1	601.3	0.4	0.6	2.1E-01	0.2	0.1	1.0
LSTAB02	04.06.2008 11:50	11.2	4.57	-24.6	21.5	370.8	0.3	0.7	5.2E-02	0.2	0.1	0.8
LSTAB03	04.06.2008 11:30	10.8	4.61	-23.6	19.5	286.3	0.3	0.8	3.3E-02	0.3	0.1	0.8
LSTAB04	04.06.2008 10:32	10.8	4.90	-12.7	16.4	186.6	0.3	0.9	6.9E-03	0.3	0.1	0.7
LSTAB05	03.06.2008 14:38	10.8	4.73	-17.8	19.4	161.5	0.3	1.2	8.9E-05	0.4	0.1	0.8
LSTBB01	12.06.2008 14:25	11.4	6.78			95.4	0.3	6.2	0	0.6	0.1	1.0
LSTBB02	12.06.2008 15:30	12.5	6.81			104.2	0.4	3.4	0	0.6	0.1	1.0
LSTBB03	03.06.2008 13:30	11.0	6.65	81.4	23.6	102.0	0.5	3.1	2.5E-03	0.5	0.2	0.9
LSTBB04	03.06.2008 13:44	11.0	6.84	89.6	23.6	109.4	0.5	3.1	0	0.5	0.1	0.9
LSTBB05	03.06.2008 14:01	11.0	6.77	84.3	23.3	96.5	0.5	2.9	0	0.6	0.1	0.9
LSTBB06	04.06.2008 14:30	9.0	6.79	94.6	24.5	98.6	0.5	3.3	0	0.6	0.2	0.9
LSTBB07	03.06.2008 14:16	11.0	6.71	63.3	21.2	104.9	0.4	3.3	6.1E-03	0.5	0.1	0.9

Source	Date and Time	Temp	pH	ANC	SC	DOC	Cl (35.453)	Ca (40.078)	Fe (55.845)	Mg (24.305)	K (39.0983)	Si (28.0855)
				µeq/L	µS/cm²	µeq/L	mg/L	mg/L	mg/L	mg/L	mg/L	mg/L
LSTWB01	12.06.2008 14:44	11.3	6.10			153.0	0.3	1.6	7.2E-03	0.3	0.1	0.8
LSTWB02	03.06.2008 13:05	11.3	6.05	16.0	15.6	143.0	0.1	1.8	3.1E-03	0.3	0.1	0.7
LSTWB03	03.06.2008 14:09	11.3	5.71	8.7	15.4	138.3	0.3	1.6	3.5E-04	0.3	0.1	0.7
LSTBS0001	11.06.2008 10:00	14.5	6.50	44.4	19.0	117.7	0.4	2.0		0.4	0.2	1.0

Source	Date and Time	Na (22.9898)	NO_3 (63.0049)	NO_2 (46.005)	SO_4 (96.0626)	Al $_{im}$ (26.9815)	pCO_2	HCO_3 (61.017)	CO_3 (60.010)
		mg/L	mg/L	mg/L	mg/L	mg/L	atm	mg/L	mg/L
LSEAB01	04.06.2008 11:15	0.2	0.1	6.8E-03	3.8	2.6E-01	1.7	0.7	6.3E-09
LSEBB01	12.06.2008 14:10	0.5	1.4	5.6E-03	4.2	1.1E-02	2.7	22.4	5.0E-04
LSEBB02	12.06.2008 14:50	0.3	1.2	1.2E-02	4.0	1.5E-02	2.8	9.9	2.2E-04
LSEBB03	12.06.2008 15:00	0.5	0.5	6.3E-03	4.0	1.1E-02	1.9	7.6	1.6E-06
LSEBB04	03.06.2008 13:38	0.4	1.4	1.3E-02	4.5	1.3E-02	2.7	8.2	6.6E-05
LSEBB05	03.06.2008 13:54	0.3	1.0	4.6E-03	4.2	6.5E-03	3.1	6.2	2.4E-04
LSEBB06	03.06.2008 14:20	1.0	0.0	6.8E-03	4.4	1.0E-02	3.5	11.3	7.2E-04
LSEBB07	04.06.2008 14:35	0.3	1.0	5.0E-03	4.2	7.6E-03	3.0	7.3	3.0E-04
LSEBS01	03.06.2008 09:30	0.2	0.5	6.3E-03	3.6	2.2E-02	2.5	2.5	2.7E-06
LSEBS02	03.06.2008 09:20	0.3	0.6	1.2E-03	4.1	1.3E-02	2.8	3.3	1.8E-05
LSEBS03	03.06.2008 09:00	0.2	0.0	4.1E-03	4.0	9.7E-02	4.0	0.0	7.3E-07
LSEBS04	03.06.2008 09:15	0.2	0.5	2.3E-03	4.2	3.2E-02	2.6	1.6	7.9E-08
LSEWB01	03.06.2008 12:44	0.3	0.8	4.7E-03	4.1	1.3E-02	3.0	16.9	1.6E-03
LSTAB01	04.06.2008 12:10	0.3	0.3	7.5E-03	3.9	1.1E-01	2.1	0.6	2.1E-08
LSTAB02	04.06.2008 11:50	0.3	0.2	3.6E-03	4.0	1.3E-01	1.7	0.8	7.9E-09
LSTAB03	04.06.2008 11:30	0.2	0.4	5.8E-03	3.9	1.1E-01	1.7	1.1	9.4E-09
LSTAB04	04.06.2008 10:32	0.2	0.5	6.4E-03	3.9	1.3E-01	2.1	0.7	3.5E-08
LSTAB05	03.06.2008 14:38	0.3	0.5	4.0E-03	3.9	4.6E-02	1.4	2.3	1.7E-08
LSTBB01	12.06.2008 14:25	0.4	1.2	7.0E-03	4.1	1.6E-02	2.6	15.1	2.1E-04
LSTBB02	12.06.2008 15:30	0.5	1.2	5.6E-03	4.1	1.3E-02	3.0	7.6	2.4E-04
LSTBB03	03.06.2008 13:30	0.5	1.1	5.4E-03	4.1	6.1E-03	2.9	6.8	1.1E-04
LSTBB04	03.06.2008 13:44	0.5	1.1	4.0E-03	4.1	9.6E-03	3.0	6.8	2.7E-04
LSTBB05	03.06.2008 14:01	0.4	1.1	6.6E-03	4.1	8.5E-03	3.0	6.3	2.0E-04

Source	Date and Time	Na (22.9898) mg/L	NO_3 (63.0049) mg/L	NO_2 (46.005) mg/L	SO_4 (96.0626) mg/L	Al_{im} (26.9815) mg/L	pCO_2 atm	HCO_3 (61.017) mg/L	CO_3 (60.010) mg/L
LSTBB06	04.06.2008 14:30	0.5	1.2	4.8E-03	4.1	9.7E-03	3.0	7.3	2.1E-04
LSTBB07	03.06.2008 14:16	0.4	1.0	5.1E-04	4.1	1.3E-02	3.0	7.1	1.5E-04
LSTWB01	12.06.2008 14:44	0.2	0.7	3.9E-03	3.9	2.9E-02	3.0	1.6	9.2E-06
LSTWB02	03.06.2008 13:05	0.2	0.3	3.3E-03	1.1	1.8E-02	2.7	5.7	7.1E-06
LSTWB03	03.06.2008 14:09	0.2	0.7	5.1E-03	3.8	2.6E-02	2.6	1.7	1.5E-06
LSTBS0001	11.06.2008 10:00	0.3	1.0		4.0	0	3.2	2.1	6.0E-05

Table 0.2: All 18 O data from longitudinal sampling campaign in June 2008 in Biscuit Brook for stream flow

Number	Sample ID	Date and Time	Flow [m^3/s]	$\delta^{18}O$ [‰]	Flow weighted $\delta^{18}O$ [‰*mm/week]	Comments	Precipitation Date
1	45049	11.01.2006 11:30	0.16	***-9.40***	***-0.05***	Winter storm	04.01.06-10.01.06
2	45094	11.01.2006 21:35	1.28	***-5.07***	***-0.22***	Winter storm	04.01.06-10.01.06
3	45095	14.01.2006 08:10	4.11	***-11.56***	***-1.64***	Winter storm	11.01.06-17.01.06
4	45096	18.01.2006 06:20	1.70	***-10.28***	***-0.60***	Winter storm	11.01.06-17.01.06
5	45423	08.03.2006 11:00	0.09	***-10.15***	***-0.03***	spring base flow	08.03.06-14.03.06
6	45476	22.03.2006 11:50	0.15	***-10.52***	***-0.05***	spring base flow	22.03.06-28.03.06
7	47386	09.08.2006 10:30	0.03	***-9.56***	***-0.01***	Summer storm	03.08.06-08.08.06
8	47447	19.08.2006 23:15	1.32	***-7.71***	***-0.35***	Summer storm	09.08.06-15.08.06
9	47389	23.08.2006 10:45	0.03	***-8.32***	***-0.01***	Summer storm	09.08.06-15.08.06
10	49035	07.02.2007 13:00	0.09	***-9.05***	***-0.03***	Snow melt	31.01.07-06.02.07
11	49079	22.02.2007 12:00	0.06	***-8.22***	***-0.02***	Snow melt	21.02.07-27.02.07
12	49110	07.03.2007 13:45	0.09	***-9.40***	***-0.03***	Snow melt	07.03.07-13.03.07
13	49223	14.03.2007 22:45	0.51	***-10.93***	***-0.19***	Snow melt	07.03.07-13.03.07
14	49183	15.03.2007 12:30	1.30	***-11.38***	***-0.51***	Snow melt	07.03.07-13.03.07/14.03.07-20.03.07
15	49247	21.03.2007 13:00	0.22	***-9.70***	***-0.07***	Snow melt	14.03.07-20.03.07/ 21.03.07-27.03.07
16	49315	23.03.2007 02:05	0.83	***-9.48***	***-0.27***	Snow melt	21.03.07-27.03.07
17	49316	24.03.2007 21:45	1.02	***-10.78***	***-0.38***	Snow melt	21.03.07-27.03.07
18	49320	27.03.2007 10:15	1.68	***-10.44***	***-0.61***	Snow melt	21.03.07-27.03.07/28.03.07-03.04.07
19	49495	15.04.2007 21:35	4.17	***-10.76***	***-1.55***	Snow melt	11.04.07-17.04.07
20	49496	16.04.2007 22:45	3.40	***-10.41***	***-1.22***	Snow melt	11.04.07-17.04.07

Number	Sample ID	Date and Time	Flow [m³/s]	δ ^{18}O [‰]	Flow weighted δ ^{18}O [‰*mm/week]	Comments	Precipitation Date
21	49405	17.04.2007 10:15	1.22	***-10.99***	***-0.46***	Snow melt	11.04.07-17.04.07/18.04.07-24.04.07
22	49762	18.04.2007 07:50	0.79	***-10.78***	***-0.29***	Snow melt	18.04.07-24.04.07
23	51023	11.09.2007 09:25	0.10	***-10.06***	***-0.04***	Late Summer/ early fall storm	05.09.07-11.09.07
24	51025	11.09.2007 10:55	3.84	***-10.24***	***-1.35***	Late Summer/ early fall storm	05.09.07-11.09.07
25	51026	11.09.2007 15:25	0.68	***-10.12***	***-0.24***	Late Summer/ early fall storm	05.09.07-11.09.07
26	50951	12.09.2007 11:15	0.14	***-9.15***	***-0.04***	Late Summer/ early fall storm	12.09.07-18.09.07

Table 0.3: All 18 O data from longitudinal sampling campaign in June 2008 in Biscuit Brook for precipitation and snow at Slide Mt.

Number	Sample ID	Time Period	Precipitation N $_i$ [mm/week]	Snowfall S $_i$ [mm/week]	Mean Snow Depth [mm/week]	δ ^{18}O [‰]	Precipitation weighted δ 18 O [‰*mm/week]	Snowfall weighted δ 18 O [‰]	Comments
1	10.01.2006	04.01.06-10.01.06	14.5	139.7	406.4	***-13.11***	***-0.36***	***-1.04***	Winter storm
2	17.01.2006	11.01.06-17.01.06	50.3	50.8	82.6	***-9.27***	***-0.88***	***-0.27***	Winter storm
3	14.03.2006	08.03.06-14.03.06	18.0	0.0	0.0	***-4.95***	***-0.17***		Spring base flow
4	28.03.2006	22.03.06-28.03.06	7.4	101.6	20.3	***-12.76***	***-0.18***	***-0.74***	Spring base flow
5	08.08.2006	03.08.06-08.08.06	6.1	0.0	0.0	***-5.30***	***-0.06***		Summer storm
6	15.08.2006	09.08.06-15.08.06	10.9	0.0	0.0	***-3.35***	***-0.07***		Summer storm
7	06.02.2007	31.01.07-06.02.07	5.8	114.3	118.5	***-17.18***	***-0.19***	***-1.12***	Winter storm
8	27.02.2007	21.02.07-27.02.07	18.3	292.1	558.8	***-8.38***	***-0.29***	***-1.40***	Winter storm/ Snow melt
9	13.03.2007	07.03.07-13.03.07	15.7	0.0	465.7	***-16.92***	***-0.50***		Winter storm/ Snow melt
10	20.03.2007	14.03.07-20.03.07	75.2	609.6	575.7	***-7.16***	***-1.02***	***-2.49***	Snow melt
11	27.03.2007	21.03.07-27.03.07	17.3	0.0	554.6	***-7.38***	***-0.24***		Snow melt
12	03.04.2007	28.03.07-03.04.07	4.1	0.0	31.8	***-9.59***	***-0.07***		Snow melt
13	10.04.2007	04.04.07-10.04.07	13.7	76.2	21.2	***-7.91***	***-0.21***	***-0.34***	Snow melt
14	17.04.2007	11.04.07-17.04.07	180.8	355.6	93.1	***-10.66***	***-3.65***	***-2.16***	Snow melt
15	24.04.2007	18.04.07-24.04.07	2.3	12.7	63.5	***-5.42***	***-0.02***	***-0.04***	Snow melt
16	11.09.2007	05.09.07-11.09.07	8.6	0.0	0.0	***-10.66***	***-0.17***		Late summer/early fall storm
17	18.09.2007	12.09.07-18.09.07	79.0	0.0	0.0	***-5.42***	***-0.81***		Late summer/early fall storm

Event Number
Event 1 baseflow
Event 1 baseflow
Event 1
Event 1